HIGHWAY RESEARCH **RECORD**

Number 337

Theory of
Pavement Design

9 Reports

HIGHWAY RESEARCH BOARD

Department of Design

W. B. Drake, Chairman
Kentucky Department of Highways, Lexington

L. F. Spaine
Highway Research Board Staff

COMMITTEE ON THEORY OF PAVEMENT DESIGN
(As of December 31, 1969)

Aleksandar S. Vesic, Chairman
Duke University, Durham, North Carolina

W. F. Abercrombie
Richard G. Ahlvin
Ernest J. Barenberg
Richard D. Barksdale
Eugene Y. Huang
W. Ronald Hudson

William J. Kenis, Sr.
Carl L. Monismith
Thomas D. Moreland
Robert G. Packard
William H. Perloff

Robert L. Schiffman
G. Y. Sebastyan
James F. Shook
Ernest B. Wilkins
Nai C. Yang

Department of Economics, Finance and Administration

R. C. Blensly, Chairman
Oregon State University, Corvallis

Kenneth E. Cook
Highway Research Board Staff

COMMITTEE ON HIGHWAY COSTS AND PROGRAMMING
(As of December 31, 1969)

Donald O. Covault, Chairman
Georgia Institute of Technology, Atlanta

Wayne C. Allison
Alvin F. Bastron
Orhan Baycu
V. O. Bradley
Ralph D. Brown, Jr.
J. P. Buckley
B. G. Bullard
S. F. Coffman
Earnest W. Elliott
Benjamin M. Givens, Jr.

A. A. Grant
James O. Granum
Gerald Grauer
Harold W. Hansen
Stearns R. Jenkins
Ralph D. Johnson
Raymond L. Kassel
Samuel L. Lipka
Edwin C. Lokken

Charles H. Moorefield
Willa W. Mylroie
G. A. Riedesel
Robert S. Scott
James R. Turner
Walter G. Wigle
H. S. Wiley
Neil H. Wilson
Reed H. Winslow

Foreword

Two aspects of pavement design theory are presented to researchers and designers in this RECORD. New mechanical models are used to describe states of stress, strain, or deflection under imposed load in the traditional approach to design theory in seven papers. In two papers, systems models are used to show how decision theory can be applied to solution of general design problems.

Experimentally determined deflection factors were compared to calculated factors by Ali, Krizek, and Osterberg for a two-layer elastic system. Calculated factors were determined using Odemark's equivalent thickness theory and Westergaard's theory with dense liquid and with elastic solid lower layers. Deflection factors were determined experimentally from model studies. Conclusions reached were that variations in Poisson's ratio significantly affect the deflection factors and that of the three procedures studied the Odemark theory gave results closest to the laboratory model results.

Rosner and Harr developed a mechanistic model to duplicate behavior of a prototype pavement used for accelerated traffic testing of aircraft landing mat systems. Numerical values for model parameters were obtained from simulation of prototype deflection patterns.

Barksdale offers an incremental nonlinear finite element theory for predicting elastic and cumulative stresses, strains, and deflections in highway pavement systems. He obtained reasonable correspondence between calculated deflections and deflections observed on a laboratory model. He concluded that an important need exists for detailed study of the influence of state of stress on material properties and for developing realistic effective stress-strain laws for the materials used in pavement construction.

Strain and deflection responses of a large-scale flexible pavement model were studied under dynamic and creep load conditions by Drennon and Kenis. Measured values were compared to values calculated using a computer program for moving loads on a viscoelastic layered system. Reasonably good correspondence was found. Of particular significance was the conclusion that response of the system to loads was time-dependent.

A theory was developed by Levey and Barenberg to evaluate the statistical nature of stresses, strains, and deflections in pavements having materials with variable physical characteristics. The method is based on a mathematical discrete element model for a layered pavement system. Results from solutions for typical systems indicate that this type of analysis is needed to establish realistic criteria for quality control during construction.

George investigated the feasibility of using vibration methods in determining elastic properties of pavement layers. The study concluded among other things that the Rayleigh wave velocity and the assumed or experimentally determined value of Poisson's ratio enable one to make a complete analysis of the elastic properties.

An approximate method is presented by Huang for determining stresses in rectangular concrete slabs due to wheel loads. A comparison of contours of principal stresses determined theoretically with loads obtained experimentally in the AASHO Road Test indicates that the pattern of stress distribution is quite similar. A theoretical analysis shows that the most critical stress in pavements with dowelled joints occurs when the load is near the edge at a distance of about 6 ft from the joint.

A framework for the systematic analysis of the decision process involved in many aspects of highway design is presented by Lemer and Moavenzadeh. Their system is designed to maximize performance, described in terms of serviceability, reliability, and maintainability. An attempt is made to show how the model may be used in practice to yield engineered highway facilities having good performance characteristics.

Optimal design in terms of minimum costs is the subject of Hejal, Yoder, and Oppenlander. The total cost of the pavement system is quantitatively described in their design model by an objective function and a minimum cost solution for each combination of material costs and design conditions. Substantial cost savings using the optimal design procedure are claimed.

—James F. Shook

Contents

Influence of Poisson's Ratio on the
Surface Deflection of Layered Systems

GALAL A. ALI, Department of Civil Engineering, Purdue University; and
RAYMOND J. KRIZEK and JORJ O. OSTERBERG,
The Technological Institute, Northwestern University

Three different theories are used to evaluate the influence of variations in
Poisson's ratio on the surface deflection function for two-layered elastic
systems. These theories are shown to be qualitatively inconsistent in ac-
counting for this effect, which may amount to 25 percent or more for cer-
tain combinations of values, and they often yield deflection factors that
differ from one another by over 100 percent for similar conditions. The
practical applicability of the theories is appraised by comparing theoret-
ical results with those obtained from a limited experimental study; this
comparison is most favorable for the equivalent thickness theory.

•EXTENSIVE STUDIES have been undertaken by many investigators to determine the
stresses and deflections in ideal elastic layered systems, and different results have
been obtained to conform with the various assumptions employed. One of the most
controversial assumptions deals with the nature of Poisson's ratio. Three of the most
important questions regarding this parameter are the following: first, does the value
of Poisson's ratio for a given material remain constant as a load history is imposed;
second, what are appropriate values to assume; and third, how do variations in Pois-
son's ratio affect the displacement field? This work is directed toward answering the
last question; the first is arbitrarily answered in the affirmative, and the second is
averted by the nature of the approach. The influence of Poisson's ratio on the deflec-
tion function is studied, and results from different theories are compared with one
another and with laboratory test results.

BACKGROUND

Various Theories

One of the earliest investigations of stresses and displacements in a half-space was
reported by Boussinesq [1]; this solution is for a one-layer system and includes the
assumption that the medium is a two-constant, linearly elastic, homogeneous, iso-
tropic, weightless half-space. The two elastic constants are the modulus of elasticity
and Poisson's ratio. Using the Boussinesq solution in conjunction with the principle
of superposition, many researchers have produced a variety of graphs and tables for
stresses and displacements resulting from specific loading conditions. Many of these
efforts include the assumption that the value of Poisson's ratio is 0.5, that is, the ma-
terial is incompressible.

Over forty years ago, Westergaard [2] suggested a method for computing the stresses
and displacements in concrete pavements; his basic assumptions are that (a) the con-
crete slab is a homogeneous, isotropic, linearly elastic, uniformly thick solid resting
on a dense liquid subgrade of constant modulus; (b) Poisson's ratio for the concrete is
0.15; and (c) the subgrade reactions are vertical and proportional to the slab deflections.
Hogg [3] and Holl [4] independently solved a similar problem with the assumption of an

elastic solid subgrade, and both of the above assumptions for the subgrade were considered in the work of Pickett, Raville, Jones, and McCormick (5).

Assuming an incompressible pavement with no flexural rigidity, Palmer and Barber (6) computed the vertical displacement under a circularly loaded area. The deformation of the pavement was neglected, and a displacement equation similar to that of Boussinesq (1) was derived. By considering displacements at any point along the vertical axis under the center of the loaded area, they concluded that, although the effect of Poisson's ratio is negligible for depths greater than the radius, it is significant near the surface. In a subsequent discussion, Barber (7) improved the above method by considering the rigidity of the pavement; later he further improved this approach by taking the pavement deformation into account.

Using the mathematical theory of elasticity, Burmister (8) presented a complete and exact solution for the displacements in a two-layer elastic system; his solution was based on the following assumptions: (a) both top and bottom layers are homogeneous and isotropic; (b) the top layer is of infinite horizontal extent but of finite vertical thickness; (c) the bottom layer is of infinite horizontal and vertical extent; (d) the two layers are in continuous contact; and (e) Poisson's ratio for both layers is 0.5. Values of the deflection factor are plotted graphically to show the influence of the thickness of the top layer and the ratio of the layer moduli. In another paper, Burmister (9) derived an expression for the total deflection at the surface of a three-layer system.

In extensions to Burmister's work, Fox (10) computed stresses at any point in a two-layer elastic system due to a circularly loaded area, Acum and Fox (11) and Jones (12) determined the stresses in a three-layer elastic system, and Pickett and Ai (13) calculated the stresses in the subgrade under a rigid pavement. In the first three works (10, 11, 12), Poisson's ratio was taken as 0.5 throughout, while in the last study (13) the values of Poisson's ratio for the two materials were varied over a limited range. Schiffman (14) solved the three-layer system for stresses and displacements; he assumed Poisson's ratio to be 0.4 for the first and third layers and 0.2 for the intermediate layer. Complete patterns for the stresses and deformations in two-, three-, four-, and five-layer systems were reported by Mehta and Veletsos (15), and they concluded that the influence of Poisson's ratio on deflection response is not negligible for many cases.

Odemark (16) used the theory of equivalent thickness and solved for the stresses and displacements in a two-layer system for which Poisson's ratio is 0.5 for both layers. This approach consists essentially of replacing the top stiffer layer with an equivalent thickness of the bottom layer material.

Poisson's Ratio

Poisson's ratio is a very difficult mechanical property to determine for most materials; for this reason, and because of the resulting mathematical simplicity, it is often assumed to be 0.5, which is the value for an incompressible material. The assumption of incompressibility has been questioned many times, and there are many documented cases where Poisson's ratio is other than 0.5. The manifest significance of Poisson's ratio on the deflection of layered systems as presented herein lends considerable support to the arguments that (a) the effect of Poisson's ratio may have an appropriate place in pavement design procedures, and (b) improved laboratory methods for determining Poisson's ratio need to be developed.

THEORETICAL ANALYSIS

In order to investigate the effect of variations in Poisson's ratio on the deflection function, expressions will be developed to include as variables the values of Poisson's ratio for the top and bottom layers. Three cases will be considered: (a) the Odemark equivalent thickness theory, (b) the Westergaard theory with a dense liquid bottom layer, and (c) the latter theory for the case where the lower layer is assumed to be an elastic solid. Only the vertical deflection, w, immediately under the center of a uniformly loaded, p, circular area of radius a resting on a two-layer elastic system will
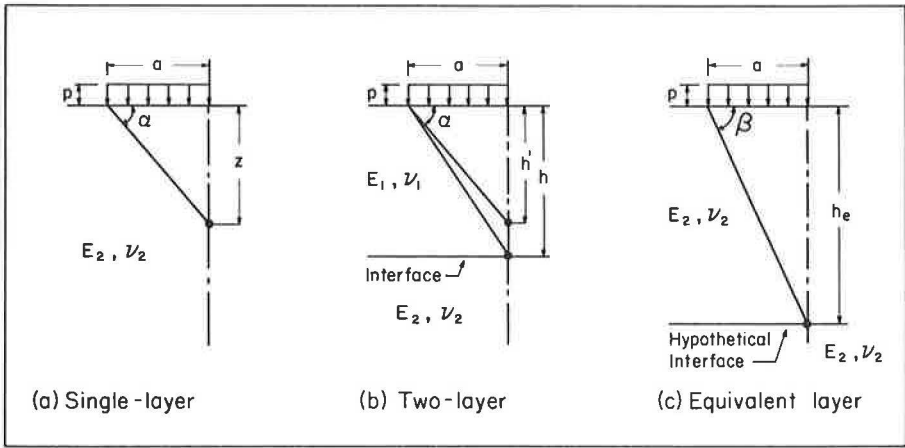
Figure 1. Geometry and notation.

be considered. Both layers are assumed to be homogeneous, isotropic, and of infinite horizontal extent; the top layer is of finite thickness, h, and the bottom layer is infinitely deep. The two layers have moduli of elasticity, E_1 and E_2, and Poisson's ratios, ν_1 and ν_2, respectively; assumed values for the parameters considered will range from 5 to 1,000 for the modular ratio, $E = E_1/E_2$; 0.5 to 3.0 for the thickness ratio, $A = a/h$; and 0 to 0.5 for each of the Poisson's ratios.

Equivalent Thickness Theory

In the equivalent thickness theory, illustrated in Figure 1, the upper layer of thickness h is replaced by an equivalent thickness, h_e, of the lower layer material according to the relationship

$$h_e = h' \left[E \frac{1 - \nu_2^2}{1 - \nu_1^2} \right]^{1/3} = Nh' \tag{1}$$

where h' equals nh and n is a coefficient that will be discussed later; stresses and displacements at the interface are assumed to be the same for the two systems. The total surface deflection, w, under the center of the loaded area for the equivalent layer case illustrated in Figure 1c is

$$w = w_a - w_b + w_c \tag{2}$$

where w_a is the surface deflection under the center of the loaded area for the single layer case illustrated in Figure 1a, w_b is the deflection at a depth h' for the same case, and w_c is the deflection at a depth h_e for the equivalent layer case shown in Figure 1c. The specific equations for these deflections follow the Boussinesq solution and may be written as

$$w_a = \frac{2\,pa}{E_1} (1 - \nu_1^2) \tag{3a}$$

$$w_b = \frac{pa}{E_1} (1 + \nu_1) \left[\cos \alpha + (1 - 2\nu_1) \tan \left(45° - \frac{\alpha}{2} \right) \right] \tag{3b}$$

and

$$w_c = \frac{pa}{E_2} (1 + \nu_2) \left[\cos \beta + (1 - 2\nu_2) \tan \left(45° - \frac{\beta}{2} \right) \right] \tag{3c}$$

$\sqrt{a^2 + z^2}$

$\sqrt{2(a^2 + z^2)}$

$\sqrt{a^2 + z^2}$

$45° - \dfrac{\theta}{2}$

$z = h_e = Nh' = Nnh,$
when $\theta = \beta$
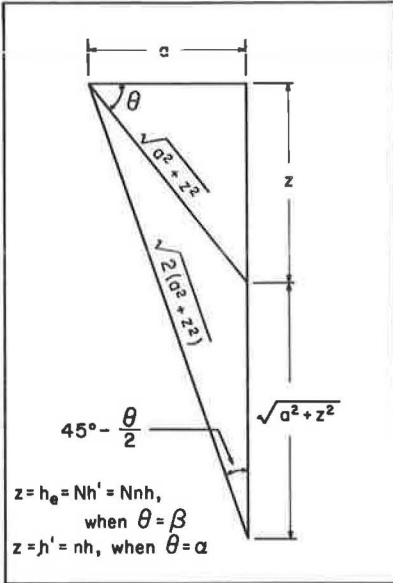$z = h' = nh,$ when $\theta = \alpha$

Figure 2. Schematic diagram for determination of trigonometric relationships.

Substituting Eqs. 1 and 3 into Eq. 2, and using $E = E_1/E_2$, $A = a/h$, and the geometrical relationships shown in Figure 2 for $\cos \alpha$, $\cos \beta$, $\tan (45° - \alpha/2)$, and $\tan (45° - \beta/2)$, we may write

$$F_T = \frac{w\,E_2}{pa} = \frac{2\,(1 - \nu_1^2)}{E}$$

$$- \frac{1 + \nu_1}{E} \left[\frac{A}{\sqrt{A^2 + n^2}} + \frac{(1 - 2\nu_1)\,A}{n + \sqrt{A^2 + n^2}} \right] \quad (4)$$

$$+ (1 + \nu_2) \left[\frac{A}{\sqrt{A^2 + N^2 n^2}} + \frac{(1 - 2\nu_2)\,A}{Nn + \sqrt{A^2 + N^2 n^2}} \right]$$

where F_T is a deflection factor that is a function of E, A, ν_1, and ν_2. For ν_1 and ν_2 equal to 0.5, N becomes $(E)^{1/3}$ and Eq. 4 reduces to the Odemark deflection equation. Although there is some experimental justification that the value for n is unity, Odemark employed it as a corrective factor and assigned it a value of 0.9 in order to make his results agree with those of Burmister; accordingly, a value of 0.9 for n is used in the following calculations. The influence of ν_1 and ν_2 on F_T is shown in Figures 3, 4, and 5 by means of a series of grid plots. Figure 3 shows the functional dependence of F_T on E for a given value of A, whereas Figure 4 indicates the variation of F_T with A for a given E. The type of behavior manifested in Figure 4b, wherein F_T reaches a maximum for a value of ν_1 between 0 and 0.5 and decreases as ν_1 is either increased or decreased, is found in cases where low values for E and high values for A are combined; this pattern is observed only for results calculated by the equivalent thickness theory and not by the subsequent two theories. Figure 5 shows a series of F_T-ν_1-ν_2 plots for arbitrarily selected values of E and A. It is significant to note that, except for cases such as depicted in Figure 4b, F_T increases monotonically as either ν_1 decreases or ν_2 increases; this is in contrast to results calculated by the other two theories.

Westergaard Theory

For an interior concentrated load, P, on a pavement, the Westergaard deflection equation for the vertical surface deflection, w, under the load is given by

$$w = \frac{P}{8\,k_2\,\ell^2} \quad (5)$$

where k_2 is the reaction modulus of the bottom layer and ℓ is the radius of relative stiffness; for the calculations performed herein, P is replaced by $p\pi a^2$. When applying this theory, it is usually assumed that the bottom layer material is either a dense liquid or an elastic solid. The principal difference in the results produced by the two assumptions lies in the expressions for ℓ. For the case of a dense liquid bottom layer, ℓ is given by

$$\ell = \left[\frac{E_1 h^3}{12\,(1 - \nu_1^2)\,k_2} \right]^{1/4} \quad (6)$$

whereas for the case of an elastic solid ℓ becomes

$$\ell = h \left[\frac{E\,(1 - \nu_2^2)}{6\,(1 - \nu_1)} \right]^{1/3} \quad (7)$$

Dense Liquid Bottom Layer—From a form of Eq. 3a and the definition for k_2, it follows that

$$k_2 = \frac{P}{w} = \frac{E_2}{2a\,(1 - \nu_2^2)} \tag{8}$$

Substituting Eqs. 6 and 8 into Eq. 5 and rearranging, we obtain

$$F_L = \frac{w\,E_2}{pa} = \left[\; 3.7\,\frac{A^3}{E}\,(1 - \nu_1^2)\,(1 - \nu_2^2)\right]^{\frac{1}{2}} \tag{9}$$

Typical plots of the deflection factor, F_L, as a function of ν_1 and ν_2 for various values of A and E are shown in Figure 6.

Elastic Solid Bottom Layer—Substituting Eqs. 7 and 8 into Eq. 5 and rearranging, we obtain

$$F_S = \frac{w\,E_2}{pa} = 2.6A^2\,(1 - \nu_2^2)\left[\frac{(1 - \nu_1^2)}{E\,(1 - \nu_2^2)}\right]^{\frac{2}{3}} \tag{10}$$
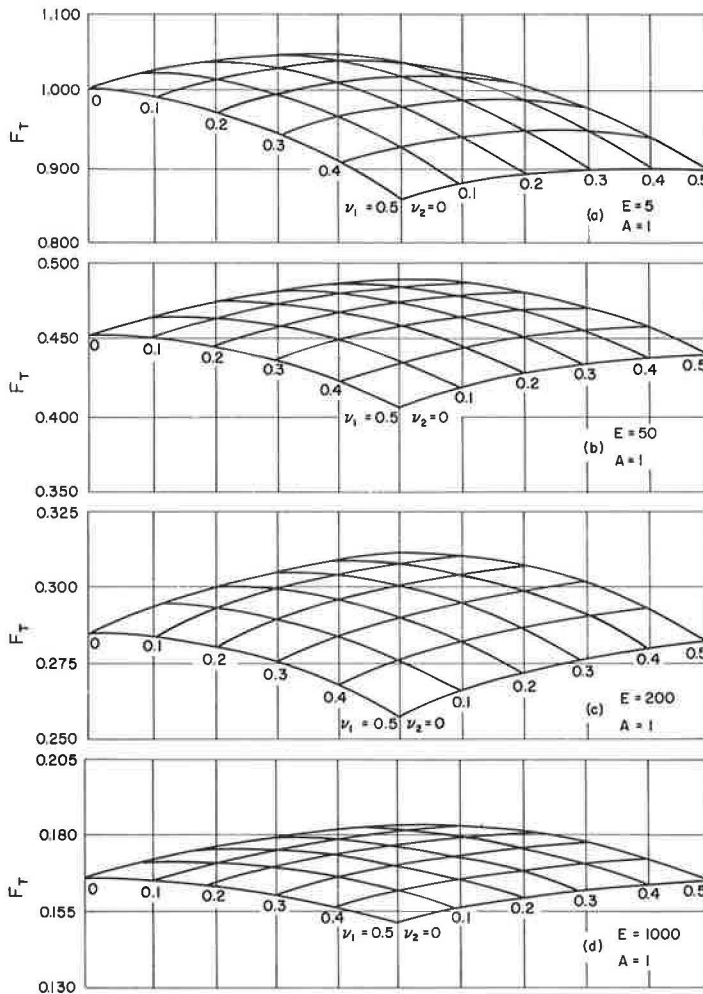

Figure 3. Typical plots of F_T-ν_1-ν_2 relationship for constant thickness ratio.
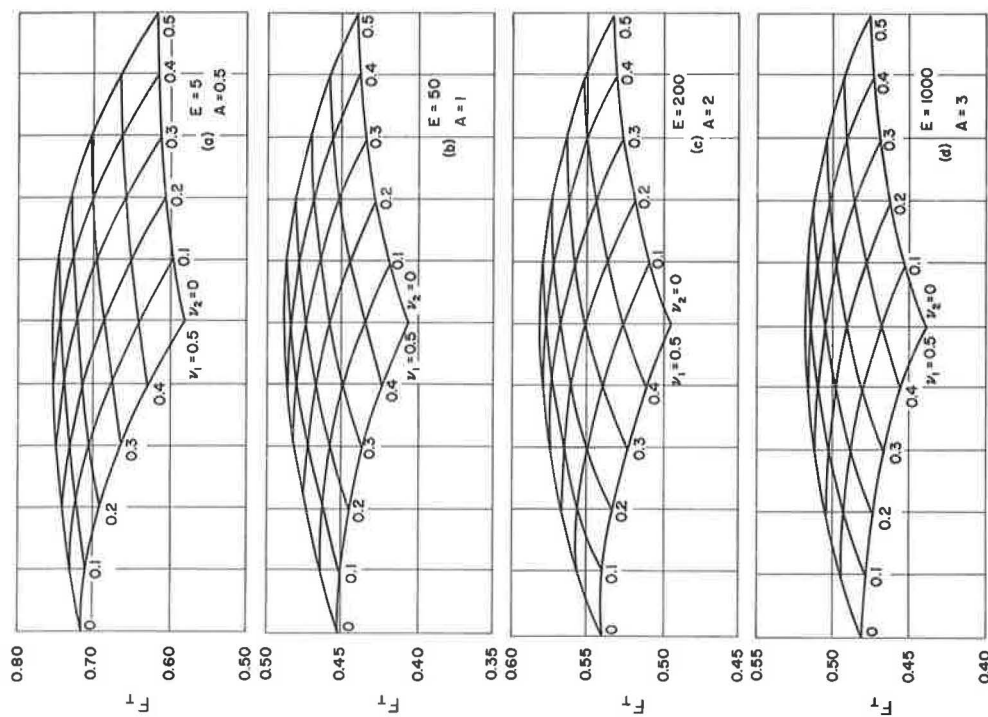
Figure 5. Typical plots of F_T-ν_1-ν_2 relationship for various values of A and E.

Figure 4. Typical plots of F_T-ν_1-ν_2 relationship for constant modular ratio.

7

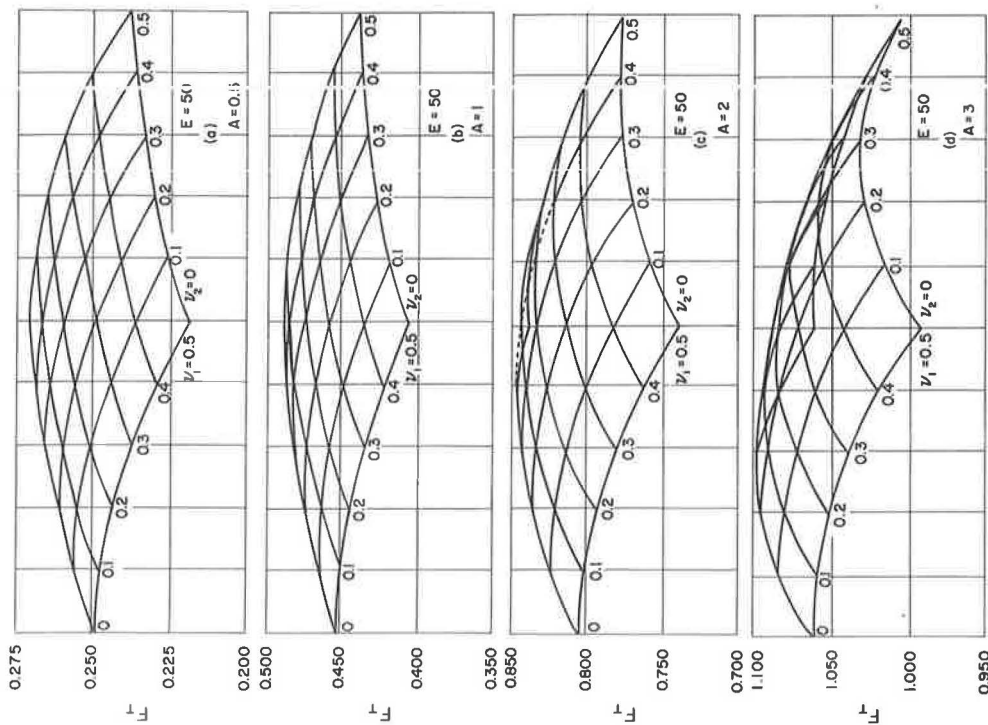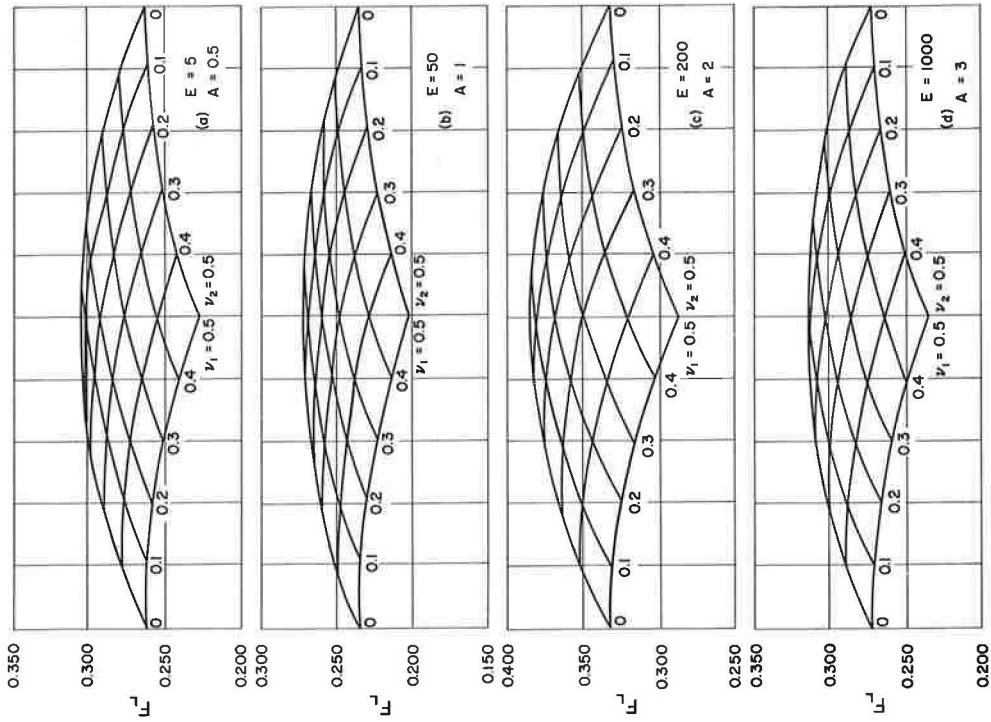Figure 7. Typical plots of F_S-ν_1-ν_2 relationship for various values of A and E.
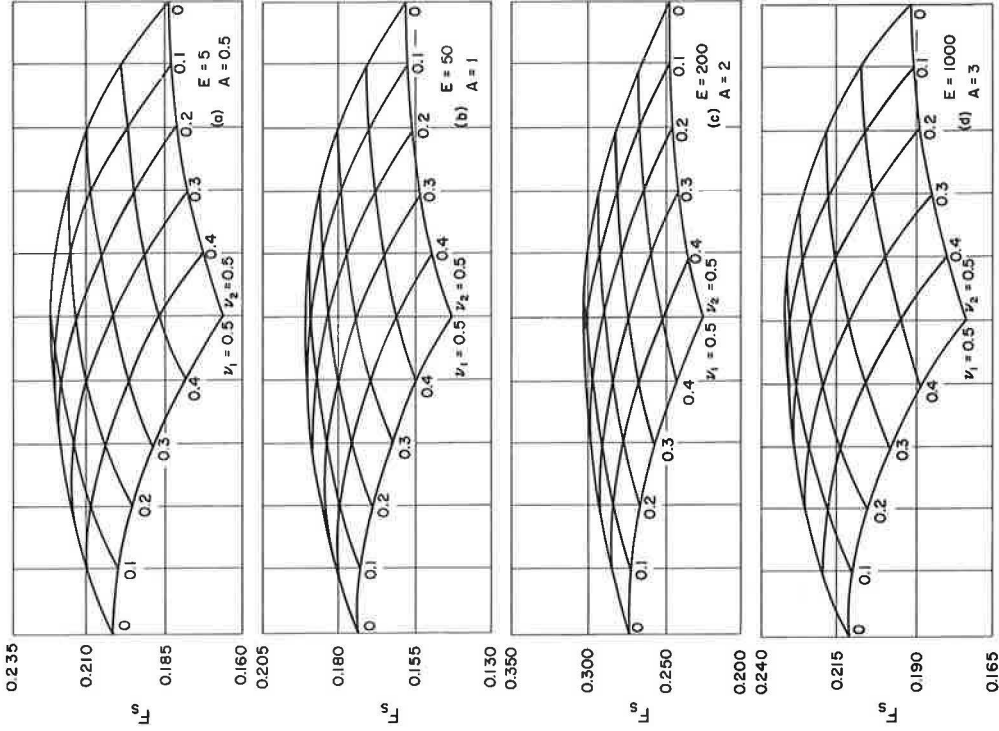

Figure 6. Typical plots of F_L-ν_1-ν_2 relationship for various values of A and E.

Typical plots of the deflection factor, F_S, as a function of ν_1 and ν_2 for various values of A and E are shown in Figure 7.

Comparison of Theories

Comparison of deflection factors obtained by each of the three approaches described is shown in Figure 8 for several arbitrarily chosen cases. Since the results of the equivalent layer theory are essentially in agreement with those of Burmister, the latter results are indirectly included in the comparison.

EXPERIMENTAL RESULTS

Description of Test Procedure

Model plate load tests were conducted on a two-layer system consisting of a lucite top layer and a polyester resin bottom layer. The top layer was 15 in. square and had thicknesses of 0.50, 0.75, and 1.00 in.; the bottom layer was 24 in. square and 6 in. thick. The system was loaded by means of rigid circular plates with radii of 0.50, 1.00, and 1.50 in.; in addition, a plate with a 0.25-in. radius was used for the system that had the 0.50-in. top layer. Loads were applied in increments of 100 lb up to a maximum of 600 lb by a Southwark hydraulic testing machine, and magnitudes were read to the nearest 0.5 lb. Six dial gages placed diagonally at a center-to-center spacing of 2.5 in. were used to measure the vertical deflection.

Test Results

The elastic properties of each material were determined by use of conventional testing procedures and found to
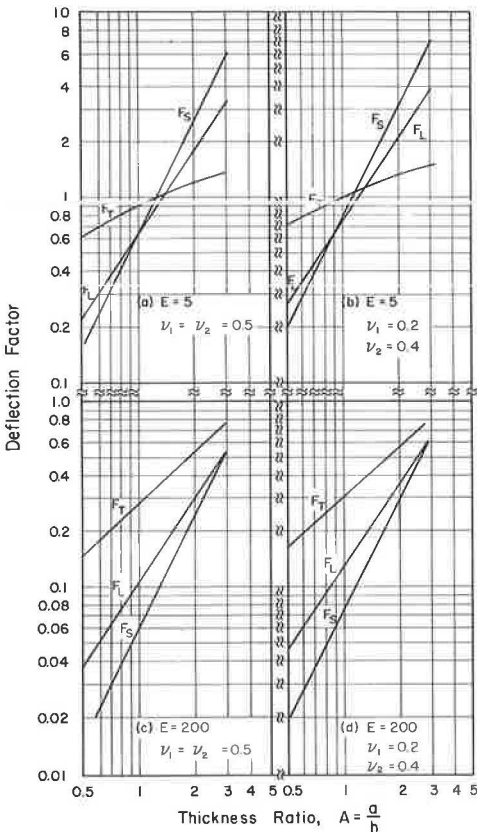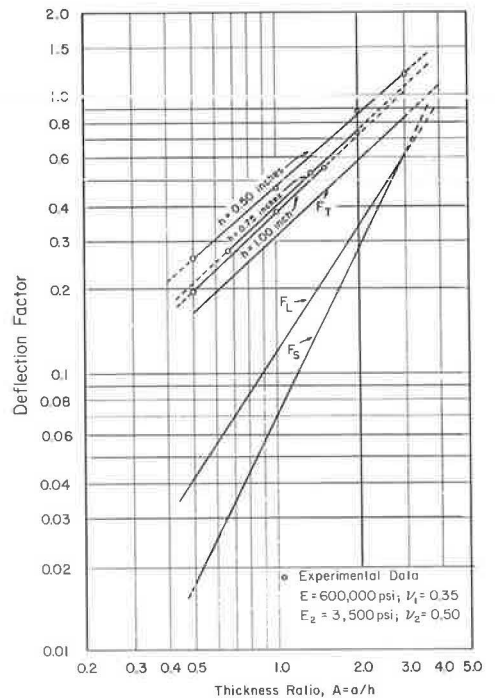

Figure 8. Comparison of theories.

Figure 9. Comparison of theoretical deflection factors with test values.

be E_1 = 600,000 psi and ν_1 = 0.35 for the lucite top layer and E_2 = 3,500 psi and ν_2 = 0.50 for the polyester resin bottom layer; hence, the modular ratio, E, is 170. Experimental deflection factors were calculated from the measured data by use of the equation $F_T = w\, E_2/pa$, where p is approximated by $P/\pi a^2$; Figure 9 shows a plot of these experimental deflection factors together with the theoretical ones calculated by the procedures described. Although the experimental deflection factors are higher than those predicted by any of the theories, they are most closely approximated by the equivalent thickness theory, which, in turn, is in close agreement with the Burmister theory. The assumption of 0.5 instead of 0.35 for Poisson's ratio of the top layer would increase the deviation between theoretical and experimental results. The apparent dependence of the experimental deflection factor values on h is not accounted for by any of the theories. It should be noted, however, that the discrepancy between theory and experiment may be caused by other differences between the idealized and practical experimental test conditions, and it would be unwise to draw more than a qualitative conclusion from the limited data presented. In addition, for many materials there is the distinct probability that Poisson's ratio, as well as other material properties, may vary during the load history.

CONCLUSIONS

Based on the limited theoretical and experimental study presented herein for a two-layer elastic system, the following conclusions can be drawn:

1. Variations in Poisson's ratio significantly affect deflection factors for many practical situations.

2. Values of the deflection factor calculated from the equivalent thickness theory generally decreased with increases in Poisson's ratio for the top layer, but they increased with increases in Poisson's ratio for the bottom layer.

3. For the Westergaard theory with either a dense liquid or elastic solid bottom layer, values for the deflection factor decreased with increases in Poisson's ratio for either the top or bottom layer.

4. The influence of variations in Poisson's ratio on the deflection function depends on the modular ratio and the thickness ratio; for high values of the latter, the influence is not as great as for lower values.

5. Discrepancies exist between deflection factors obtained from laboratory tests and those calculated from the various theories; however, the laboratory results compare most favorably with those determined from the equivalent thickness theory. Although a quantitative evaluation of these discrepancies is not possible herein, it is entirely conceivable that they may result from the over-idealized assumptions on which the theories are based, since these assumptions are seldom satisfied in practical situations.

ACKNOWLEDGMENT

REFERENCES

1. Boussinesq, J. V. Application des potentiels a l'étude de l'équilibre et du mouvement des solides élastiques. Gauthier-Villars, Paris, 1885.
2. Westergaard, H. M. Computation of Stresses in Concrete Roads. HRB Proc., Vol. 5, pp. 90-112, 1925.
3. Hogg, A. H. A. Equilibrium of a Thin Plate, Symmetrically Loaded, Resting on an Elastic Foundation of Infinite Depth. Philosophical Magazine, Series 7, Vol. 25, pp. 576-582, 1938.
4. Holl, D. L. Thin Plates on Elastic Foundation. Wiley and Sons, New York, pp. 71-74, 1939.

5. Pickett, G., Raville, M. E., Jones, W. C., and McCormick, F. J. Deflections, Moments and Reactive Pressures for Concrete Pavements. Bull. No. 65, Engineering Experiment Station, Kansas State College, 1951.

6. Palmer, L. A., and Barber, E. S. Soil Displacement Under a Loaded Circular Area. HRB Proc., Vol. 20, pp. 279-286, 1940.

7. Barber, E. S. Discussion on Flexible Surfaces. HRB Proc., Vol. 20, pp. 330-331, 1940.

8. Burmister, D. M. The Theory of Stresses and Displacements in Layered Systems and Applications to the Design of Airport Runways. HRB Proc., Vol. 23, pp. 126-148, 1943.

9. Burmister, D. M. The General Theory of Stresses and Displacements in Layered Systems. Jour. Appl. Phys., Vol. 16, pp. 89-94, 126-187, 296-302, 1945.

10. Fox, L. Computation of Traffic Stresses in a Simple Road Structure. Proc. Second Internat. Conf. on Soil Mech. and Found. Eng., Rotterdam, Vol. 2, pp. 236-246, 1948.

11. Acum, W. E. A., and Fox, L. Computation of Load Stresses in a Three-Layer Elastic System. Geotechnique, Vol. 2, No. 4, pp. 293-300, 1951.

12. Jones, A. Tables of Stresses in Three-Layer Elastic Systems. HRB Bull. 342, pp. 176-214, 1962.

13. Pickett, G., and Ai, D. K. Y. Stresses in Subgrade Under Rigid Pavement. HRB Proc., Vol. 33, pp. 121-129, 1954.

14. Schiffman, R. L. The Numerical Solution for Stresses and Displacements in a Three-Layer Soil System. Proc. Fourth Internat. Conf. on Soil Mech. and Found. Eng., London, Vol. 2, pp. 169-173, 1957.

15. Mehta, M. R., and Veletsos, A. Stresses and Displacements in Layered Systems. Structural Research Series, No. 178, Civil Engineering Studies, Univ. of Illinois, 1959.

16. Odemark, N. Investigations as to the Elastic Properties of Soils and Design of Pavements According to the Theory of Elasticity. Statens Vaginstitut, Stockholm, 1949.

Identification of Subgrade Characteristics
From Prototype Testing of Landing Mats

JOHN C. ROSNER, Department of Civil Engineering, Arizona State University; and
MILTON E. HARR, Department of Civil Engineering, Purdue University

•SURFACE MATERIALS distribute wheel loads to the subgrade in a complicated manner, and the exact mechanism through which distribution is accomplished has not been defined. The consensus is, however, that the surface materials distribute loads in a manner similar to that of a beam or flat plate (1, 6, 10). Regardless of the load transfer mechanism chosen or the sophistication attached thereto, characterization of the subgrade is made presently from indicators (properties) obtained from selected samples imposed to artificial stress conditions. These indicators are then employed with design charts and/or formulas, which have been judiciously tempered by experience, to estimate the life of a pavement system.

Present design procedures have merit as long as the proposed traffic loading and subgrade conditions can be related adequately to past experience. However, application of these pavement design procedures to future traffic demands may prove unsatisfactory, and hence other design approaches should be sought to accommodate future needs. The hypothesis is forwarded in this paper that such developments are consequent upon the mechanistic modeling of pavements to reflect their behavior as demonstrated in prototype tests.

Mechanistic simulation of prototype tests provides a means whereby the system parameters can be determined from the pavement behavior under actual stress conditions. In addition, such an approach permits investigation of the pavement system at times other than failure.

DESCRIPTION OF PROTOTYPE TESTS

In 1966, accelerated traffic tests simulating aircraft taxiing operations were conducted by the Corps of Engineers (4) on test sections surfaced with landing mats. Numerous combinations of wheel configurations, loads, tire pressures, and subgrade strength were investigated. The wheel configuration varied from that of a single wheel up to a combination of 12 wheels; loadings varied from 35,000 to 273,000 lb; and tire pressures ranged from 50 to 250 psi. Two soils were used as subgrade materials. One soil was a "fat clay (CH)" with a liquid limit of 58 and a plasticity index of 31, while the other soil was a "fat clay (CH)" with a liquid limit of 61 and a plasticity index of 37. The in-place, initial strength of these subgrades as indicated by CBR values ranged from 1.1 to 9.0.

The tests were made on the modified T11 mat (designated herein as Item 1), which is a lightweight, extruded aluminum panel with an abrasive surface, and on the M8 mat (Item 2), which is a heavy deep-ribbed steel mat. The moment of inertia per foot of width of these two mats is 1.368 in.^4 and 0.618 in.^4 respectively. Both mats were placed on the subgrade in a masonry type of arrangement, as shown in Figure 1.

The behavioral characteristics and performance of the mat surfaces, whether loaded or unloaded, are well documented in the Corps of Engineers' publication (4) for each test at the various coverage levels. The data, single-wheel and dual-wheel, from this series constitute the basis of the investigation reported herein.

MECHANISTIC ANALYSIS

Model Development

A mechanistic model was sought whose deflection behavior reflected the action of observed landing mats. Initial consideration was given to the selection of a representative structural load transfer element. Following earlier findings of the Corps of Engineers (2), a membrane and thin plate were quickly eliminated as possibilities.

Figure 1. Arrangement of mat elements within the traffic lane.

A beam of infinite length was selected as the mechanistic equivalent of the mat. This selection was predicated on several prevailing conditions. First, actual field operations and test procedures employed by the Corps of Engineers (4) demonstrated that the mat elements extend laterally for an appreciable distance outside the normal traffic lane. Second, the transverse joints in the mat surface (necessitated by the construction procedure) provided virtually no moment transfer from one row of mats to the next (Fig. 1). Also, tests (2) on the M8 mat indicated that the transverse rigidity was approximately 150 times larger than the longitudinal rigidity.

A second approximation was necessary to "idealize" the soil media. Because prototype tests (4) indicated that the "average deflection" increased with the number of coverages, a conventional elastic solid model was not thought to be directly applicable. The observed behavioral characteristic was accommodated by employing a "quasi-elastic" model wherein parameters are permitted to be coverage-dependent.

The width of the infinite beam was taken as the length of a rectangle whose area was equivalent to the tire print area and whose width was equal to the maximum width of the tire print.

In addition, the following assumptions were made:

1. The end joint connections provide total shear and moment transfer between mat elements;
2. The wheel loads can be represented by uniformly distributed loads;
3. The beam obeys Eulerian conditions regardless of the stress level;
4. The beam and the soil always remain in contact; and
5. Horizontal displacements within the soil media are negligible.

The validity of the assumption of complete moment transfer was investigated by Rosner (8). Results indicated that the effectiveness of the end joint connections was approximately only 10 to 15 percent less than that of the mat elements.

Mat-soil parameters were established by analytical simulation of the prototype test data. This was achieved through a modification of the general variational method of analysis developed by Vlasov and Leont'ev (9).

Imposing the foregoing assumptions, the response of the mat-soil model was expressed as

$$\frac{d^4 V(\eta)}{d\eta^4} - 2r^2 \frac{d^2 V(\eta)}{d\eta^2} + s^4 V(\eta) = \frac{p(x)L^4}{EI} \qquad (1)$$

where

$$r^2 = \frac{tL^2}{EI} = \frac{1 - \mu_0}{2L} \int_0^H \Psi^2 dy \qquad (2)$$
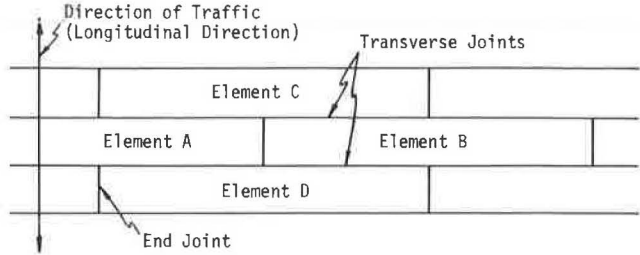
$$s^4 = \frac{kL^4}{EI} = 2L \int_0^H \left[\frac{d\Psi(y)}{dy} \right]^2 dy \tag{3}$$

and

$$L = \sqrt[3]{\frac{2EI(1 - \mu_0^2)}{E_0\delta}} \tag{4}$$

and where

> E is the modulus of elasticity of the beam (mat),
> E_0 is the modulus of elasticity of the soil,
> H is the thickness of the soil layer,
> I is the moment of inertia of the beam,
> k is a foundation modulus that determines the compressive strains in the foundation,
> L is an elastic characteristic of the model,
> $p(x)$ is a uniform loading function,
> t is a foundation modulus that determines the shearing strains in the foundation,
> $V(\eta)$ is the generalized deflection,
> δ is the width of the beam,
> μ_0 is Poisson's ratio of the soil, and
> $\Psi(y)$ is a function representing the distribution of displacement with depth (y).

It should be noted that Eq. 1 differs significantly from the governing relationship for an infinite beam on a Winkler foundation. The third term on the left-hand side of Eq. 1 arises from consideration of the normal strains within the soil; the coefficient on this term is analogous to the Winkler spring constant. The second term of Eq. 1 accounts for the presence of shearing strains within the soil; this term does not appear in the Winkler model. The coefficients for these two terms can be related to the distribution of displacement with depth as shown in Eqs. 2 and 3.

Tests conducted by the Corps of Engineers (2) indicated an asymptotic attenuation of displacements with depth. Functional representation of this type of displacements may take many forms. One convenient form, suggested by Vlasov and Leont'ev (9), assumes a ratio of hyperbolic functions as

$$\Psi(y) = \frac{\sinh \gamma \left(\frac{H - y}{L} \right)}{\sinh \frac{\gamma H}{L}} \tag{5}$$

where y is the distance from the subgrade surface and γ is a dimensionless parameter that reflects the rate of attenuation of displacement with depth.

With the distribution of displacements described by Eq. 5, the stresses can be expressed as

$$\sigma_y = \frac{E_0}{1 - \mu_0^2} V(x) \frac{d\Psi(y)}{dy} \tag{6}$$

and

$$\tau_{xy} = \frac{E_0}{2(1 + \mu_0)} \frac{dV}{dx} (x)\Psi(y) \tag{7}$$

A representation of the distribution of the above stresses on a vertical section through the soil mass is given in Figure 2.

With the form of $\Psi(y)$ taken as in Eq. 5, any variation in the rate of attenuation of the displacement can be incorporated by judicious selection of the parameter γ (Fig. 3). The value of γ could not be established directly from any previous studies. Hence, a simulation procedure was evolved that could yield reasonable measures of this parameter from the "average deflection" patterns.

For simplicity it was assumed that the soil media ex-

Figure 2. Distribution of stresses with depth.

tended to infinite depth. Under this assumption, the model characteristics k and t in Eqs. 2 and 3 become

$$k = \frac{E_0 \delta}{2(1 - \mu_0^2)} \frac{\gamma}{L} \tag{8}$$

$$t = \frac{E_0 \delta}{8(1 + \mu_0)} \frac{L}{\gamma} \tag{9}$$

Parameter Indentification

The model characteristics k and t (Eqs. 8 and 9 are functions of γ in addition to the conventional elastic constants, E_0 and μ_0. Previous studies of beams on elastic foundations indicated that variation of μ_0 generally has a negligible effect on resulting deflection patterns. In this study μ_0 is assigned a value of 0.4 as had previously been suggested by Pickett (6, 7). Any error introduced by this assumption can be compensated for by the remaining parameters $\overline{E}_0$ and γ as they are identified in the simulated procedure.

Loads were imposed on the developed mat-soil model similar to those of the prototype tests. The "steep descent" method (5) was employed for the identification of the model parameters. The criterion imposed was to minimize an error functional (the sum of the square of the differences between the actual deflection and the model deflection of at least 9 discrete points).
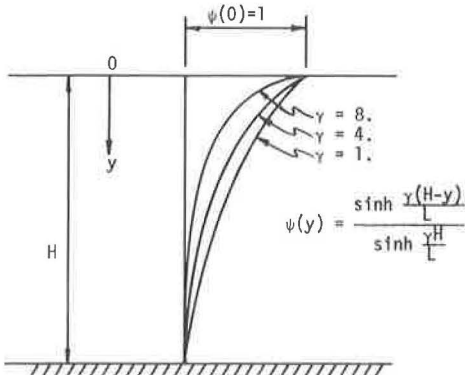
Figure 3. Distribution of displacement with depth.

The foregoing procedure was applied initially to data gathered from the Corps of Engineers' test designated as section 1, lane 2, item 1, for zero coverages. The initial values assumed for E_0 and γ were 100 psi and 1.55 respectively. A minimum of the error functional of 0.060 was achieved when $E_0 = 750$ psi and $\gamma = 1.598$; this is indicated as trial 1 in Figure 4. To determine whether the minimum obtained was global rather than local, another trial was performed. Trial 2 (Fig. 4), which was initiated with $E_0 = 200$ psi and $\gamma = 6.00$, produced a minimum of 0.079 when $E_0 = 280$ psi and $\gamma = 6.006$. From these results it was apparent that the surface of the error functional was definitely not bowl-like in form. Additional trials were made as indicated in Figure 4. As can be seen from the figure, the error functional possessed a curved

Figure 4. Behavior of error functional (section 1, lane 2, item 1).

valley of minimal values that for all practical purposes could be considered identical.

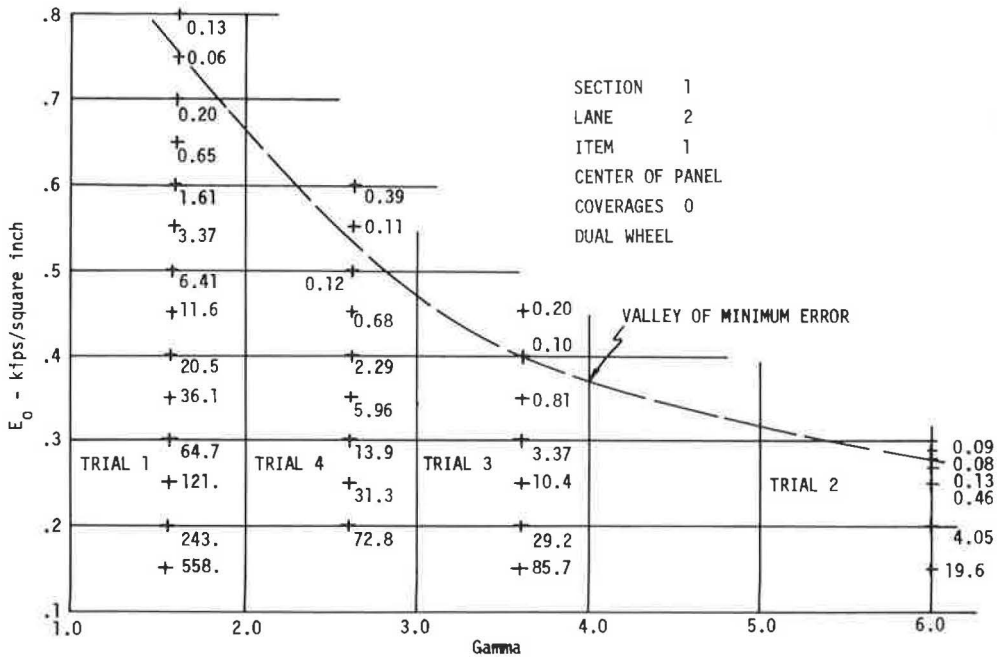It was apparent that unique values of E_0 and γ could not be obtained with the selected form of the error functional. Fortunately, as can be seen in Table 1, the values of the parameter k varied only slightly along the valley of the error functional. This behavior was found to be general (8), and hence representative values of the characteristic k were generated.

Since the line of steepest descent for all trials (Fig. 4) was essentially parallel to the E_0 axis, a modification was incorporated into the identification procedure. Values of 1.0, 2.5, 4.0, 5.5, 7.0, and 8.5 were assigned to the parameter γ and for each of these values E_0 was incremented until the error functional was minimized. This procedure was subsequently employed for the determination of the parameter k for all relevant test sections and at all coverage levels.

Because of the insensitivity of the error functional to large change in γ, it was concluded that the developed procedure was not satisfactory. Preliminary studies (Fig. 5) indicated that the magnitude of the computed deflections was not sensitive to changes in γ. However, as γ increased, deflections in the near vicinity of the loads did become larger and attenuated more rapidly with lateral distance than the observed pattern. This seemed to indicate that the value of γ was related to the rigidity of the mat; that is, the more flexible the mat, the larger the deflection under the load and the more rapid the return to the undeflected position.

The parameter γ was established by a trial-and-error procedure using generated computer model deflections. The value of k (previously and independently determined) was held constant for each coverage level while different values were assigned to γ. The "correct" value of γ was established

TABLE 1

VALUES OF k ALONG THE VALLEY OF
THE ERROR FUNCTIONAL

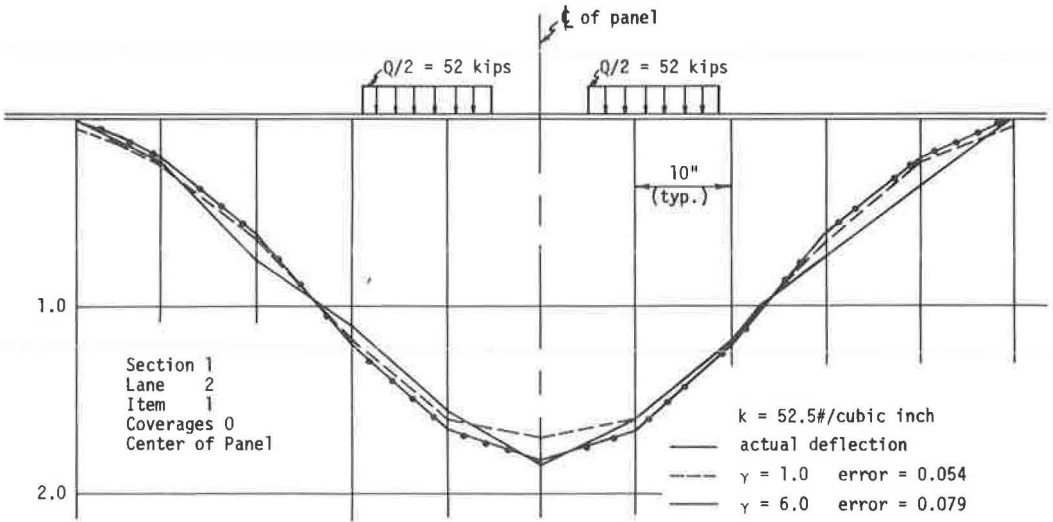| Section 1 E_0	Lane 2 γ	Item 1 Error	Zero Coverage k
750 psi	1.598	0.060	52.5 pci
530 psi	2.620	0.095	52.4 pci
400 psi	3.608	0.100	51.0 pci
280 psi	6.006	0.079	52.8 pci

Figure 5. Influence of the parameter γ on the deflection pattern.

by comparing the computed model deflection configuration to the prototype deflection pattern. After the parameter γ had been established, slight modifications were made in the initial value of the parameter k to improve the correspondence between deflection patterns. This procedure was followed in all subsequent cases to obtain measures of both γ and k values.

RESULTS

Values of the parameters γ, E_0, k, and the error functional for two typical test sections are given in Table 2. Displaying the magnitude of k against the number of coverages (Fig. 6) it can be observed that, in general, the magnitude of the parameter k decreases with coverage. Similar behavior was also observed for the dual-wheel tests (8).

It was found that the magnitude of k at any coverage level could be established as a function of the initial value. This relationship was established empirically as

$$k_N = \frac{k_{INT}}{N^{0.0485}} \tag{10}$$

where k_{INT} is the k value at zero coverage and k_N is the k value after N number of coverages. The value of k_{INT} was found to correlate with several standard soil properties: water content, dry density, and CBR (obtained at the test site). It was found for the prototype tests that k_{INT} could be established from the relationship

$$k_{INT} = 164.0 + 3.0 \, CBR - 5.4w \, \gamma_d \tag{11}$$

where CBR is the average CBR for the upper 18 in. of subgrade and w γ_d is in pounds per cubic foot.

Observations of the "average deflection" patterns of the prototype tests indicate that the curvature, in general, increased with increasing number of coverages. The identification procedure demonstrated that the value of γ also increased with coverages and

TABLE 2

COMPARISON OF THE VARIABILITY OF THE CHARACTERISTIC k

| γ	E_O, psi	k, pci	Error	E_O, psi	k, pci	Error
		Section 2	Lane 3	Item 1		
		Coverage zero			Coverage 600	
1.0	800	36	0.139	680	29	0.040
2.5	420	38	0.108	350	30	0.043
4.0	290	37	0.105	250	30	0.043
5.5	230	37	0.103	200	31	0.044
7.0	190	37	0.104	170	32	0.050
8.5	170	38	0.102	150	32	0.061
		Section 9	Lane 21	Item 2		
		Coverage zero			Coverage 20	
1.0	540	25	0.080	510	24	0.064
2.5	280	26	0.058	270	25	0.045
4.0	200	27	0.055	190	25	0.043
5.5	160	27	0.054	160	28	0.051
7.0	140	29	0.058	130	27	0.041
8.5	120	29	0.053	110	26	0.052
		Section 9	Lane 21	Item 2		
		Coverage 200			Coverage 300	
1.0	480	22	0.626	460	21	0.166
2.5	250	23	0.528	240	22	0.128
4.0	180	24	0.510	170	22	0.126
5.5	160	28	0.597	160	28	0.365
7.0	120	24	0.509	120	24	0.127
8.5	110	26	0.500	110	26	0.182
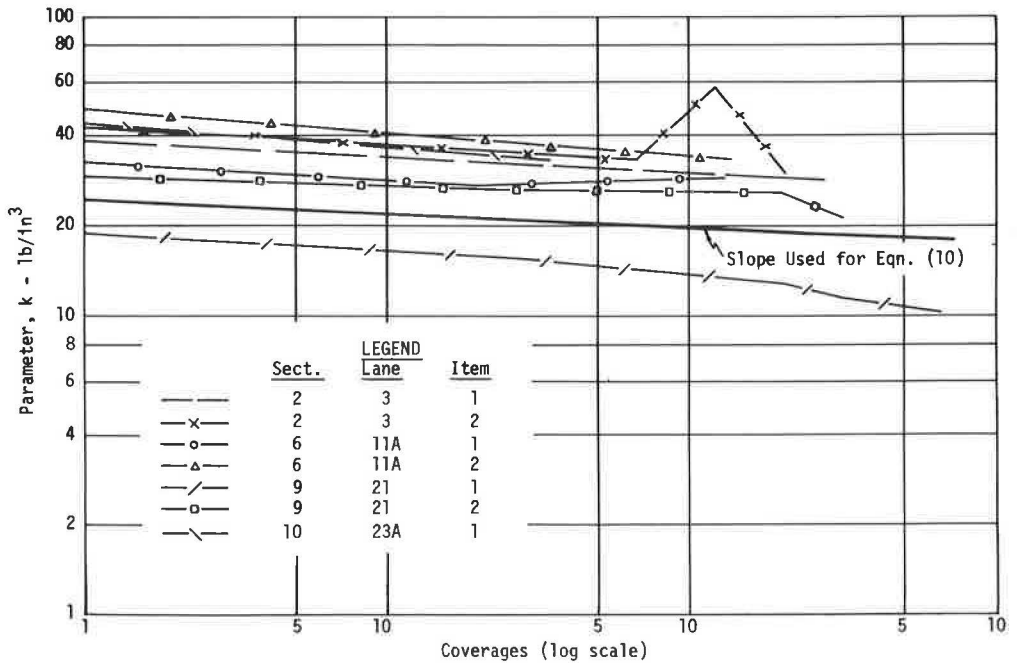
Figure 6. Variation of parameter k with coverage for single-wheel tests.

TABLE 3

COMPARISON OF DEFLECTION PATTERNS

Distance (in.)	Actual Deflection (in.)	Estimated Deflection (in.)	Distance (in.)	Actual Deflection (in.)	Estimated Deflection (in.)
		Section 2	Lane 3	Item 1	
		$k_{INT} = 35.5$ pci	$\gamma_{INT} = 1.00$		
	Zero Coverages - Error = 0.139			600 Coverages - Error = 0.164	
99	0.10	0.20	90	0.00	0.09
102	0.15	0.26	102	0.42	0.38
105	0.19	0.33	112	0.71	0.76
112	0.41	0.54	120	1.00	1.11
117	0.59	0.71	132	1.19	1.41
122	0.88	0.87	142	0.96	1.19
129	1.20	1.03	146	0.88	1.03
132	1.17	1.04	152	0.71	0.77
142	0.82	0.87	162	0.38	0.38
152	0.61	0.54	174	0.00	0.09
162	0.27	0.26			
170	0.00	0.11			
		Section 9	Lane 21	Item 2	
		$k_{INT} = 25.5$ pci	$\gamma_{INT} = 1.75$		
	Zero Coverages - Error = 0.063			300 Coverages - Error = 0.149	
108	0.00	0.12	108	0.00	0.18
114	0.20	0.24	114	0.28	0.36
124	0.55	0.56	120	0.57	0.58
134	0.90	0.93	124	0.59	0.75
144	1.15	1.11	132	1.00	1.12
154	1.00	0.93	134	1.15	1.20
164	0.70	0.56	144	1.32	1.41
174	0.20	0.24	154	1.27	1.20
179	0.00	0.14	160	1.00	0.94
			164	0.80	0.76
			174	0.32	0.36
			179	0.00	0.21

TABLE 4

COMPARISON OF SIMULATED TO CALCULATED VALUES OF k_{INT}

| Section	Test Lane	Item	k, pci		Section	Test Lane	Item	k, pci	
			Simulated	Calculated				Calculated	Calculated
1	1	1	48.5	59.3	6	12	2	36.0	36.7
1	2	1	50.5	66.1	9	21	1	14.0	11.9
2	3	1	35.5	18.5	9	21	2	25.5	20.2
2	3	2	41.0	35.1	9	22	1	10.0	11.2
2	4	1	19.0	15.9	9	22	2	16.0	13.5
2	4	2	31.5	38.3	10	23A	1	37.5	27.1
3	5	1	16.0	17.0	10	23A	2	27.5	31.7
3	5	2	21.0	32.7	10	23B	1	32.5	27.1
3	6	1	12.5	20.4	13	28	1	11.0	11.6
3	6	2	18.0	29.2	13	28	2	25.0	25.3
6	11	1	34.0	20.6	13	29	1	18.0	11.7
6	11	2	50.5	41.8	13	29	2	28.0	24.2
6	12	1	22.0	29.4					
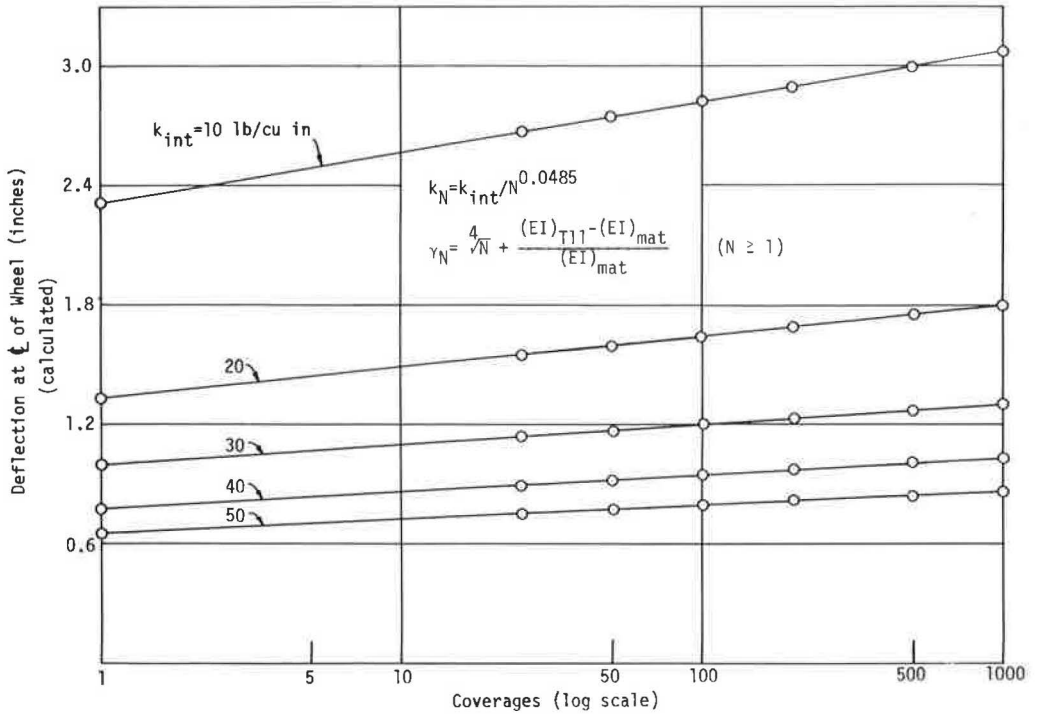
Figure 7. Influence of k_{INT} on maximum deflection.

became slightly larger with decreasing mat rigidity. The relationship for γ_N was established as

$$\gamma_N = \sqrt[4]{N} + \frac{(EI)_{T11} - (EI)_{MAT}}{(EI)_{MAT}} \quad (N \geq 1) \tag{12}$$

where N is the specific number of coverages, $(EI)_{T11}$ is the rigidity per foot of width of the T11 aluminum mat, and $(EI)_{MAT}$ is the rigidity per foot of width of the mat being investigated.

With the parameters k_{INT} and γ_N defined, the system characteristic t may be found from Eqs. 8 and 9. Some typical computed deflection patterns obtained using Eqs. 10 and 12 are given in Table 3. Some observed deflection patterns are also given.

In Table 4 are given values of k_{INT} obtained from the identification procedure and from Eq. 11. It is noted that the largest discrepancies occur for those sections where the simulated values were high. From Figure 7, it can be observed that small variations in the subgrade strength, as reflected by the subgrade modulus, have appreciable influence on the deflection characteristics of the load transfer element.

SUMMARY AND DISCUSSION

The model characteristics k and t (Eqs. 8 and 9), are functions of γ in addition to the conventional E_0 and μ_0 parameters. The "steep descent" method used for identification failed to produce unique values of the parameters E_0 and γ (Fig. 4). However, the error functional was found to possess a valley of minimums along which the value of the characteristic k was found to be essentially constant.

The simulation of the "average deflection" patterns (Table 2) indicated that the value of the model parameter k increased slightly with increases in γ. For a specific value of γ (as shown in Table 2) the magnitude of k was found to decrease with the number of coverages. Computations indicated that the magnitude of k was more sensitive to the number of coverages than to the value of the parameter γ. The validity of the developed expression for k_N (Eq. 10) is demonstrated in Table 2 and Figure 6.

As noted in Figure 5, variations in the parameter γ were reflected primarily as alterations of the deflection pattern curvature. The representative value of γ was established from the similarity of model deflection curvature for various values of γ with prototype deflection curvature. From this comparison it was noted that the curvature, and thus γ, increased with coverages and decreased with increasing mat rigidity. This behavior is expressed by Eq. 12.

The simulated values of the characteristic k at zero coverages were in all cases less than 53 pci. In this range, the model deflections were found to be quite sensitive to the magnitude of k_{INT} (Fig. 7).

CONCLUSIONS

On the basis of assumptions made herein, the following conclusions appear warranted:

1. A mechanistic model can be developed that is capable of duplicating the behavior of prototype landing mat systems under static loads.

2. Numerical values for parameters entering the model can be obtained from simulation of prototype deflection patterns.

3. Model parameters can be correlated with established soil properties.

4. Contrary to prevailing opinion, the subgrade modulus (k) decreased as trafficking progressed and the associated model behavior is extremely sensitive to the magnitude of the subgrade modulus.

ACKNOWLEDGMENT

REFERENCES

1. Burmister, D. M. Theory of Stresses and Displacements in Layered Systems and Applications to the Design of Airport Runways. HRB Proc., Vol. 23, 1943, pp. 126-144.
2. U.S. Army Corps of Engineers. Theoretical Landing Mat Studies. Tech. Memorandum No. 3-418, Waterways Experiment Station, Vicksburg, Miss., Oct. 1955.
3. U.S. Army Corps of Engineers. Engineering Tests of Experimental T11 Aluminum Airplane Landing Mat. Tech. Report No. 3-634, Waterways Experiment Station, Vicksburg, Miss., Sept. 1963.
4. U.S. Army Corps of Engineers. Aircraft Ground-Floatation Investigation. Tech. Documentary Report AFFDL-TDR-66-43, Parts I, II, III, IV, V, VII, X, XI, and XIII. Air Force Flight Dynamics Laboratory, Wright-Patterson Air Force Base, Ohio, 1966.
5. Noble, B. The Exploration of Functional Relationships—An Aspect of Optimization. Applications of Undergraduate Mathematics in Engineering. Macmillan, New York, 1967.
6. Pickett, G., et al. Deflections, Moments, and Reactive Pressures for Concrete Pavements. Kansas State College Bulletin No. 65, Oct. 1951.
7. Pickett, G. Analytical Studies of Landing Mats for Forward Airfields. Final Report to Corps of Engineers, Waterways Experiment Station, Vicksburg, Miss., Dec. 1951.
8. Rosner, J. C. Theoretical Study of Landing Mat Behavior. Doctoral thesis, Purdue Univ., Aug. 1969.

9. Vlasov, V. Z., and Leont'ev, N. N. Beams, Plates, and Shells on an Elastic Foundation (translated from Russian). Israel Program for Scientific Translations, Jerusalem, 1966.

10. Westergaard, H. M. Stresses in Concrete Pavements Computed by Theoretical Analysis. Public Roads, Vol. 7, No. 2, 1926, pp. 25-35.

A Nonlinear Theory for Predicting the Performance of Flexible Highway Pavements

RICHARD D. BARKSDALE, School of Civil Engineering, Georgia Institute of Technology

A nonlinear theory is proposed for the structural analysis of flexible highway pavements. The proposed theory uses a nonlinear incremental approach based on finite element theory. The nonlinear problem is solved by applying each load repetition to the solid continuum in small increments. This procedure, in effect, reduces the nonlinear problem to that of successively solving a large number of elastic problems. A plastic load concept using cumulative plastic strain is developed that makes possible placing all of the nonlinear effects in the load vector. Using this approach, the system stiffness matrix needs to be decomposed only once. As the external load is incrementally increased or decreased and the modulus changes, essentially all that has to be done to calculate the new displacements of the system is to solve an upper triangular matrix by back-substitution. The plastic load approach using the concept of cumulative plastic strains is perfectly general, and the theory is applied to problems involving the application of large numbers of wheel load repetitions and viscoelastic creep loadings.

•IN THE DESIGN of flexible highway pavement systems, apparently the most important structural considerations are rutting of the surfacing due to the accumulation of permanent shear deformations and fatigue cracking of the surfacing which can also lead to rutting (1, 2). At the present time, the structural components of flexible pavement systems are usually designed by either empirical or semi-rational methods based on ultimate strength or elastic theory (3). The presently used design methods cannot rationally account for either important variations of elastic and plastic material properties with increasing numbers of load repetitions or the occurrence of cumulative deformations (rutting) in the pavement system.

Several linear elastic (4-8) and nonlinear elastic (9) theories have been proposed and, at least to some extent, verified for predicting the elastic response of pavement systems subjected to a single wheel load. Very few theories, however, have been proposed and verified for predicting the response of pavement systems under time-dependent creep or repeated wheel loads. Although not directly related to pavement systems, interesting theories and related model studies that deserve mentioning have been presented by Majerus and Tamekuni (10) and by Gallagher, Padlog, and Bijlaard (11).

Monismith and Secor (12) performed a comprehensive investigation to verify a linear viscoelastic theory that used the correspondence principle and characterized the material properties by a 4-element spring and dashpot model. They attempted to verify the theory using an idealized model pavement system consisting of a thin asphaltic concrete slab resting on a bed of closely spaced springs. Even after modifying the linear theory to account for differences in tensile and compressive material properties, the calculated center deflections of the model were found to be considerably less than the measured deflections shortly after the application of a creep loading.

Barksdale and Leonards (2) developed a method using material properties obtained from repeated load triaxial tests for predicting both elastic and permanent deflections and stresses in 3- and 4-layer pavement systems subjected to repeated wheel loads.

The linear theory used consisted of applying the correspondence principle to elastic layered theory and inverting the solution using the collocation inversion technique. A comparison of both the elastic and permanent surface deflections measured at the AASHO Road Test with those calculated showed reasonable agreement considering the many uncertainties involved in making a comparison of this nature. The disadvantages of this theory are, however, that the elastic modulus cannot be varied with number of wheel load applications, elastic and plastic properties cannot be varied within each layer with changes in stress state, and the plastic material properties must be evaluated by a trial-and-error process.

A general nonlinear theory that can be used to calculate both the elastic and plastic response of layered pavement systems is proposed in this paper. This theory is suitable for use as the basis for a rational, flexible pavement design procedure. A cumulative strain concept is combined with the finite element approach to give a very powerful and general method for the structural analysis of flexible pavement systems. This theory is extended to include repeated loadings and nonlinear viscoelastic creep problems. The problem of a simplified model pavement subjected to a single step function loading is used to show the validity of the proposed nonlinear, viscoelastic theory.

THEORETICAL DEVELOPMENT

The elastic finite element method was originally developed in the aircraft industry as a generalization of matrix structural methods of analysis. A detailed description of the finite element method applied to linear problems has been presented by Zienkiewicz and Cheung (13). Complicated nonlinear elasticity problems can often be reduced by iterative techniques to the problem of successively solving a large number of related linear elastic problems (11, 13, 14, 15, 16, 17). Iterative methods that have been used include direct iteration, in which the total loading is applied in one increment, or incremental methods, where the load is applied in small increments and a constant or variable modulus is used for each iteration (13). When iterative methods are used to solve nonlinear problems, careful attention must be given to whether or not the iterative solution has converged to within an engineering degree of tolerance of the mathematically correct answer.

Linear Elastic Finite Element Theory

As a first approximation, the layered pavement system problem can be idealized as one of axial symmetry. An elastic axisymmetric solid continuum may be represented as an assemblage of a finite number of discrete ring-shaped elements. Each adjacent element in the solid that comes together at a common point is interconnected by frictionless pins called nodes. By requiring that equilibrium of forces and compatibility of element displacements at all the nodes in the system are satisfied under the application of external loads, the continuum problem is reduced to that of solving a large system of simultaneous linear equations. Fortunately, the system of equations usually has a large number of zero terms, which greatly reduces the number of calculations required to solve the system.

A finite element computer program for solving elastic axisymmetric problems was developed and later modified for nonlinear material properties. Rectangular, ring-shaped elements were used in the program to approximate the continuum, and the displacement components were assumed to vary linearly over each element. The corresponding stiffness of each element was numerically evaluated using 3-point Gaussian quadrature in both directions. After assembling the system stiffness matrix and load vector, the resulting system of simultaneous linear equations was solved using Choloski decomposition, taking into consideration the bandwidth of the system stiffness matrix. In formulating the load vector, distributed surface loadings were lumped at the nodes using consistant energy concepts. Inertia forces were neglected throughout this investigation. A comparison was made for the elastic half-space problem between deflections and stresses calculated using the proposed finite element theory, those obtained using a finite element program written by Wilson (18), and those calculated using elastic half-

space theory. Good agreement was shown to exist between the stresses and deflections calculated using the different methods.

Incremental Nonlinear Elasticity Theory

The incremental approach can be used to solve nonlinear problems by dividing the total load on the structure into small, equally spaced increments. By following this approach the task of solving nonlinear problems can be reduced to one of solving a relatively large number of linearly elastic ones. Essentially what is done using the proposed procedure is to obtain for each load level, using an iterative procedure, a modulus for each element that is compatible with the corresponding stress state or effective stress. Effective stress-strain laws and a detailed explanation of the method are given elsewhere (19).

The effective stress path followed in this investigation using an iterative procedure subsequently described is shown in Figure 1. An initially guessed elastic modulus E^e is used to calculate the stress state for the first load increment which results in a movement along the stress path from o to a in Figure 1. A new modulus is then determined using the initially calculated stress state based on E^e. A new stress state is then calculated using the total modulus E just calculated. Repeating this iterative procedure would cause a gradual movement from point a to a point near b provided a sufficient number of similar iterations are carried out for the first load increment. The next load increment is then added to the previous increment. The modulus defined by line o-b is used to calculate the first approximate stress state for the second load increment resulting in a movement from b to c on the effective stress path. The correct plastic load increment, $\bar{\epsilon}^p$, for the new load level can be determined using the final plastic load for the first load increment and similar triangles oab and ozc, when the indicated stress path is followed. The same iterative procedure described for the first load increment is repeated again for the second load increment resulting in a movement from c to the vicinity of d. The same procedure is carried out with the addition of each successive load increment until the total desired load is applied to the solid.

The plastic strain, $\bar{\epsilon}^p$, associated with any deviation from the elastic strain, $\bar{\epsilon}^e$, calculated using the initial elastic modulus can be treated exactly like an initially known strain state applied to the solid, such as that due to temperature effects or erection errors. A fictitious load matrix can then be calculated which places all the plastic
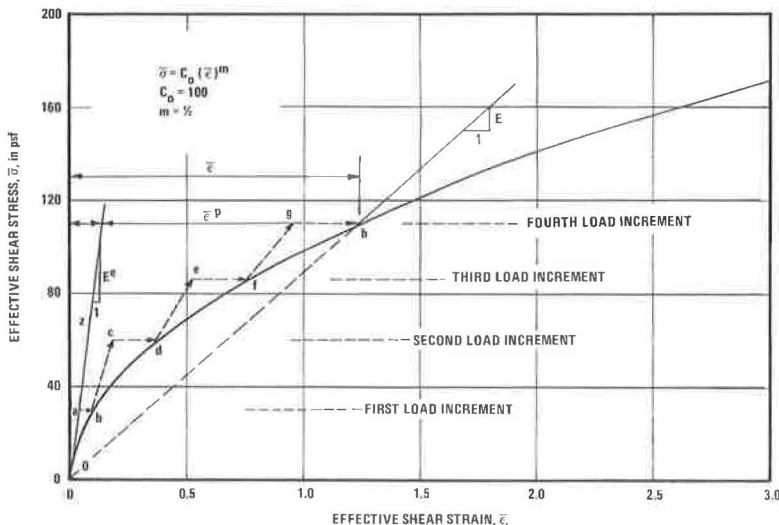

Figure 1. Effective stress path followed using proposed iterative procedure.

effects in the loading. Handling the plastic effects in this way makes possible the solution of nonlinear problems without ever changing the system stiffness matrix from the one initially calculated for the first load increment. The stiffness matrix therefore needs to be decomposed or inverted only one time and successively solved for each iteration and load increment using a different total load vector.

If Poisson's ratio remains constant, it is not necessary when calculating the fictitious load matrix to evaluate the associated volume integral during the entire iterative procedure (19). The contribution to the load matrix due to the plastic strains in each element can be evaluated for each successive iteration by simply multiplying the previously calculated elastic stiffness matrix of each element times the appropriate node displacement vector and a ratio of the total modulus to the plastic modulus. Both elastic and plastic deviations from an initially assumed elastic modulus can be placed in the load vector. Therefore, the elastic stiffness matrix, which involves a complicated volume integral, needs to be evaluated only one time during the solution of a nonlinear problem.

The nonlinear theory just presented was incorporated into the elastic finite element computer program described in the previous section. The nonlinear theory and computer program were initially verified for the problem of a long, hollow cylinder subjected to a uniform internal pressure (20). The stresses obtained using the nonlinear program were found for all degrees of nonlinearity studied to be within less than 5 percent of the values obtained by Nadai (20). The number of load increments required to give good convergence was found to depend upon the degree of material nonlinearity.

Repeated Wheel Load Applications

The proposed nonlinear finite element theory can be readily extended for highway pavements to include large numbers of repeated wheel loadings. Assume that the moving wheel loads can be replaced by a series of stationary, repeated loadings. This idealization, in effect, neglects the influence of inertia forces. Furthermore, assume that only a relatively few wheel loadings are applied very near the edge of the pavement so that an axisymmetric loading can be used to represent the loading and pavement structure. Finally assume a normal surface loading and small deflection theory. A discussion of these assumptions and their implications is given elsewhere (19).

The material properties for the nonlinear analysis of highway pavements subjected to large numbers of wheel applications can be obtained from repeated load triaxial tests. Repeated load tests would be performed on the surface, base, and subgrade materials using an appropriate range of deviator stresses and confining pressures. The stress state and deflections at the end of the first load cycle can be calculated by applying and then removing the wheel load to the pavement system in small increments. During unloading the permanent cumulative strain in each element can be treated in the same way the fictitious plastic strain was handled in the earlier theory. Previous laboratory studies (21, 22) have shown that the average loading modulus and the accumulation of permanent strain during each load repetition changes relatively slowly with increasing number of load applications. From an engineering standpoint, the material properties can therefore be assumed either to remain constant for a certain number of load repetitions or else to vary in some predetermined manner. The number of load repetitions during which the modulus and cumulative strain would be assumed constant would be determined from the results of the repeated load triaxial tests. Fortunately, this interval would, in general, tend to increase logarithmically with the increase in the number of load repetitions. Using the plastic strain concept, this approach would require, at most, reevaluating the system stiffness matrix and decomposing it each time the material properties are changed. This approach not only permits the use of nonlinear material properties but also makes it possible to vary both the elastic and plastic material properties with the number of load repetitions. This approach, therefore, greatly generalized the previous work done by Barksdale and Leonards (2).

Nonlinear Viscoelastic Creep Problems

The problem now is to illustrate how the nonlinear finite element theory can be readily used to predict the response of nonlinear pavement systems subjected to stationary

creep loadings. Time-dependent problems may be solved by using finite element techniques either by marching forward in small increments of time (11, 23, 24, 25) or else by directly applying the correspondence principle (2, 10). Applying the correspondence principle to problems involving step loadings and inverting the transformed solution often results in considerably less numerical calculations than solving the same problem using a step-by-step method. The correspondence principle, however, could not, in general, be used to solve nonlinear problems involving arbitrary variations of loading with time. Use of the correspondence principle in solving linear viscoelastic pavement problems has already been described (2). This same approach can also be used in solving nonlinear viscoelastic creep problems with only the minor modifications described in this section.

Appropriate tension and compression creep tests would be performed at stress levels selected so as to cover the range of anticipated stress states to which the material would be subjected under actual loading. For each type of test, a linear n-element Kelvin model could then be readily fitted to the experimental data obtained for each stress level by using the collocation method proposed by Schapery (26). Using the Kelvin model, the operational creep compliance $\bar{D}_c(p)$, as a function of transformed time p, could be calculated for all stress levels for a particular type of test. This operation, in effect, would generate a family of curves in the transformed $\bar{D}_c(p)$-p plane relating operational creep compliance, stress level, and time. Each curve would correspond to a stress level at which a test was performed. At each desired instant of transformed time, a relationship could be obtained between the stress state and the operational creep compliance by cross-plotting these results. This procedure would give the relationship between stress state and operational compliance at a certain instant of operational time which is analogous to the information obtained from a time-independent, nonlinear stress-strain curve. A relationship having this form between stress state and operational creep compliance for given values of operational time p can be readily used in the proposed method of nonlinear stress analysis. This nonlinear viscoelastic approach is equivalent to assuming that the material behaves linearly for small incremental changes in stress state and is similar in overall concept to the proposed time-independent, nonlinear incremental theory.

The transformed time-dependent response $\zeta(p)$ to a creep loading could be readily calculated at a finite number of transformed times by applying the correspondence principle and using the material properties evaluated as described above. The transformed solutions could then be inverted back to the real time plane by applying a collocation inversion method (27).

NONLINEAR VISCOELASTIC MATERIAL CHARACTERIZATION

This section describes the evaluation and characterization of the nonlinear viscoelastic material properties of a sand asphalt. Specimens of sand asphalt were subjected to both uniaxial tensile and triaxial compression creep states of stress to evaluate the effects of stress state and time on the material properties. All tests were performed in constant-temperature chambers at a temperature of 77 ±0.5 F. The material properties were then characterized in a form suitable for use in the proposed nonlinear viscoelastic theory. All samples tested had $6\frac{1}{2}$ percent by total weight of a 120-150 standard penetration grade asphalt cement. The aggregate used was a fine, well-graded crushed granite having a maximum grain size of $\frac{3}{8}$ in.

Uniaxial Tensile Creep Tests

The tensile creep properties of the sand asphalt specimens were determined by means of a uniaxial creep test. The 1 x 1 x 5-in. specimens used in this series of tests were cut from 1 x 6 x 6-in. samples prepared by static compaction. Axial tensile step loadings of 2.0, 3.9, 5.6, and 7.5 psi were applied to specimens in order to cover the approximate range of stress levels estimated before the development of the theoretical analysis. The average density of the tensile specimens was 141.7 pcf (±1.4 percent).
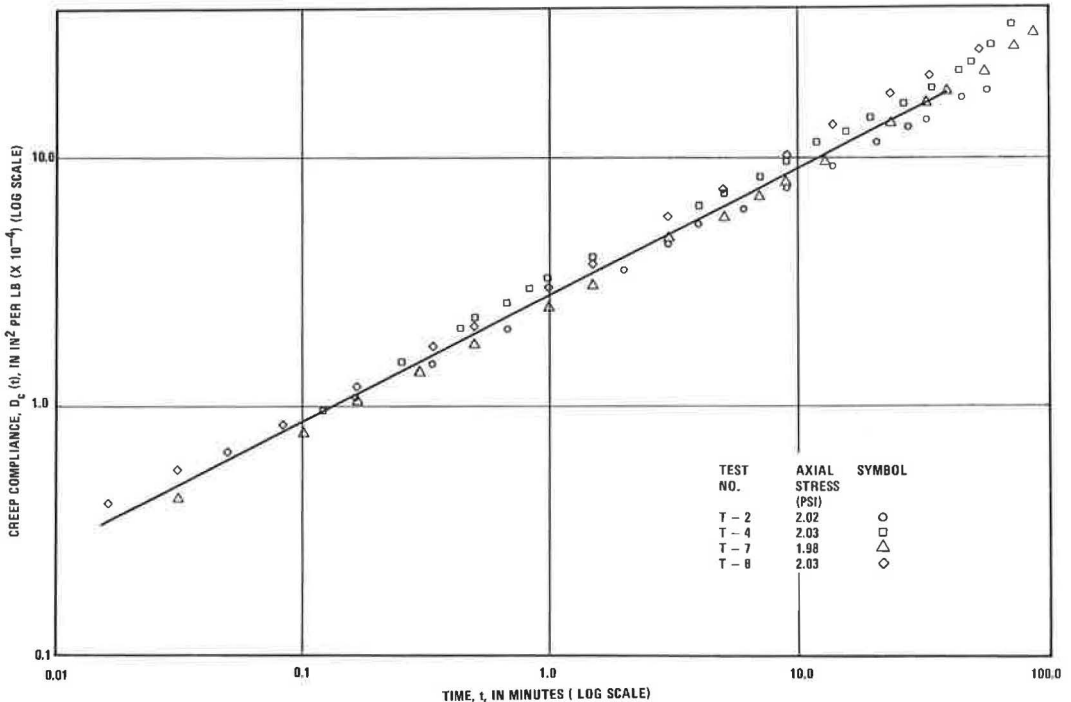
Figure 2. Experimental tensile creep compliance curve for sand asphalt at 77 F and an axial stress of 2.0 psi.

The tensile specimens were orientated with their long axis vertical in an aluminum loading frame. Each specimen was subjected to a creep loading by placing circular lead weights on a load hanger.

Typical test data and the corresponding average creep compliance curve as a function of time for the tests performed at a stress level of 2.0 psi are shown on a log-log plot in Figure 2. The creep compliance is just the reciprocal of the creep modulus and is equal to the time-dependent strain divided by the constant stress. The creep compliance as a function of time was found for a given stress level to be linear over almost 2 log cycles of time. All test data were corrected for the small deformations that occurred in the wood end tabs and loading system. The approximate influence of stress level on creep compliance is shown in Figure 3. Some of these curves have been slightly shifted so as to give consistent results for each successive stress level. These results, although based on a limited number of tensile creep tests, indicate that, at times greater than about 0.5 min, the creep compliance increases as the stress level goes from 2.0 to 7.6 psi. On the other hand, for times less than about 0.5 min, the creep compliance becomes smaller as the stress level is increased.

The viscoelastic material characterization theory described earlier was used to develop a mathematical set of models from the experimentally measured creep material properties suitable for use with the proposed nonlinear viscoelastic theory. A 16-element Kelvin model was fitted to each of the 4 tensile creep response curves shown in Figure 3. A mathematical model was thus obtained for the operational creep compliance as a function of transformed time for each of the 4 stress levels at which tensile creep tests were performed. The relationship between axial stress level and operational creep compliance at 11 values of p spaced approximately evenly between 0.01 and 100 was then obtained by cross-plotting the results from the operational creep compliance curves for each stress level. Typical results of this operation, which give the relationship between axial stress level and operational creep compliance at a given
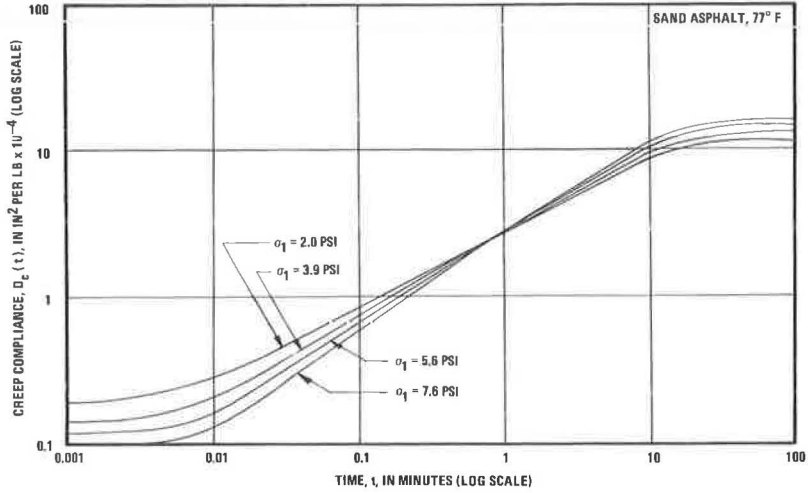
Figure 3. Influence of axial stress on tensile creep compliance.

instant of operational time p, are shown in Figure 4 for p = 0.1. This operational time corresponds to a real time of roughly 5 min. These relationships between axial stress level and operational creep compliance are in a form suitable for use in the proposed nonlinear viscoelastic theory. These curves would be, for example, the nonlinear viscoelastic equivalent to a plot of the modulus of elasticity as a function of axial stress obtained from a uniaxial tension test performed at a constant strain rate.
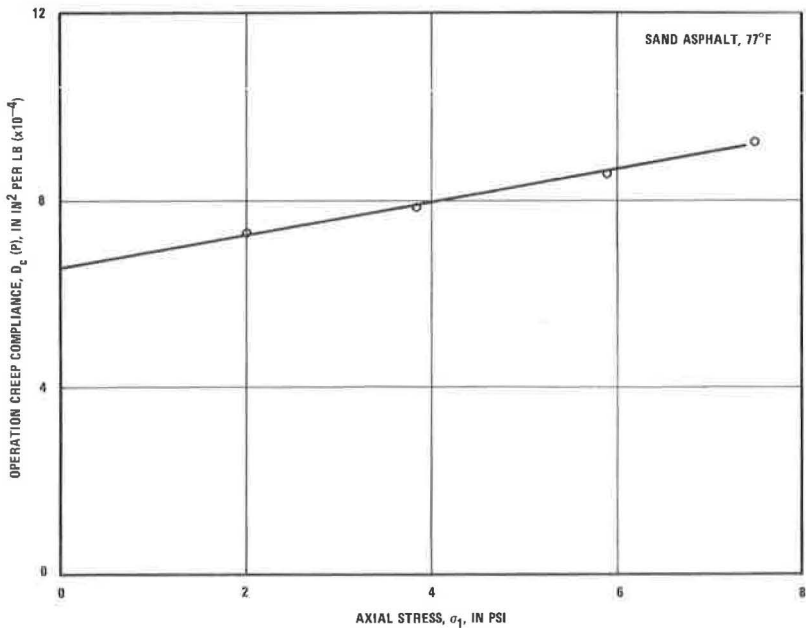

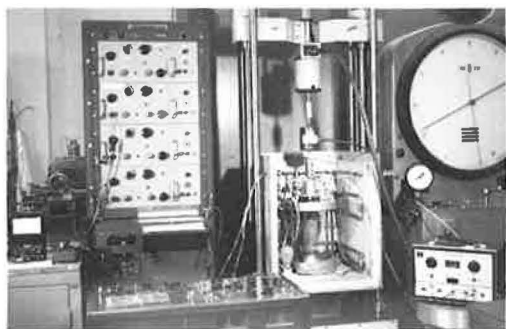Figure 4. Variation of operational tensile creep compliance with axial stress for p = 0.1.

Figure 5. Compressive creep test apparatus.

For all stress levels, lateral deformations at the mid-height of the specimen were measured in one plane by using either two Collins LVDT displacement transducers wired in series or else two 1/10,000-in. Federal dial indicators. Values of Poisson's ratio were calculated from the lateral deflection measurements made at the center of the specimens from the relationship

$$\nu = \frac{1}{2}\left[1 - \frac{1}{\epsilon_a}\frac{\Delta V}{V}\right] \tag{1}$$

where ν = Poisson's ratio, ΔV = volume change, V = initial volume, and ϵ_a = axial strain. This approximate relationship was derived from the theory of linear elasticity, assuming the radial and tangential strains were equal. The change in volume that occurred during the creep tests was estimated by assuming that the end cross-sectional areas did not change and the deformed shape of the specimen could be approximated by plane surfaces. At a given instant of time the calculated values of Poisson's ratio were found to vary quite widely from one test to the next. However, when average values were plotted against the logarithm of time, Poisson's ratio was found to decrease almost linearly from a value of 0.32 at 0.5 min to approximately 0.11 at the end of 10 min.

Compression Creep Tests

The compressive creep properties of statically compacted cylindrical sand asphalt specimens approximately 2.9 in. in diameter and 6.0 in. in height were evaluated for confining pressures of 0, 15.0, and 35.0 psi and 3 deviator stresses in order to determine the effect of stress state on the material properties. The average density of the compressive specimens was 144.2 pcf ($\pm$0.9 percent). The compressive creep tests were performed between 20 and 50 days after compaction of the specimen. All tests were performed using a triaxial test cell that was placed inside a constant-temperature chamber as shown in Figure 5. A step function loading was applied to the specimen by means of a pneumatically operated Bellofram connected in series with a load cell and a small aluminum loading head. The Bellofram was activated by electrically opening a quick-release valve.

Lateral displacements at the mid-height of the specimen were measured throughout the tests by means of a lateral deflectometer. Also, final deflection profiles for a number of the specimens were measured using vernier calipers at the end of the creep tests. These data were used in estimating the end deformations and the deflected shape of the sample at selected times during the test. Poisson's ratio was calculated using the volume change relationship given in Eq. 1. The deflected sample profile was assumed to be a parabola with lateral deformations occurring at the top but no deformations at the bottom. These approximate calculations indicated that Poisson's ratio gradually increased with time. Apparently, however, this change is not very large. The average value calculated from 12 tests that included all confining pressures indicated a value of 0.50 for Poisson's ratio, assuming it is time-independent. The calculated variation from the average value, however, was found to be relatively large in both directions.

A typical measured compressive creep compliance response for the test performed at a confining pressure of 15 psi and a deviator stress of 19.0 psi is shown in Figure 6, together with the data from each individual test. All curves were corrected for the deformations occurring in the plexiglass end caps and the base of the triaxial cell. The creep compliance, as a function of the logarithm of time, was found at very small times to gradually increase at an increasing rate with time. By an elapsed time of
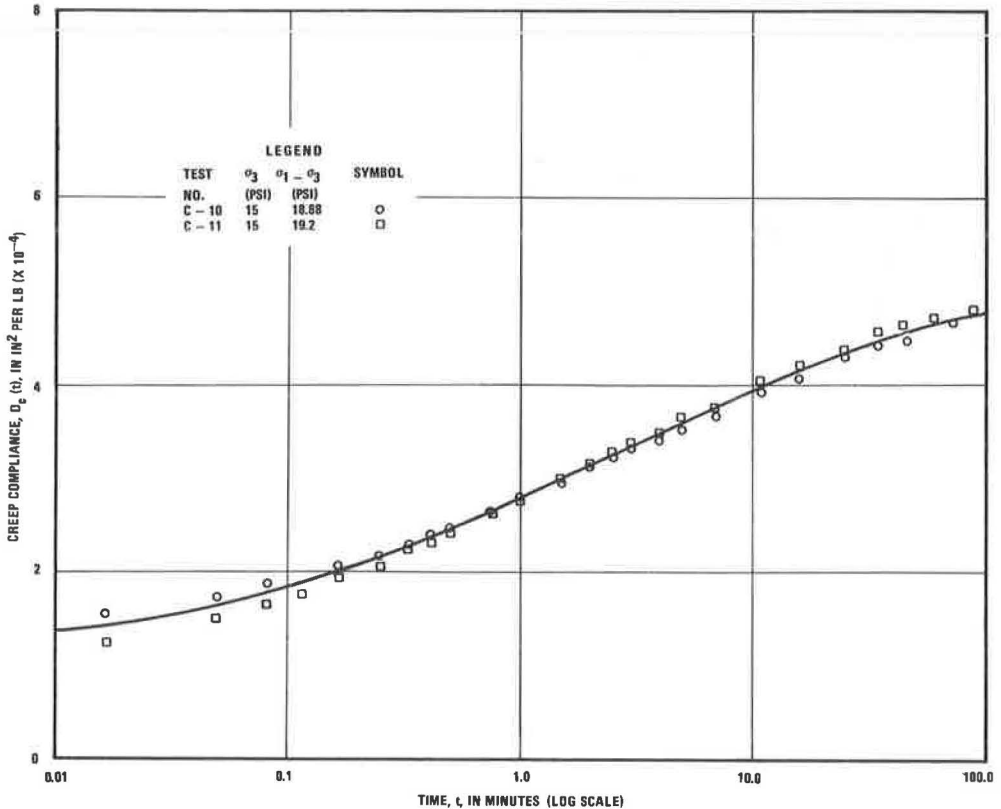
Figure 6. Experimental compressive creep compliance curves for sand asphalt at 77 F and a confining pressure of 15 psi.

approximately 0.1 min, the increase in creep compliance had become almost directly proportional to the logarithmic increase of time. The creep compliance, after remaining almost proportional to the logarithm of time for 2 to 3 log cycles, then started either to asymptotically approach an equilibrium value or else to get larger at a rapidly increasing rate, indicating approaching failure. Since failure of the specimen under a constant creep loading was not being investigated, the tests were discontinued after approximately 100 min if failure had not occurred before this time. Failure or indications of impending failure were observed during the 100-min testinng period only in specimens subjected to deviator stresses greater than 45 psi.

An 11-element Kelvin model was fitted to the experimental compressive creep compliance curves following the same procedure used in reducing the tensile test data. Using the Kelvin model representations, the operational creep compliance was calculated and plotted as a function of operational time for each creep test. The relationship between operational creep compliance, confining pressure, and deviator stress was obtained by cross-plotting the operational creep compliance curves at each desired instant of operational time. Typical results obtained for operational times $p \leq 6$ (which correspond roughly to real times ≥ 0.1 min) are shown in Figure 7 for $p = 0.04$. For this time range the operational creep compliance was found to apparently decrease as the confining pressure and deviator stress were increased, although a more detailed investigation is needed. The test results indicate that, at constant confining pressures, as the deviator stress is increased the rate of decrease in the operational creep compliance becomes smaller. For operational times $p > 6$ the operational creep modulus was found to increase as the confining pressure was increased and decrease as the
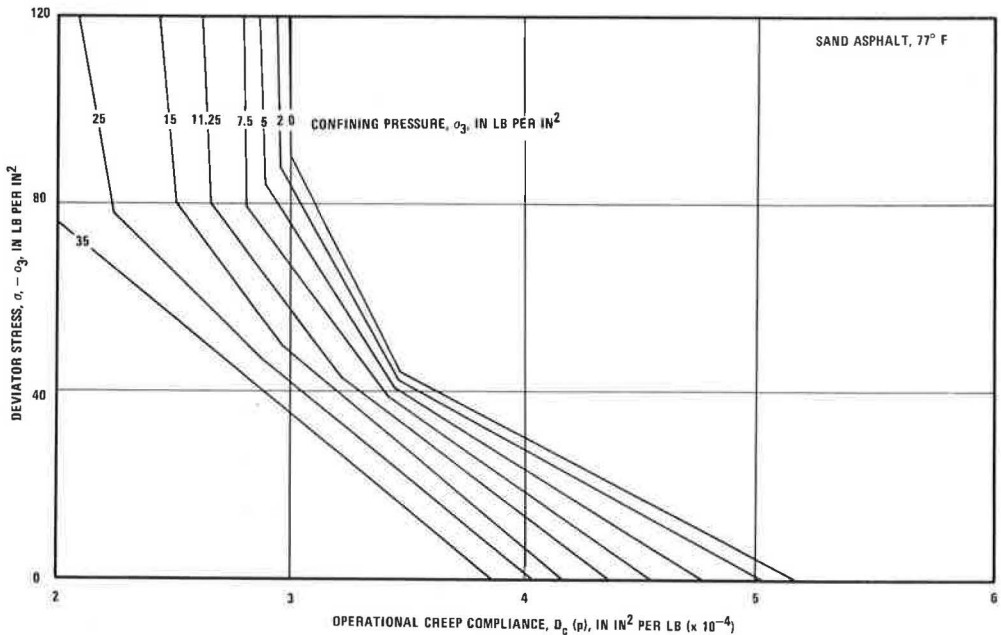
Figure 7. Influence of deviator stress and confining pressure on the compressive operational creep compliance for p = 0.04.

deviator stress increased. The same values of operational time p were used in reducing both the tensile test data and compression test data so that the material characterization could later be used in the nonlinear viscoelastic analysis.

Discussion of Tests

In performing a creep test, a certain finite rise time is required for the total applied load to become fully supported by the specimen. During this rise time the stress on the sample is increasing, and the sample is influenced to an unknown degree by impact effects. For these reasons the results of the creep tests should be considered valid only for times greater than about 10 times the rise time (28). The average measured rise time for the tensile creep tests was found to be 0.10 sec and for the compressive creep tests, 0.16 sec. Therefore, in characterizing the tensile and compressive creep properties for use together in a theoretical analysis, these properties should be considered valid only for times greater than about 1.6 sec after the specimens began to carry load.

In all of the creep tests performed, the axial specimen deformation was determined by averaging the axial deformation occurring on each side of the sample at equal distances from the center. This averaging procedure compensates for the effects of any bending due to eccentricity of load and gives more reproducible results than if only one value of deflection is measured at some distance out from the center. The recorder-transducer systems were calibrated periodically as close to the test setup position as possible by applying a known set of deformations to the transducers and measuring the corresponding movement of the recorder pen. This method of calibration eliminates any variations in transducer and recorder calibration factors, the effects of wire resistances, and ground loop errors that may occur in the electrical system. For both the tensile and compressive creep tests, the measured axial deformations were corrected for deformations occurring in the end caps and support system.

No matter how carefully a series of tests is performed, some experimental errors are always introduced. Assuming that all measurements were made correctly, most

of the possible errors, such as eccentricity of loading, strain concentrations, piston friction, and deformations in the system that were not corrected for, would tend to give an apparent modulus somewhat lower than the actual modulus and shorter apparent times to failure. Piston friction was found to be apparently small, and approximate corrections were applied to account for at least part of the deformations occurring in the loading system. Although care was taken in performing the tests, eccentricity of loading was probably one of the more important experimental errors, particularly for the tensile creep tests.

Both the tensile and compressive creep test results show a relatively large scatter in calculated values of Poisson's ratio. Probably one important cause of this scatter is that the change in shape of the sample did not occur symmetrically about its midheight, as is assumed in the reduction of the data. Furthermore, some scatter is probably partly due to the small deformations involved and the approximate equation used to reduce the data. The tensile test results may also have been influenced by anisotropy in a cross-sectional plane normal to the long axis of the specimen due to compaction. Large cracks parallel to the axis of the sample were observed in the compression specimens that failed. Cracks may also open up at lower stress levels, causing the calculated Poisson's ratio to be greater than 0.50. No matter what the cause, Poisson's ratio is apparently sensitive to the details of the test and deserves further study.

MODEL PAVEMENT STUDY

The only manner by which at least a partial evaluation of a theory can be made is to compare the predicted response of either a model or prototype pavement with experimentally measured response values. For this investigation, a small-scale idealized pavement model was chosen for verifying the proposed theory. The model selected consisted of a circular sand asphalt slab 1 in. thick and $18\frac{1}{2}$ in. in diameter resting on a bed of linearly elastic springs. The slab was subjected to an approximately uniform step loading applied at its center over a radius of 1 in. The surface deflections predicted using the proposed nonlinear viscoelastic theory were then compared with the experimentally measured values.

Model Tests

The circular asphalt slab was prepared using the same aggregate gradation and $6\frac{1}{2}$ percent asphalt cement content as was used in preparation of the samples from which the material properties in creep were evaluated. The asphalt slab was statically compacted to the desired thickness by a 2-stage compaction procedure using, in each stage, the full capacity of a 450,000-lb constant strain rate testing machine and a specially designed mold and loading assembly.
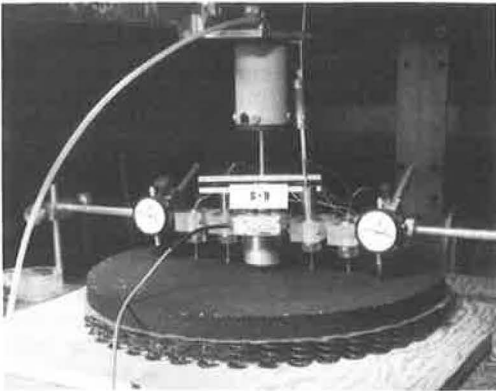
The sand asphalt slab used in the model study was supported on 113 springs placed in 5 concentric rings. The stiffness of each spring was determined by calibration to be linear with their stiffnesses varying between 15.0 and 17.0 lb/in. In order to minimized the effect of variation in spring stiffness, the springs were grouped together so that the maximum variation of spring stiffness from the average within any one concentric ring of springs was less than $+0.5$ lb/in.

A total of 4 model tests were performed at a temperature of 77 F ($\pm$1 F) in a large constant-temperature room. The pavement

Figure 8. Model pavement represented by an $18\frac{1}{2}$-in. diameter sand asphalt slab resting on a spring base.

model is shown in Figure 8. A 2-in. diameter step load of 33.5 lb was applied at the center of the model through a $\frac{3}{8}$-in. thick rubber cushion that was glued on the bottom of an aluminum loading head. The rubber cushion was used to reduce impact effects and to obtain as uniform a contact pressure as possible over the loaded surface. The step load was applied using the pneumatic apparatus previously described. The average load rise time for the 4 model tests was determined to be 0.15 sec. The deflection creep response to the step loading was measured across a single diameter of each slab by using 5 Collins self-excited LVDT transducers and 2 dial indicators. All transducers and dial indicators were zeroed just before the step load was applied to the specimen. Therefore, the reference datum for all measurements was the slab profile just before application of the step loading.

The average measured deflected surface profiles along a diameter for all 4 tests at times of 5 sec, 1 min, and 10 min after the application of the step load are shown in Figures 9 through 11. All points on the surface of the slab moved downward at the instant of load application, and the deflected surface profile had a bowl-shaped appearance at each successive instant of time. The central portion of the slab moved downward quite rapidly at first with a decreasing rate of movement with increasing time throughout the test. The outside edge of the slab, however, after an initial downward movement lasting less than 1 min, tended thereafter to move slightly upward but not enough to result in a net deflection above the reference datum.

Theoretical Prediction of Slab Response

The time-dependent response of the slab was calculated using the previously described nonlinear viscoelastic theory and the experimentally evaluated material properties. The transformed p-multiplied deflections $p\zeta(p)$ were calculated for the same 11 approximately equally spaced values of p between 0.01 and 100 used in characterizing the tensile and compressive operational creep compliance data. In the nonlinear viscoelastic finite element analysis, the $18\frac{1}{2}$-in. diameter slab was represented as an assemblage of 225 rectangular, ring-shaped finite elements, as shown in Figure 12.

Since there was no bond between the sand asphalt slab and the spring base, tensile forces could not physically be transmitted from the slab to the base. Therefore, the asphalt slab was assumed to rest on 3 to 5 concentric circles of linear springs depending on whether or not the slab was theoretically in contact with the particular ring of
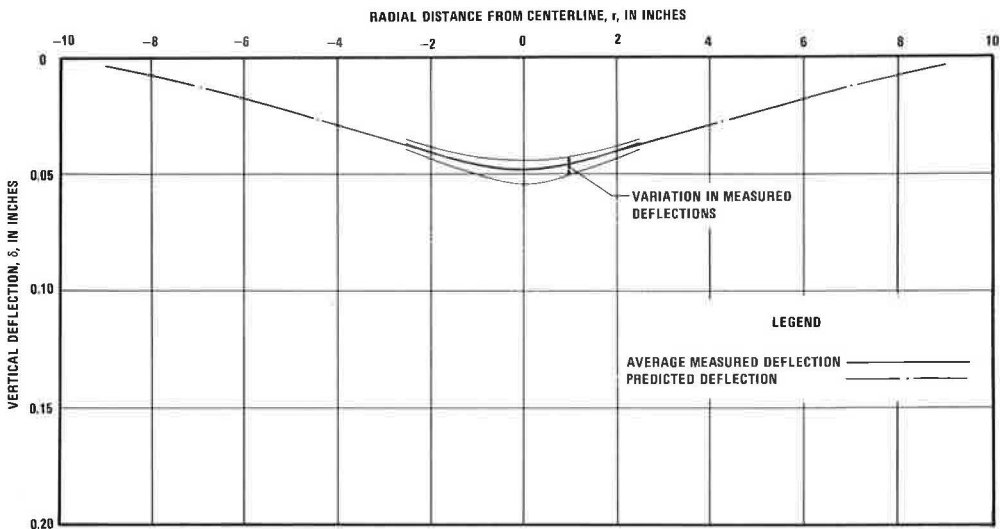

Figure 9. Comparison of measured and predicted surface deflection profiles of the model pavement after 5 sec.
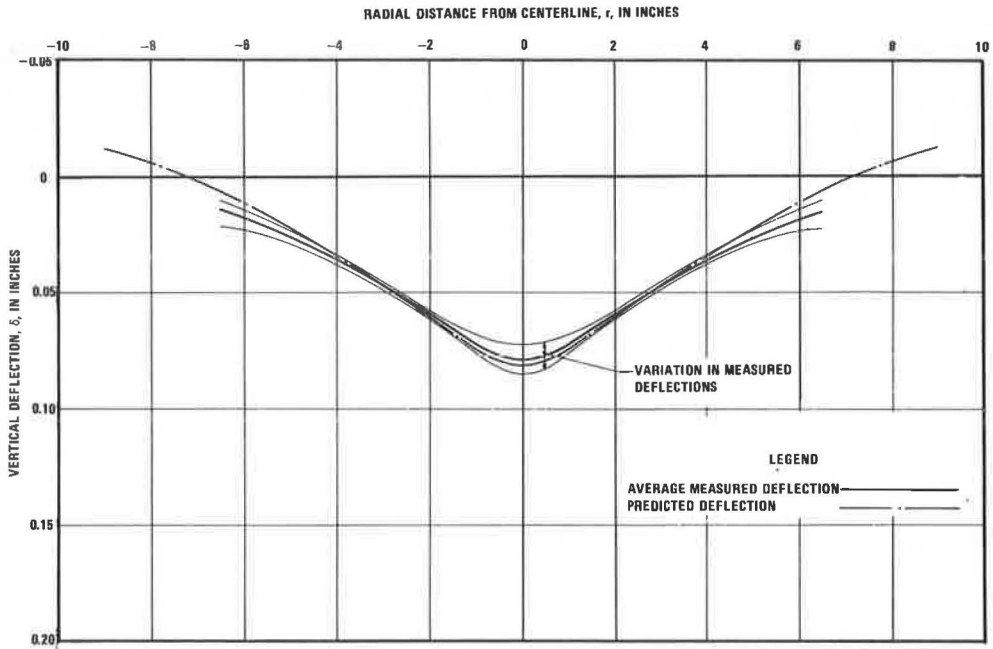
RADIAL DISTANCE FROM CENTERLINE, r, IN INCHES

Figure 10. Comparison of measured and predicted surface deflection profiles of the model pavement after 1 min.

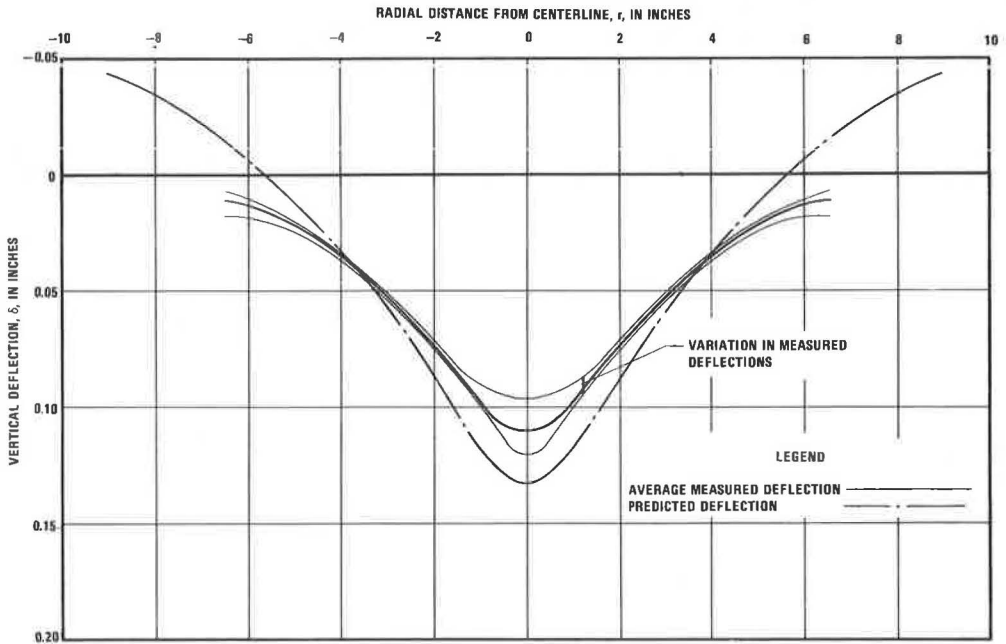RADIAL DISTANCE FROM CENTERLINE, r, IN INCHES

Figure 11. Comparison of measured and predicted surface deflection profiles of the model pavement after 10 min.
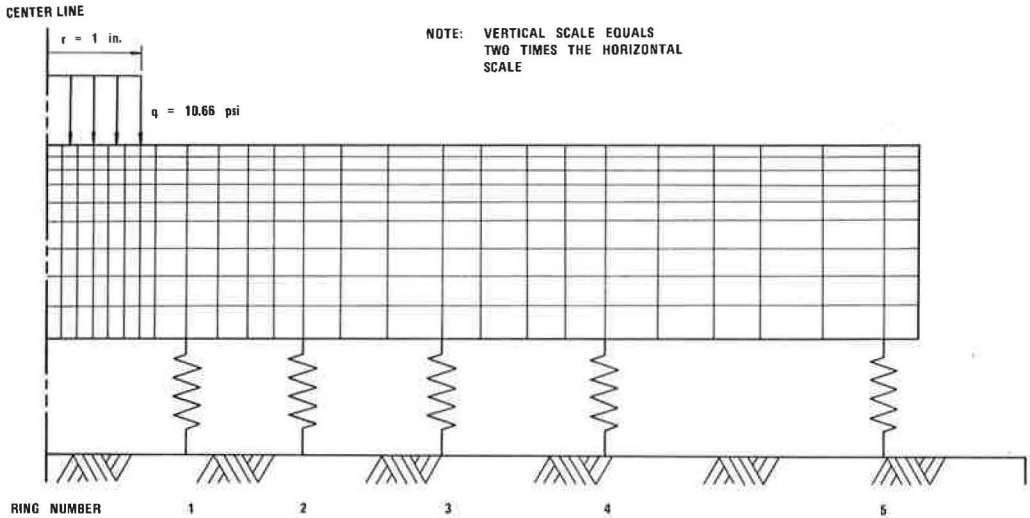
Figure 12. Finite element idealization of the model pavement system.

springs at each instant of operational time. The presence of the 5 concentric groups of linear springs was handled in the theoretical analysis by treating the force on each node connected to the springs like any other external node force. In this way the spring effect for each concentric ring of springs can be handled by simply adding the total spring stiffness for each ring into the correct position in the system stiffness matrix.

If under the imposed loading the volume of an infinitesimal element located at the center of each finite element increased, the entire element was assumed to be in a state of tension. For a tensile stress state, the effective stress law proposed by Nadai [20] was used in selecting the appropriate tensile creep compliance, using the uniaxial tensile creep test data. If in applying the volume change criteria a compressive state of stress was found to exist in an element, the two larger principal stresses (tension is defined as positive) were averaged to obtain an approximate confining pressure. For the desired instant of operational time, the operational creep compliance was selected from the corresponding set of material properties, such as those shown in Figure 7, for instance, using the compressive deviator stress and average confining pressure. For computational purposes, all material property data used in the nonlinear computer analysis were approximated by as many straight line segments as necessary to ensure a good fit. Using the procedure outlined above, for each load level and iteration the stress state at the center of each element was calculated and used to obtain the appropriate operational creep compliance.

In a preliminary study to determine the required number of load increments and iterations per load increment to use in order to ensure convergence, the nonlinear finite element analysis for the asphalt slab was performed at the operational time $p = 0.04$, using 9 load increments and a total of 3 iterations for each increment of load. The same problem was then solved using 18 load increments and 3 iterations per increment. This study indicated that the theoretically calculated slab deflections changed less than 1 percent, whereas the stresses in the slab changed by as much as 15 percent. Furthermore, this and the rest of the study indicated that performing several iterations within a load increment apparently had little effect on the results except in a few elements that were on the borderline between the tensile and compressive zones in the slab. Based on this limited study, 14 load increments with either 2 or 3 iterations for each increment were chosen for use in the remaining theoretical calculations. For other material properties, problem geometrics, and load configurations, the requirements for convergence would, in general, be different. After the p-multiplied values of

response were calculated for each value of operational time, the results were inverted back to the real time plane using a 5- to 7-term Dirichlet series (2).

To determine if the creep properties evaluated from the compacted specimens were actually representative of those of the $18\frac{1}{2}$-in. diameter slab, $1 \times 1 \times 2$-in. specimens were cut from near the center after testing the slab. A limited number of tensile and compressive creep tests were performed on these small specimens. The compressive creep properties were found to be almost identical to those measured using the cylindrical specimens, and the tensile creep properties of the slab were found to agree reasonably well with those measured from the 6-in. tensile specimens.

A very good agreement between the theoretical profiles and the measured ones exists up to an elapsed time of about 4 min. By the end of 10 min, the calculated and measured profiles still compare favorably. The theoretical profiles did indicate that the edges of the slab should lift up off the spring base at a time slightly less than 1 min, whereas the measured deflections indicated that the outside edges of the slab did not lift up at all. This discrepancy is probably at least partly due to the fact that the measurements on the model were taken using the deflected profile of the slab just before the loads were applied as the zero reference. During several of the model tests, the outer two rows of springs were observed not to be in contact with the slab.

GENERAL DISCUSSION

The fact that the calculated center deflections for times greater than approximately 1 min became increasingly larger than the measured deflections can be explained if the measured stiffness of the sand asphalt is assumed to be less than the actual stiffness. Almost all experimental errors, such as eccentricity of load, system and end cap deformation, and strain concentrations, would tend to give an experimentally measured stiffness of the sand asphalt less than the actual stiffness. The tensile test specimens failed at times between approximately 8 and 100 min, with the time to failure decreasing as the stress level increased. The time required to cause tensile failure at the same stress level was found to be greatly influenced by seemingly minor details of either the test or the method of specimen preparation or possibly both. All the tensile specimens failed at times of less than 2 hours. However, when subjected to the applied loading for as long as 10 hours, the model pavement did not visibly fail. One possible explanation for this behavior is that at relatively large times the actual stiffness of the slab is indeed greater than the experimentally measured apparent stiffness of the tensile specimens.

The theoretical study shows that, for the model pavement studied using 14 load increments and 3 iterations for each increment, in general the modulus of each element changes only a very small amount from the first to the final iteration. An exception to this occurs when an element is apparently just on the verge of going from a tensile state to a compressive state of stress. In this case, which apparently occurs in only a very few elements, the modulus tends to oscillate between the appropriate tensile and compressive value. Considering all factors for the numerical solution of the problem solved in this investigation, it is concluded that apparently a total of 2 iterations for each load level is sufficient. Based on the work of others and on the very limited number of problems solved during this investigation, it is intuitively felt that as many load increments as possible should be used with only a total of one or two iterations made within each load increment. For moderately nonlinear material properties, 10 to 20 load increments may often be found to give good results. For strongly nonlinear material properties, however, as many as 20 to 40 or more iterations may be required. It should be emphasized that in either instance convergence of the numerical calculations should be studied for each specific problem.

In applying the theory to the idealized model pavement it is assumed that as the external load is incrementally increased the stress state acting on each element either remains the same or always changes in the same direction. This assumption means that unloading of a given element during the incremental application of the external load is assumed to never occur. For most pavement problems, application of the load should not result in a condition of unloading in most of the elements. A few elements

may, however, undergo some unloading and introduce an unknown but probably small error into the analysis. The theory developed is perfectly general and a condition of unloading can be readily included using the plastic strain concept.

Tremendous progress has been made in the last few years toward developing numerical step-by-step and iterative methods of stress analysis suitable for solution using high-speed digital computers. These numerical approaches can be used to solve time-dependent problems whose materials exhibit both nonlinear and anisotropic properties. This rapid advancement of theory has resulted in a very definite need for reevaluating presently used methods of material testing and characterization. In particular, a great need now exists for more research on the effect of stress state on material properties and the development of realistic effective stress-strain laws for the materials used in pavement construction, which often undergo high volume changes and exhibit quite different properties in tension and compression.

SUMMARY AND CONCLUSIONS

The problem of developing a rational theory that can be used in predicting the performance of flexible highway pavement systems is very complicated because of the large number of wheel load repetitions, complex material properties and pavement geometry, and cyclic environmental changes that occur during the life of the pavement. The proposed incremental nonlinear finite element theory offers a quite general approach to the problem of predicting both elastic and cumulative stresses, strains, and deflections in highway pavement systems. The proposed plastic strain concept incorporated in the finite element theory results in a practical method for handling the variation of both elastic and plastic material properties with increasing numbers of wheel load applications. The material properties for use with this theory would be evaluated from either repeated-load triaxial tests or other suitable dynamic tests. Variations of the material properties with tensile and compressive stress states, confining pressures, deviator stresses, environmental changes, and changes with age or number of load applications can all be readily considered using the proposed nonlinear theory. The most important assumptions made in this theory are that (a) inertia forces in highway pavements as a first approximation can be neglected, (b) the surface loading is normal to the pavement, and (c) axisymmetry of the load and pavement structure is maintained.

This study and other investigations indicate that the rate of convergence using the incremental nonlinear approach is dependent on the type of loading, the geometry of the solid, the manner in which the load is applied, and the degree of material nonlinearity. For these reasons, the convergence of the iterative numerical calculations for nonlinear problems should always be carefully studied for each specific problem investigated.

The nonlinear theory developed in this investigation and also other numerical methods are presently available for the comprehensive analysis of complex structural mechanics problems. These relatively new theories which can handle complicated nonlinear material properties have resulted in a very definite need for reevaluating presently used methods of material characterization. An important need now exists for a detailed study of the influence of stress state on material properties, and for developing a realistic effective stress-strain law for the class of materials used in pavement construction.

A nonlinear engineering theory suitable for predicting the structural response of flexible pavement systems subjected to repeated loads was presented and verified for the case of a hollow cylinder and an idealized model pavement system subjected to a creep loading. The next step is to verify the proposed theory for either a full-scale pavement test section subjected to repeated wheel loads or else a full-scale laboratory test pavement subjected to either stationary or moving repeated loads.

ACKNOWLEDGMENTS

38

REFERENCES

1. The AASHO Road Test: Report 5—Pavement Research. HRB Spec. Rept. 61E, 1962.
2. Barksdale, R. D., and Leonards, G. A. Predicting Performance of Bituminous Surfaced Pavements. Proc. Second Internat. Conf. on the Structural Design of Asphalt Pavements, July 1968, pp. 321-340.
3. Vesic, A. S., and Domaschuk, L. Theoretical Analysis of Structural Behavior of Road Test Flexible Pavements. NCHRP Rept. 10, 1964.
4. Burmister, D. M. Evaluation of Pavement Systems of the WASHO Road Test by Layered System Methods. HRB Bull. 177, 1958.
5. Peattie, K. R. A Fundamental Aproach to the Design of Flexible Pavements. Proc. Internat. Conf. on the Structural Design of Asphalt Pavements, Univ. of Michigan, 1963, pp. 403-411.
6. Whiffin, A. C., and Lister, N. W. The Application of Elastic Theory to Flexible Pavements. Proc. Internat. Conf. on the Structural Design of Asphalt Pavements, Univ. of Michigan, 1963, pp. 499-521.
7. Coffman, B. S., Kraft, D. C., and Tamayo, J. A Comparison of Calculated and Measured Deflections for the AASHO Test Road. Proc. AAPT, Vol. 33, Feb. 1964, pp. 54-90.
8. Seed, H. B., Mitry, F. G., Monismith, C. L., and Chan, C. K. Prediction of Pavement Deflections From Laboratory Repeated Load Tests. Dept. of Civil Engineering, Univ. of California, Rept. No. TE-65-6. Oct. 1965.
9. Duncan, J. M., Monismith, C. L., and Wilson, E. L. Finite Element Analysis of Pavement. Highway Research Record 228, 1968, pp. 18-33.
10. Majerus, J. N., and Tamekuni, M. Effects of Material Nonlinearity and Failure Criteria Upon Solid-Propellant Integrity. Journal of Spacecraft, Vol. 3, No. 3, March 1965, pp. 393-399.
11. Gallagher, R. H., Padlog J., and Bijlaard, P. P. Stress Analysis of Heated Complex Shapes. American Rocket Society Journal, Vol. 23, May 1962, pp. 700-707.
12. Monismith, C. L., and Secor, K. E. Viscoelastic Behavior of Asphalt Concrete Pavements. Proc. Internat. Conf. on the Structural Design of Asphalt Pavements, Univ. of Michigan, 1963, pp. 476-498.
13. Zienkiewicz, O. C., and Cheung, Y. K. The Finite Element Method in Structural and Continuum Mechanics. McGraw-Hill, London, 1967, p. 72.
14. Argyris, J. H. Elasto-Plastic Matrix Displacement Analysis of Three-Dimensional Continua. Journal of the Royal Aeronautical Society, Vol. 69, 1965, pp. 633-636.
15. Mentel, T. J. Study and Development of Simple Matrix Methods for Inelastic Structures. Journal of Spacecraft and Rockets, Vol. 3, No. 4, April 1966, pp. 449-457.
16. Wilson, E. L. Finite Element Analysis of Two-Dimensional Structures. Rept. 68-2, Univ. of California, Berkeley, June 1963.
17. de Veubeke, F. B. (Ed.). Matrix Methods of Structural Analysis. Agardograph 72, Pergamon Press, 1964.

18. Wilson, E. L. A Digital Computer Program for the Finite Element Analysis of Solids With Non-Linear Material Properties. Univ. of California, Dept. of Civil Engineering, Berkeley, 1965.

19. Barksdale, R. D. Analysis of Layered Pavement Systems. School of Civil Engineering, Georgia Inst. of Technology, 1969.

20. Nadai, A. Theory of Flow and Fracture of Solids. McGraw-Hill, New York, 1950, pp. 252-274.

21. Larew, H. G., and Leonards, G. A. A Strength Criterion for Repeated Loads. HRB Proc., Vol. 41, 1962, pp. 529-556.

22. Seed, H. B., Chan, C. K., and Lee, C. E. Resilience Characteristics of Subgrade Soils and Their Relation to Fatigue Failures in Asphalt Pavements. Proc. Internat. Conf. on the Structural Design of Asphalt Pavements, Univ. of Michigan, 1963, pp. 611-636.

23. White, J. L. Finite Elements in Linear Viscoelasticity. Paper presented at the Second Conf. on Matrix Methods in Structural Mechanics, Wright-Patterson A. F. B., Oct. 1968.

24. Zienkiewicz, O. C., Watson, M., and King, I. P. A Numerical Method of Viscoelastic Stress-Analysis. Internat. Journal of Mechanical Sciences, Vol. 10, No. 10, Oct. 1968, pp. 807-828.

25. Greenbaum, G. A., and Rubinstein, M. F. Creep Analysis of Axisymmetric Bodies Using Finite Elements. Nuclear Engineering and Design, Vol. 7, April 1968, pp. 379-397.

26. Schapery, R. A. A Simple Collocation Method for Fitting Viscoelastic Models to Experimental Data. Guggenheim Aeronautical Laboratory, California Inst. of Technology, SM 61-23A.

27. Schapery, R. A. Approximate Methods of Transform Inversion for Viscoelastic Stress Analysis. Proc. Fourth U. S. National Congress of Applied Mechanics, ASME, Vol. 2, 1962, pp. 1075-1085.

28. ICRPG Solid Propellant Mechanical Behavior Manual. Chemical Propulsion Information Agency, CPIA Publ. No. 21, Sept. 1963.

Response of a Flexible Pavement to Repetitive and Static Loads

CLARENCE B. DRENNON and WILLIAM J. KENIS,
Federal Highway Administration, U.S. Department of Transportation

The paper describes the strains and deflections observed upon loading a full-scale, asphaltic concrete pavement model with a water-filled bag. The specimen, 10 by 10 ft by 8 ft deep, was carefully prepared to ensure uniform materials whose properties could be reproduced. Tests were conducted at constant temperature with three modes of loading: (a) 0.1-sec load and 0.9-sec unload, (b) 0.5-sec load and 0.5-sec unload, and (c) constant load creep. Cyclic tests were 1,000 cycles long, creep tests 900 sec. Load intensities of 10, 20, 40, and 80 psi were applied. The total deflections observed were viscoelastic in nature and increased linearly with load. The dynamic component of strain and of deflection was also linear. Total deflections and strains were affected only slightly by conditioning of the pavement with increased cycles and intensity of load. The accumulated deflection increased linearly with load, but during a test the deflection at a distance of 12 to 20 in. from the center of load would eventually decrease with increase in repetitions. This rise in the pavement is believed due to a differentiation of viscoelastic properties with depth at locations determined by the geometry of the pavement and of the loaded area. Strains show a similar phenomenon in similar locations on the surface from the beginning of loading, being tensile upon load and accumulating compressive strain. The strains were small, under 30 microin. per in. in the areas affected by directional reversal. The largest strain measured was 470 microin. per in. Further research is needed to explain the "12-in. rise" and the opposite accumulation of strain.

• THE RESEARCH reported herein is part of the Federal Highway Administration's National Program Task, "Rational Design of Flexible Pavements". It is primarily concerned with defining certain primary responses of a full-scale flexible pavement subjected to static and repetitive loads under controlled laboratory conditions. Little emphasis is placed, at this time, on defining limiting responses such as fatigue or permanent deformation. However, a basic premise of this research is that the use of mathematical models which are insensitive to prediction of primary responses may be of little value for use in a concept that attempts to predict pavement distress and performance.

The ability of a model to predict the response of a prototype pavement under field or laboratory conditions is a measure of the adequacy of the model (1). In a very complex system such as a flexible pavement, more than one mathematical model may be necessary to trace the paths of interrelated failure mechanisms as they propagate from a primary response to pavement distress. Indeed, it may be proper to establish a framework of various models, properly interfaced, to tie together the primary and limiting responses in order to predict the behavior of the pavement at any time under any conditions.

The mathematical model most popularly used to describe the primary response of a pavement system to environment and loading is that which combines the geometry and material properties into a system of equations that can be solved satisfying specific boundary conditions. The n-layer elastic theory is an example of such a representation that has received wide use to date (2, 3, 4). Work at the Road Research Laboratory (5) on asphalt concrete is attempting to explore the interactions between rate of loading, rest period, and configuration of the load wave form.

In this report typical responses obtained from the experimental testing of the flexible pavement under various load stimuli are presented and evaluated. Boltzmann's superposition integral is utilized to predict responses due to sinusoidal repeated loading from the response due to static loading. These predictions are compared with the measured results, and system linearity and effects due to load duration and repetitions are analyzed. Work conducted at Purdue University (6) utilizes a similar concept to characterize asphaltic concrete whereby the responses from sinusoidal loading in the form of transfer functions can be used to predict responses due to static loading.

Future work in connection with this study will involve testing of a flexible pavement identical to the one described in this study except for a thinner surface course. Comparisons will be made between the actual measured responses and theoretically predicted responses obtained through the use of various mathematical models and characterizations of the pavement component materials.

PREDICTION THEORY

A necessary condition for a system to be linear is that the principle of superposition applies. Boltzmann's superposition principle as applied to elastic and viscoelastic systems is utilized as an indicator of the time-dependency and linearity of the system. Boltzmann's superposition principle states that when an excitation function $e_1(t)$ produces a response function $w_1(t)$, a second excitation function $e_2(t)$ produces a second response function $w_2(t)$, and any other $e_n(t)$ produces $w_n(t)$, then

$$e_1(t) + e_2(t) + \ldots + e_n(t) \to w_1(t) + w_2(t) + \ldots + w_n(t) \tag{1}$$

or

$$\sum_{k=1}^{n} e_k(t) \to \sum_{k=1}^{n} w_k(t) \tag{2}$$

which must hold for a linear system (7). When n identical excitations are applied to the same part of a linear system the following expressions must also hold:

$$\sum_{k=1}^{n} e_k(t) = ne_1(t) \to \sum_{k=1}^{n} w_k(t) = nw_1(t) \tag{3}$$

Now if the time-varying excitation function $e(t)$ is approximated by a series of step functions $\Delta e(\tau)$ successively displaced in time t by an amount $\Delta \tau$, then by the principle of superposition the following is obtained (7):

$$w(t) = e(0) w_u(t) + \int_0^t \frac{de(\tau)}{d\tau} w_u(t-\tau)d\tau \tag{4}$$

The integral in Eq. 4 is known as the "superposition integral" or Duhamel's integral. The "system function" $w_u(t)$ is the response of an initially relaxed linear system to a unit step input, and $w(t)$ is the response of the system to load $e(t)$. When $w_u(t)$ is replaced by the response to a step load function of any magnitude, it is labeled a response function $R(t)$, which is comparable to the creep responses obtained by experimentation. The response function $R(t)$ is approximated by an exponential Dirichlet series,

$$R(t) = \sum_{i=1}^{n} G_i \exp - (t-\tau) \delta_i \tag{5}$$

where G_i and δ_i are the coefficients selected using the least-squares curve fit method (8). When the excitation function is a sine-squared function such that

$$e(t) = \begin{cases} \sin^2 \omega t & 0 < t \leqslant \text{duration of } e(t) \\ 0 & \text{Duration of } e(t) < t \leqslant \text{period of } e(t) \end{cases} \tag{6}$$

then Eq. 4 becomes

$$w(t) = \int_0^t \frac{d \sin^2 \omega t}{d\tau} \sum_{i=1}^{n} G_i \exp - (t-\tau)\delta_i \tag{7}$$

The solution to Eq. 7 was obtained by a computer program written under contract by the Massachusetts Institute of Technology (8). The program output is a time-varying function that represents total and accumulative displacement (defined later) for a sine-squared time configuration of the excitation load function for any specified period and duration.

MATERIALS

A 3-layer flexible pavement system consisting of a clay subgrade, crushed stone base, and asphalt concrete surface was constructed in a 10 × 10 ft × 8 ft deep concrete test pit. The density of the compacted lifts of the clay subgrade averaged 106.7 lb per cu ft, which was 97 percent of AASHO T-99. The average moisture content at the beginning of testing was 17.7 percent, which was slightly higher than the 16.3 percent optimum moisture from T-99.

The crushed stone base course was placed in two lifts and had an average compacted thickness of 8.16 in. and density of 147.3 lb per cu ft at 5 percent moisture by the sand cone method. Laboratory density by AASHO T-180 was 157.5 lb per cu ft with optimum moisture of 6.2 percent.

The asphaltic concrete was a commercially available $^3/_8$-in. nominal maximum size asphaltic concrete designated S-5 in the specifications of the Virginia Department of Highways. The density of the compacted asphaltic concrete was determined by nuclear gage measurements that were correlated with 5 cores drilled in nonload areas of the pit. The compacted thickness was 6.62 in. and the average density was 151.0 lb per cu ft. Figure 1 shows the rolling of the asphalt concrete.

INSTRUMENTATION AND ENVIRONMENT

An enclosure built over the entire test pit area allowed the temperature to be maintained to within ±1 F of the desired temperature, 72 F, during the tests. Temperature of the asphaltic concrete pavement was measured by thermocouples at $\frac{1}{2}$, $2\frac{1}{2}$, $4\frac{1}{2}$, and $6\frac{1}{2}$-in. depths at two locations. Temperature and moisture content in the subgrade were measured by Soiltest MC-310A Soil Moisture Cells.

Vertical pressure in the soil subgrade was measured by two types of soil pressure cells. All cells were first calibrated in an airtight triaxial chamber and then one cell of each type was calibrated in a 5 × 5 × 5 ft pit of compacted clay and at depths similar to those used in the prototype and under essentially uniform stress distribution with depth.

Pressure cell, strain gage, and LVDT locations are shown in Figure 2, and a schedule of the strain gage and LVDT locations is given in Tables 1 and 2 respectively.
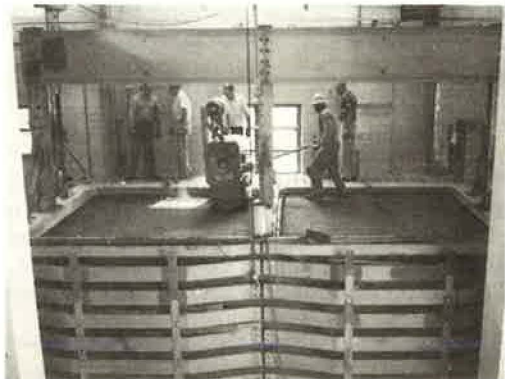

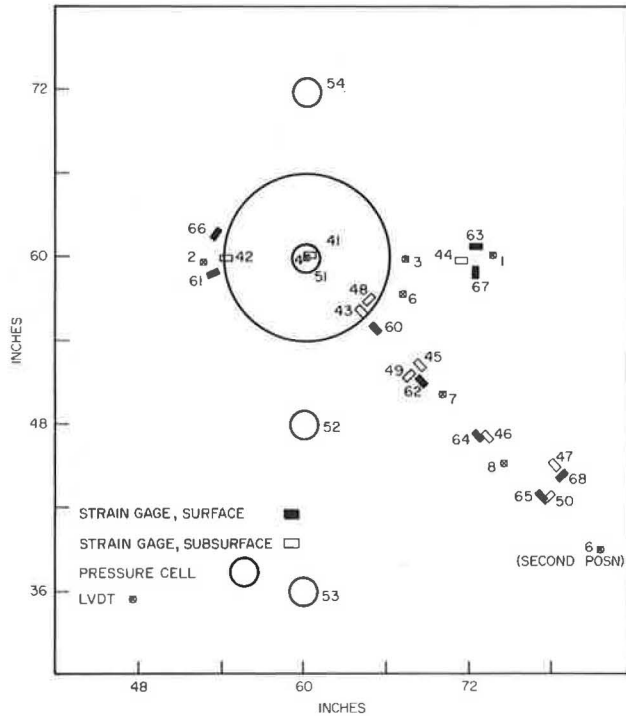Figure 1. Preparing the asphalt concrete surface.

Figure 2. Load cell, LVDT, and strain gage placements.

Radial and transverse strains on the surface and on the underside of the asphaltic concrete were measured by 0.75-in. long Micro-Measurement encapsulated 120-ohm temperature-compensated strain gages. Installation of the strain gages beneath the asphaltic concrete was accomplished by laying down a very thin layer of sand asphalt, averaging $3/8$-in. thick, which covered a slightly greater area than the area to be gaged. Output of the strain gages was measured by including the mounted gage as the one active arm in a 4-arm Wheatstone bridge. Temperature compensation necessary for the surface gages was attained by using dummy gages identically mounted on the asphaltic concrete surface of an adjacent identically prepared pavement.

Deflection of the surface of the pavement was detected by Schaevitz linear variable differential transformers readable to 0.0001 in. The LVDTs were supported by aluminum channel beams bolted

TABLE 1

STRAIN GAGE LOCATIONS

	Subsurface		Surface
Gage No.	Radial Distance From Center of Load (in.)	Gage No.	Radial Distance From Center of Load (in.)
41	0.0	60	7.16
42	6.00	61	6.82
43	5.57	62	12.31
44	11.13	63	12.16
45	11.32	64	17.85
46	17.78	65	24.10
47	23.42	66	6.89
48	5.51	67	12.10
49	11.43	68	24.12
50	24.58		

TABLE 2

LVDT LOCATIONS

LVDT No.	Radial Distance From Center of Load (in.)	LVDT No.	Radial Distance From Center of Load (in.)
1	13.5	6	7.54 (30.0 after test 80-1)
2	7.63		
3	7.75	7	13.79
4	0.0	8	20.50
5	11.5 (Subgrade)		

to the walls of the pit as shown in Figure 3, which also shows the LVDT arrangement and a view of the adjustable holder for the LVDTs. LVDT 5, a subsurface device, became inoperable and produced no usable data.

Pavement loading was accomplished with MTS Systems Corporation's electronic servo-type hydraulic equipment. The load was transmitted to the pavement through a water-filled doughnut-shaped rubber bag 12 in. in diameter with a $2\frac{1}{4}$-in. diameter center hole, also shown in Figure 3. A doughnut-shaped rubber pad of 109.14 sq in. was placed under the water bag to reduce the radial strain on the surface caused by friction.

TEST SEQUENCE

Haversine load functions as shown in Figure 4 and a step function were selected as the excitation configurations. Duration of loading was varied in order to determine this effect on the response of the pavement. Table 3 gives the period and duration for each type of test. A static (creep) test was run at each load level to obtain a characterization of the pavement system. Tests were conducted at four levels of load
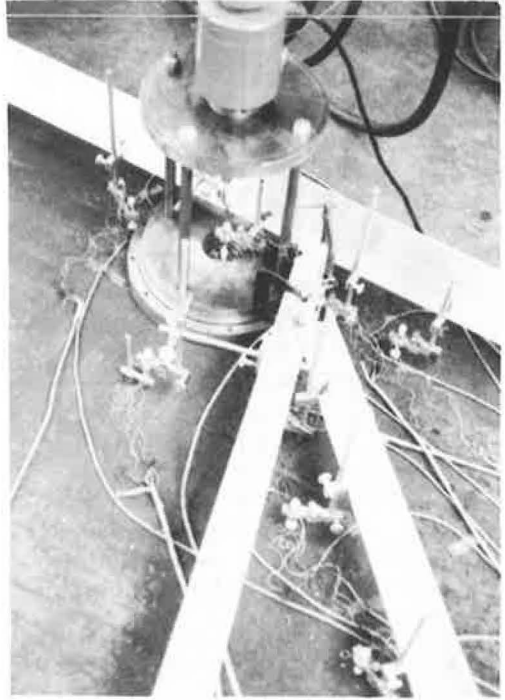

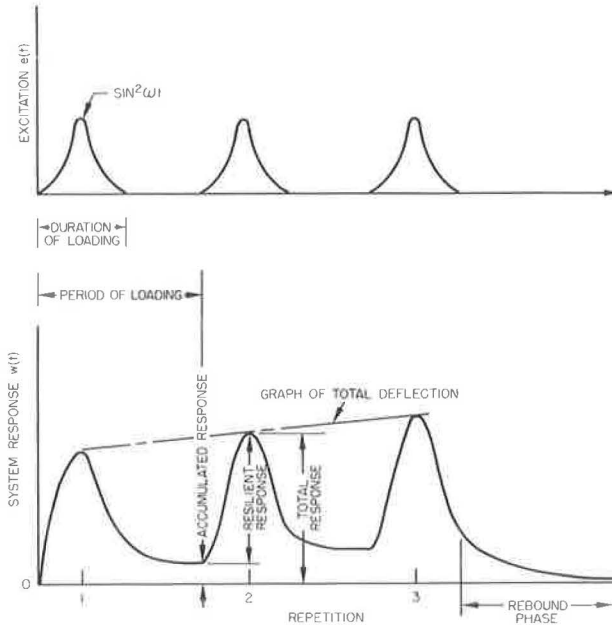Figure 3. Arrangement of LVDTs and rubber bag.

Figure 4. Excitation and pavement response functions.

intensity in the following sequence: 10, 20, 40, 80, 40, 20, 10 psi. At each of the first four load levels, tests were conducted in the sequence A, B, C, A, B, C; at the last three load levels, only one A, B, C cycle was conducted. Tests are numbered in essentially the order performed at each level. Tests with (d) after their number were those performed in descending order after the last 80-psi test.

TABLE 3
PERIOD AND DURATION OF TESTS

Type of Test	Desig-nation	Load Duration (sec)	Period of Loading	No. of Applications of Load
Repeated	A	0.1	1 sec	1,000
Repeated	B	0.5	1 sec	1,000
Static (Creep)	C	—	15 min	1

A total of 42 tests were performed on the pavement. Of this number, 35 were analyzed; 28,000 repetitions of load and 210 minutes of static loading were applied to the pavement.

EXPERIMENTAL RESULTS

Average pressures recorded under the center of the load for type A and type B tests for each of the four load levels increase linearly with load, as shown in Figure 5. Observed values for other cells as well as the accumulated pressures on the center cell were erratic.

Deflection is classified as accumulated, resilient, and total, as illustrated in Figure 4. The accumulated deflection is that which remains in the pavement after removal of the load and immediately before the application of the next repetition. Resilient deflection is that deflection which takes place during application of the load, and total deflection is the sum of the accumulated and resilient deflections at any repetition.

Total center deflection vs. repetitions for LVDT 4 is shown in Figure 6, which indicates a linear relationship between deflection and load. This was observed for all types of tests and is also shown for LVDT 2 in Figure 7. The successive tests for each load level replicate each other extremely well.

A pavement would normally be expected to condition, that is, to densify so that deflections of later tests are in all cases less than that for earlier tests of the same load and type; however, the conditioning that does take place is insignificant under load within the range of measurement. Conditioning is observable in the rate and amount of
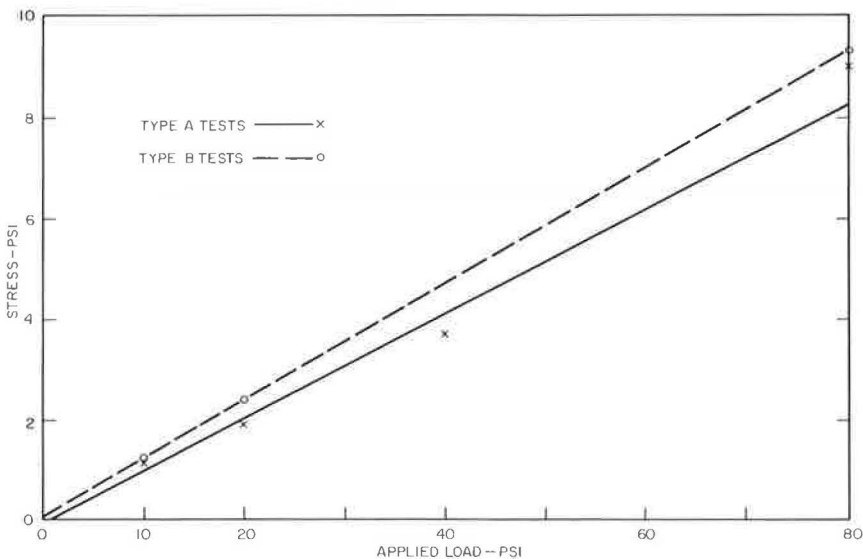

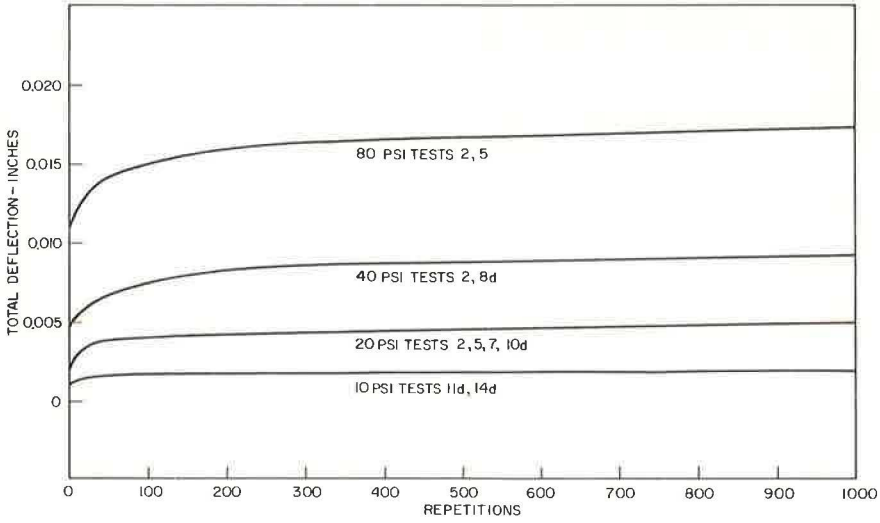Figure 5. Center pressure cell, resilient stress vs. applied load.

Figure 6. Effect of load, type B tests, LVDT 4 (center).

recovery of the accumulated deflection during the rebound phase. In that situation, most of the irrecoverable deflection was essentially completed after the 40-psi series.
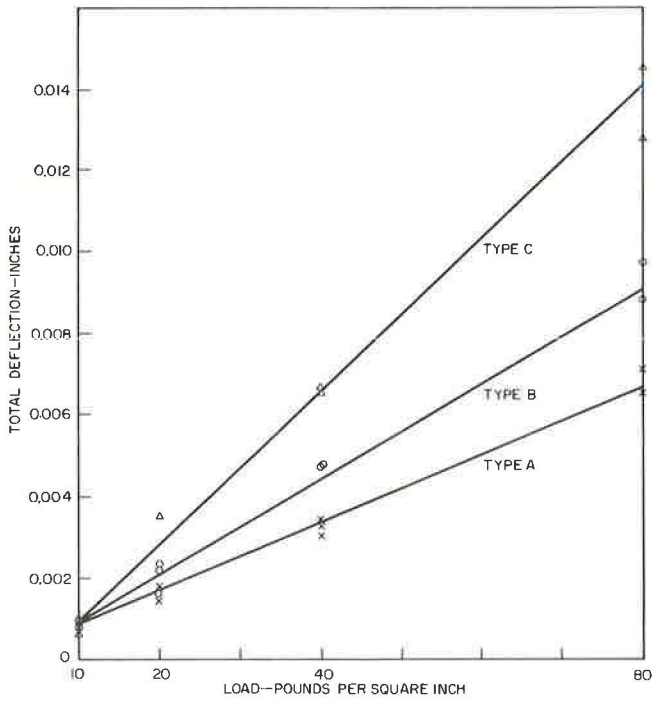

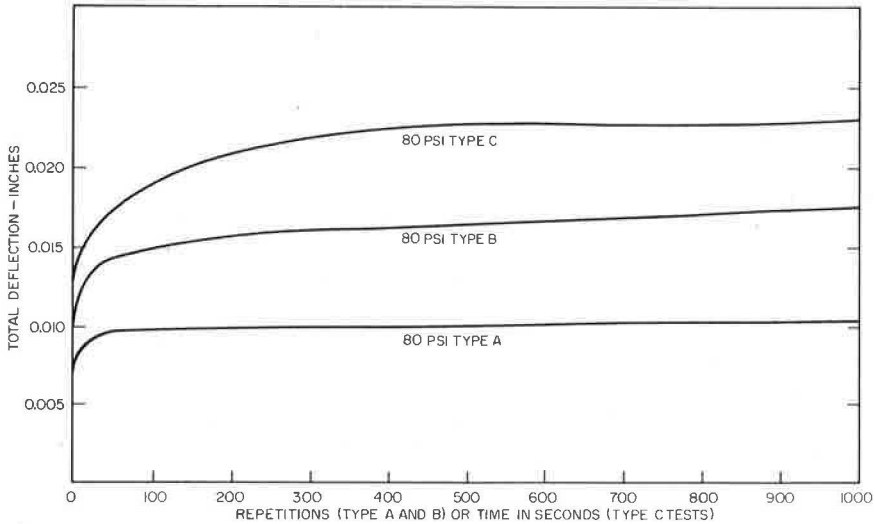Figure 7. Total deflection vs. applied load at repetition 600, LVDT 2.

Figure 8. Effect of load duration: total deflection, LVDT 4 (center), 80 psi.

Figure 8 is a plot of total center deflection vs. time for the three types of tests at 80 psi. The effect of load duration on displacement is quite obvious at this load level, e.g., the type C test producing the greatest and the type A test the least amount of deflection. At distances greater than 13.8 in., the effect of the load duration on deflection becomes less significant.

Figure 9 shows the accumulated and resilient components of the total deflection for a type A and a type B test at the 40-psi load level. The resilient deflection as well as
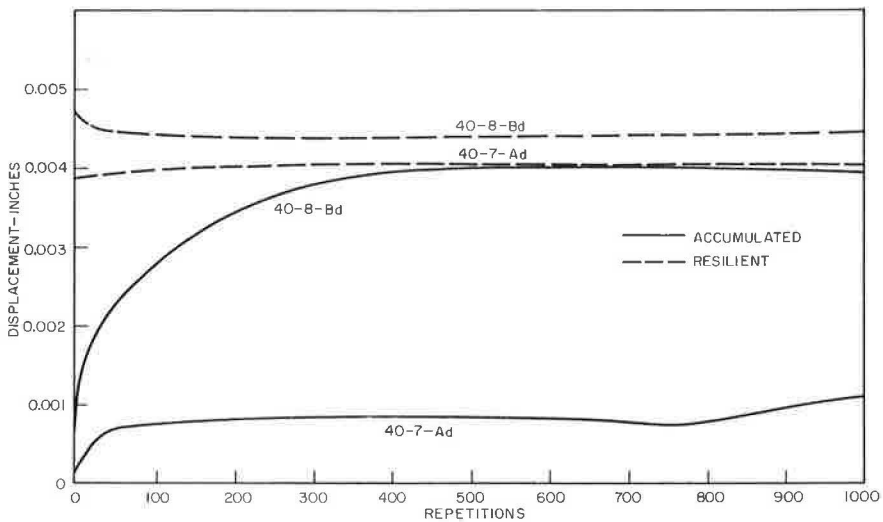

Figure 9. Effect of load duration: resilient and accumulated deflection, LVDT 4 (center), 40 psi.

the accumulative deflection for all type B tests is consistently higher than that of the type A tests, reflecting the effect of longer load durations. A large part, usually 30 to 40 percent of the total accumulated deflection at the center of the loaded area and 60 to 80 percent at more remote locations, occurs in the first 5 repetitions of the load.

A paradox that appeared in the tests is a lessening of accumulated deformation (an apparent rise in the unloaded pavement profile) at distances of 12 to 13 and sometimes up to 20 in. from the center of the load. The unloaded pavement profile seems to reach a maximum deflection at around 60 repetitions, with the most visible bulge at about 600 repetitions. Figure 10 depicts the pavement cross section and shows this effect for a type C test.

Strains were also separated into resilient and accumulative components. The resilient strain remained fairly constant for each individual test for most gages and is basically linear for both surface and subsurface gages, as shown in Figure 11 for the 12-in. radial surface and subsurface gages (62 and 45).

Figure 12 is a plot of type B test total strain vs. repetitions for the 12-in. radial subsurface gage (45). This figure indicates a linear increase in total strain with load and is typical of all subsurface gages and of surface gages located within approximately 8 in. from load center for type A and B tests. A nonlinear variation of total strain is, however, typical for all surface gages located over 11 in. from load center for type A and B tests. These gages register tension under load but show accumulation of strain in compression. This "opposite" effect is shown in Figure 13 for gage 62 along with the strain response for radial gage 60, which acts as would be expected, i. e., the accumulation of strain is in the same direction as the resilient strain. It is interesting to note that this "opposite" effect occurs in the same general area of the pavement surface as does the rise in the unloaded displacement profile.

In type C tests the 7-in. surface and subsurface gages register strains that continuously increase under sustained load. All other gages, including the center subsurface gage (41), exhibit a reversal of the direction of straining. A plot of creep strain for gage 41 is shown in Figure 14.

Figures 15 and 16 are representative cross sections of surface and subsurface radial and transverse strains observed at repetition 60. Notice that the subsurface resilient strains are in general larger than the surface resilient strains. A point of inflection is indicated in both the surface and subsurface radial gages. No inflection point is indicated in the transverse strain profile.

ANALYSIS

Total and accumulated displacements for type A and B tests were predicted for center and 7.75-in. radial locations using the Boltzmann superposition principle. Comparisons with measured values are shown in Figures 17 through 20. The predicted values were obtained by fitting a Dirichlet series to the creep curves obtained at a
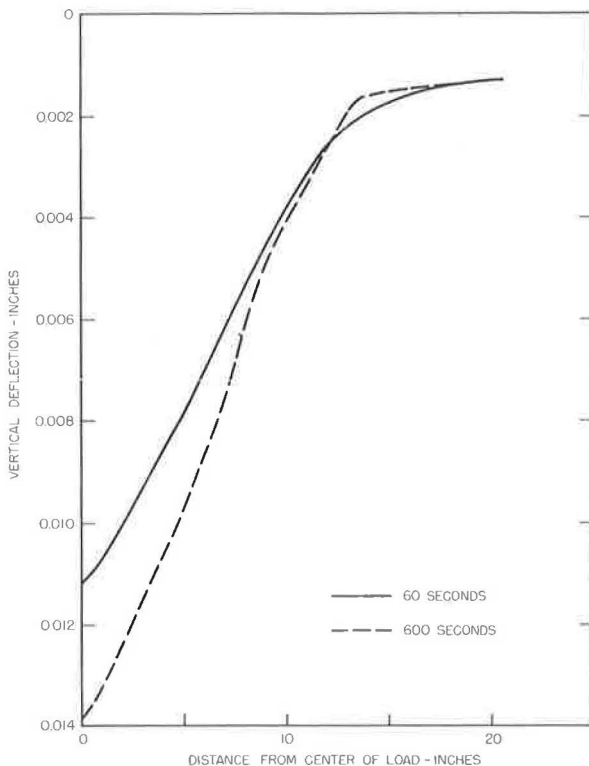
Figure 10. Cross section 40-3-C.
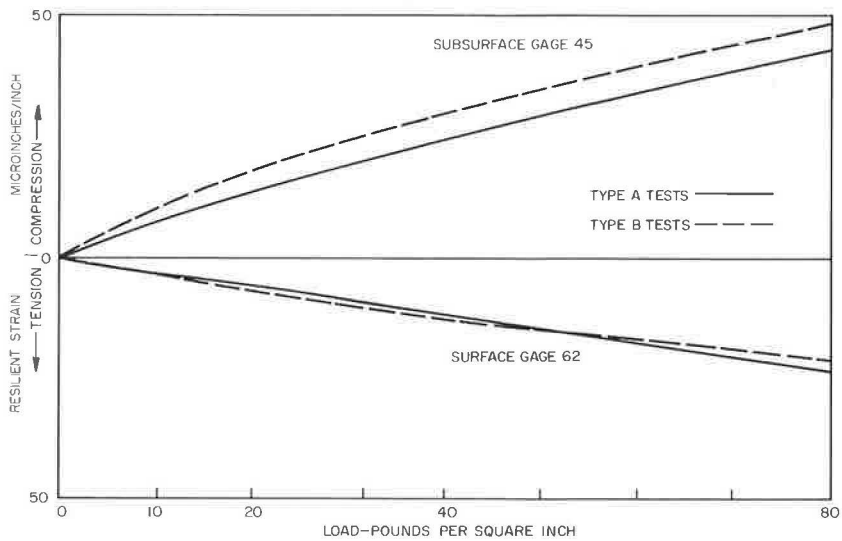
Figure 11. Resilient strain at repetition 300, 12-in. radial surface and subsurface gages.
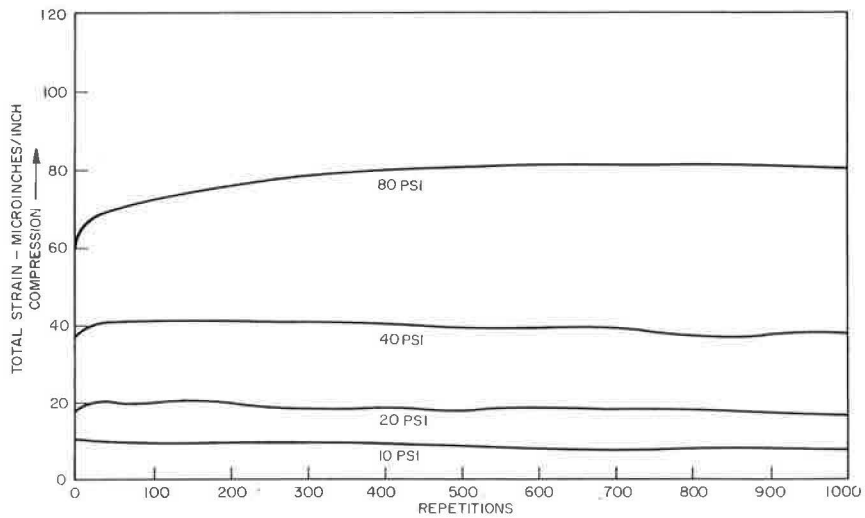
Figure 12. Effect of load on total strain: gage 45, 12-in. radial subsurface, type Bd tests.
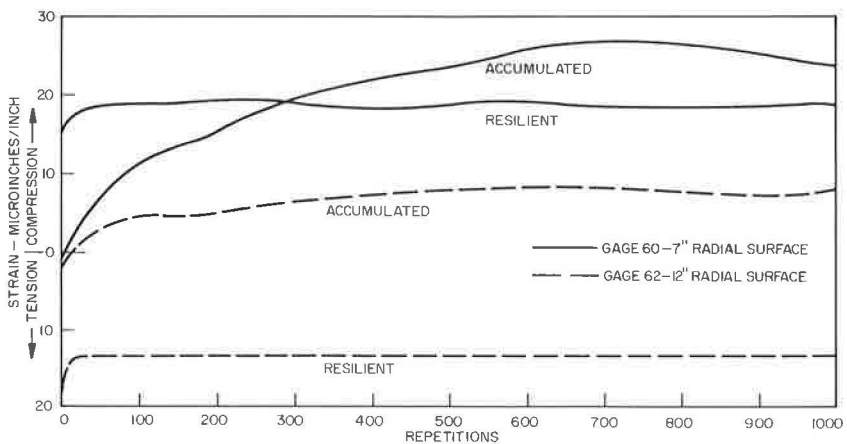
Figure 13. Resilient and accumulated strain for a 7- and 12-in. radial surface gage, test 40-8-Bd.

50
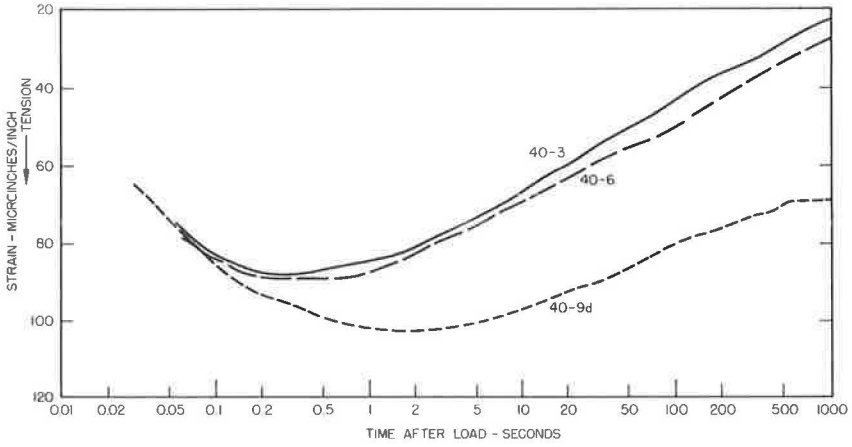
Figure 14. Strain under creep loading: type C tests, gage 41, center subsurface, 40 psi.
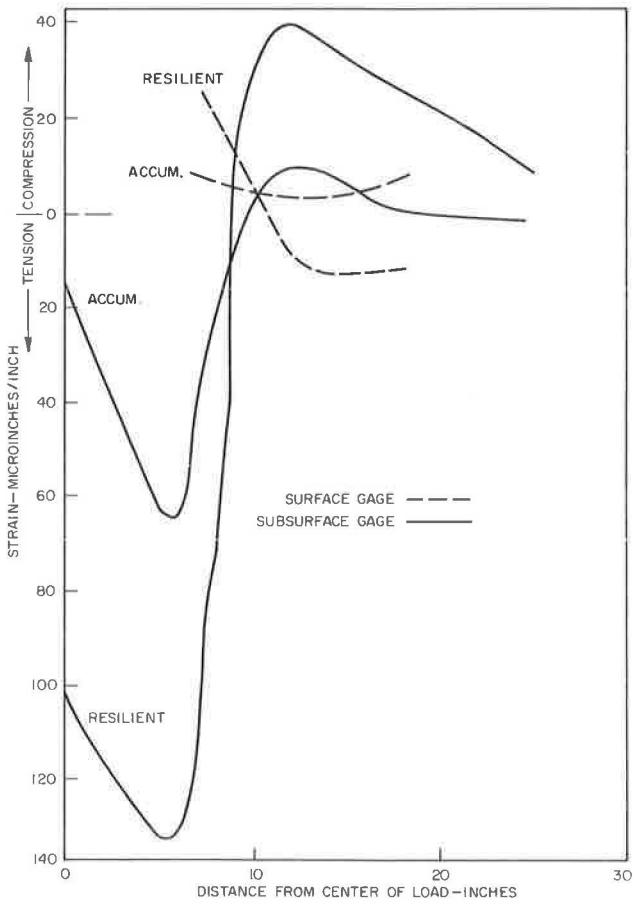
Figure 15. Cross section of test 40-8-Bd, radial strain at repetition 60.
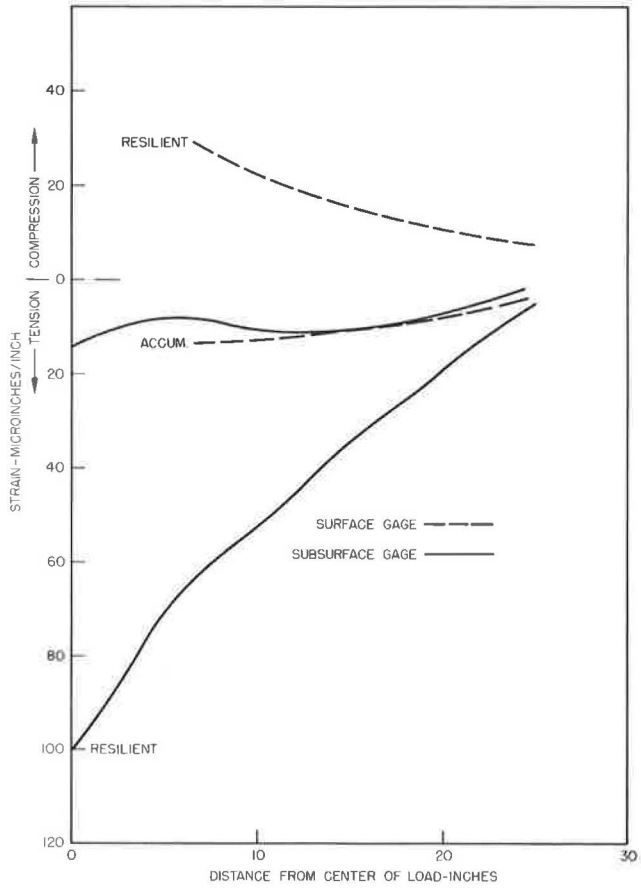
Figure 16. Cross section of test 40-8-Bd, transverse strain at repetition 60.
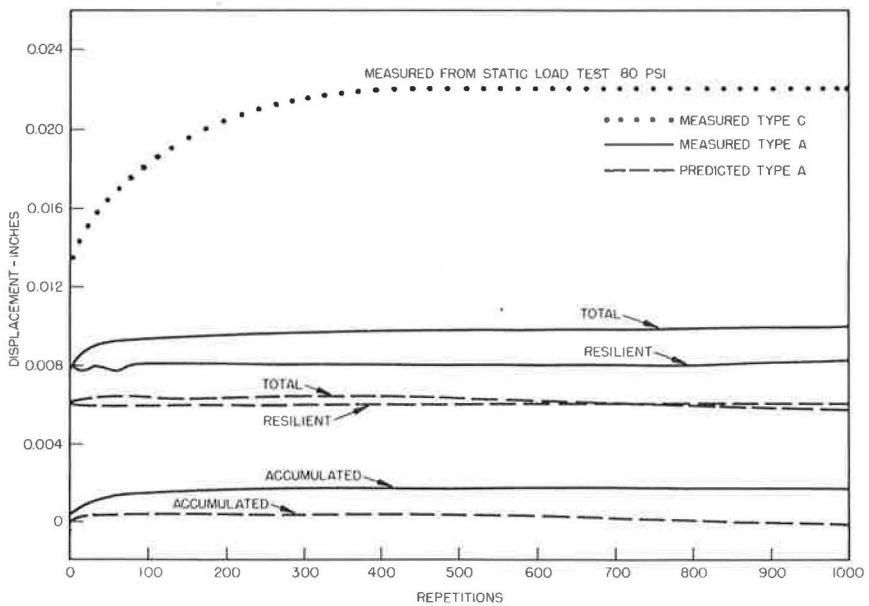
Figure 17. Predicted center surface displacements, type A, 80 psi.

52
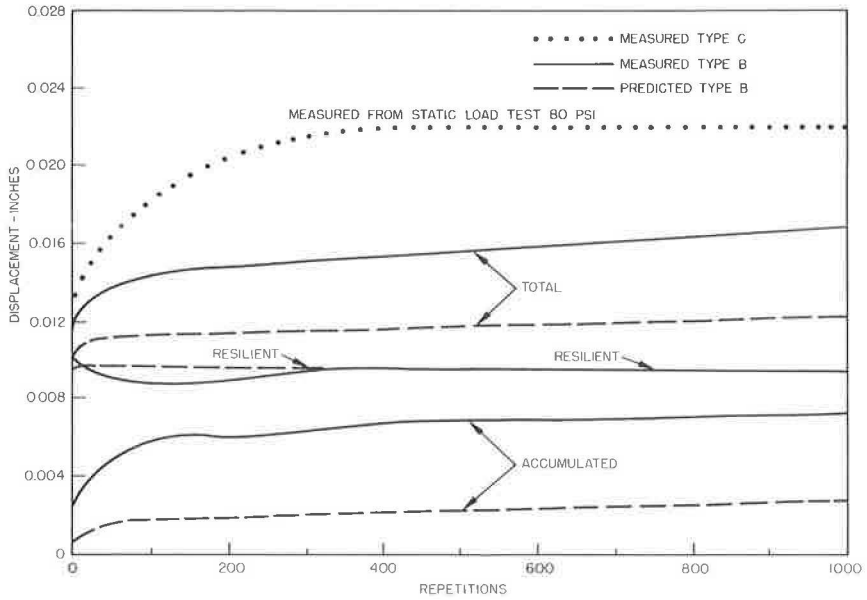
Figure 18. Predicted center surface displacements, type B, 80 psi.

specified LVDT location. The coefficients G_i and δ_i were obtained from the fitted curve and used as input to the computer solution of the superposition integral, Eq. 7. The resulting predicted displacements for an 80-psi type A and B test at load center are shown
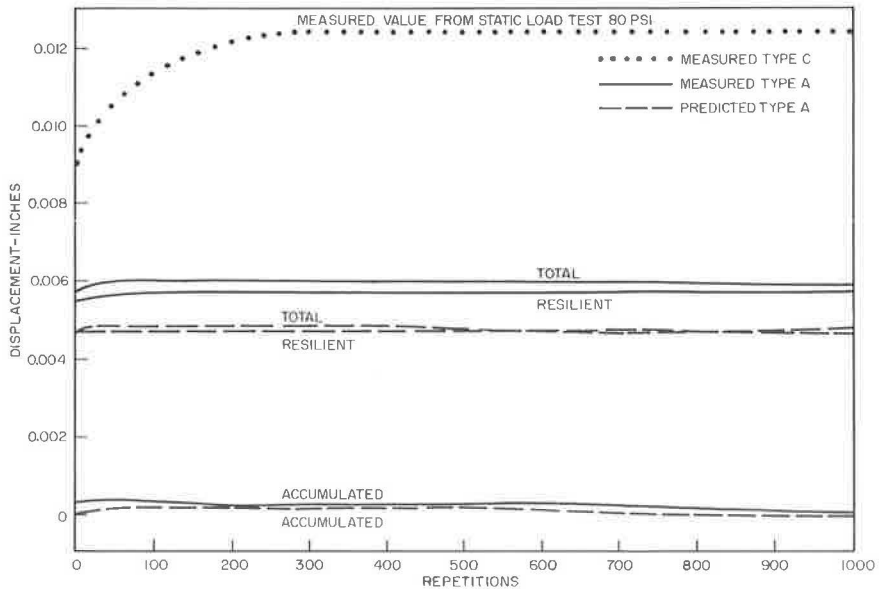
Figure 19. Predicted displacements at 7.75 in., type A, 80 psi.
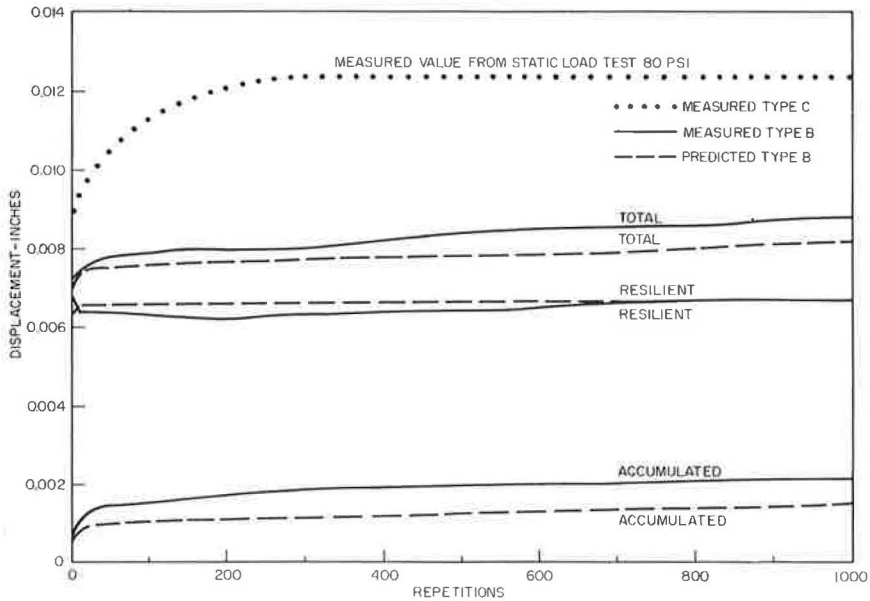
Figure 20. Predicted displacements at 7.75 in., type B, 80 psi.

in Figures 17 and 18 respectively. Similar trends were obtained for the 80-psi type A and B test at 7.75-in. from load center, as shown in Figures 19 and 20 respectively.

A measure of the degree of linearity and time-dependency of the system may be obtained by comparing measured and predicted values. It is interesting to note the excellent agreement between measured and predicted resilient displacements for type B tests, as shown in Figures 18 and 20. Predicted and measured resilient displacements for type A tests also agree rather well, although to a lesser extent.

The time-dependent nature of the system is revealed from comparisons of both predicted and measured resilient displacements with the limiting (values beyond 400 sec) displacement measured in static (creep) tests. Ratios of measured limiting static displacement to measured resilient displacement range from 2.0 to 2.7, whereas ratios of predicted resilient displacement to measured resilient displacement range from 0.75 to 1.04.

Also shown in the figures are values of accumulated and total displacements. The most significant accumulated displacement curve is shown in Figure 18 for type B 80-psi tests. The discrepancy observed between measured and predicted accumulative displacement could be attributed to the conditioning experienced by the pavement during the first 5 to 10 repetitions of load. However, a cursory investigation of the creep recovery curves suggests that better approximations of accumulated values may be obtained by using both the creep curve and the creep recovery curve as input to the superposition integral. Only the creep curve was used in this analysis.

Negligible amounts of accumulated displacement are predicted for the type A tests and consequently resilient values approach total values. This is reflected in the measured resilient displacements, which are almost identical to the total displacements.

CONCLUSIONS

1. Observations of the total, accumulative, and resilient deflections as well as of the strains that occur during repetitive and creep tests all point toward the time-dependent nature of the system.

2. Observed deflections are basically linear with load for each specific type of test. Observed resilient strains also tend to be linear with load for each type test.

Gages that exhibit an "opposite" or reversal effect produce total strains that are basically nonlinear with load.

3. A rise in the unload displacement profile of the pavement is noted in the same general area (11 to 20 in. from load center) as the "opposite" effect exhibited by strain gages.

4. The use of superposition integral to predict resilient and accumulative displacements from a system creep test reflects the linear time-dependent nature of the flexible pavement for the load levels and time configurations used.

REFERENCES

1. Hudson, W. R., Finn, F. N., McCullough, B. F., Nair, K., and Vallerga, B. A. Systems Approach to Pavement Design. Final Report, NCHRP Project 1-10, Highway Research Board, March 1968.
2. Coffman, B. S. Pavement Deflections From Laboratory Tests and Layer Theory. Proc. Second Internat. Conf. on the Structural Design of Asphalt Pavements, Univ. of Michigan, 1967.
3. Monismith, C. L., Seed, F. G., Mitry, F. G., and Chan, C. K. Prediction of Pavement Deflections From Laboratory Tests. Proc. Second Internat. Conf. on the Structural Design of Asphalt Pavements, Univ. of Michigan, 1967.
4. Klomp, A. J. G., and Niesman, T. W. Observed and Calculated Strains at Various Depths in Asphalt Pavements. Proc. Second Internat. Conf. on the Structural Design of Asphalt Pavements, Univ. of Michigan, 1967.
5. Raithby, K. D., and Sterling, A. B. The Effect of Rest Periods on the Fatigue Performance of a Hot-Rolled Asphalt Under Reversed Axial Loading. Paper presented at 1970 AAPT annual meeting.
6. Swami, S. A., Goetz, W. H., and Harr, M. E. Time and Load Independent Properties of Bituminous Mixtures. Highway Research Record 313, 1970, pp. 63-78.
7. Cheng, D. K. Analysis of Linear Systems. Addison-Wesley Inc., 1959.
8. Moavenzadeh, F., and Elliott, J. F. Moving Load on Viscoelastic Layered System. Interim report prepared for Bureau of Public Roads by the Massachusetts Institute of Technology.

A Procedure for Evaluating Pavements With Nonuniform Paving Materials

JAMES R. LEVEY, Illinois Division of Highways; and
ERNEST J. BARENBERG, Department of Civil Engineering, University of Illinois

A procedure was developed to evaluate layered systems with nonuniform material properties. The procedure consists of defining the layered system by a physical model consisting of mass points tied together by springs and bars. The variability of the material is simulated by assigning different characteristics of the material properties to springs connecting the mass points. Assignment of values representing the material properties is done on a random basis. The random values are generated in a manner that produces a model with mean characteristics corresponding to the mean properties of the materials in the various layers of the pavement, and with a coefficient of variation compatible with the coefficient of variation of the corresponding paving material.

Results from the study show that the response of the layered system is influenced by the statistical characteristics of the materials. The statistical nature of the response is influenced by both the variability of the material and the nature of the variability. A large area with slightly less than average stiffness has a greater influence on the response of the system than a large difference in stiffness over a small area. Thus, detailed analyses are necessary to obtain a comprehensive understanding of the behavior of the system. Much work still needs to be done to obtain a complete picture of the statistical nature of pavement response. Preliminary results strongly indicate a need for the type of analysis presented in the paper as a guide for establishing realistic quality control criteria for paving materials. With results from such a procedure it is possible to establish a cost benefit from higher quality control criteria.

•PAVING MATERIALS, because of their heterogeneous nature, have natural or inherent variations in their physical properties. This natural variability is compounded by nonuniformity in the material due to construction processes and techniques. Taken together, these variations may have a profound effect on the behavior and performance of pavement systems.

Little is known about the manner and extent of influence that material variability has on the behavior of pavements. It is known that pavements do exhibit significant variations in response to loads (1, 2, 3, 4), and this variability can often be attributed to nonuniformity in the paving materials. What is not clear is what role the variability in the various layers of the pavement plays in the nonuniform behavior of the overall pavement.

To evaluate the effects of nonuniform paving materials on the behavior of pavements it is necessary to (a) know the effect of the magnitude of material variability on the behavior of the pavement system, (b) know the effects of the size of the defect on the behavior of the pavement system, and (c) know the magnitude of variability of in-place paving materials. In this paper, a procedure is developed that can deal directly with items a and b. Item c can be evaluated indirectly by correlating the observed behavior of actual pavements with the results obtained from the procedure outlined here.

It is important to know the relationships between material variability and pavement behavior due to the increased use of statistical quality control techniques. The present statistical quality control plans are based on the present level of control being delivered. The procedure developed herein can be used to evaluate various levels of material variability so that the optimum level of control can be determined.

Knowledge of the effect of defect size and severity on pavement performance is important for aiding inspectors in applying non-statistical sampling techniques. If the material is only slightly substandard or if the quantity of defective material is small, the decision between acceptance and rejection becomes unclear. The procedure presented here can be used to determine whether the substandard or defective material is critical, i.e., whether it would cause a noticeable decrease in pavement performance. The relationship between the size of the critical defect and its deviation from the standard would define the characteristics of the critical defect.

The specific objective of this paper is to describe the procedures developed to evaluate the statistical nature of load-induced stresses, strains, and deflections in pavements having materials with variable physical characteristics. While the procedure can be applied to a three-dimensional problem, the example solutions and applications given in this paper are limited to the two-dimensional plane strain case because of limited capacity of available computer systems.

DEVELOPMENT OF THE SOLUTION PROCEDURE

The method for determining the response of the pavement system due to variable material properties is based on a mathematical discrete element model. By using this type of model to represent the pavement system, the material properties can be varied from point to point, and in this way the variability of the material properties can be incorporated into the solution. The nature of the variability of the response can be determined by randomly selecting for every point in the model values for the material properties from their respective statistical populations and repeatedly solving the layered structural system using sets of material properties selected on a random basis. A sufficient number of solutions must be developed to evaluate the statistical nature of the pavement response.

Discrete Element Model

The discrete element mathematical model used in this work was developed by Ang and Harper ($\underline{5}$, $\underline{6}$). The physical analog of the mathematical model consists of a two-dimensional rectangular grid of mass points connected on the diagonals by stress-strain elements. The mass points form the basis for deflection analysis while stresses, strains, and their relationships are defined at the intersections of the stress-strain elements, i.e., at the stress points. A typical section of the physical model is shown in Figure 1.

In mathematical terms, the model used is the central finite difference approximation of the basic differential equations from the theory of elasticity assuming plane strain. From the theory of elasticity the differential equations for relating deflection and strain are
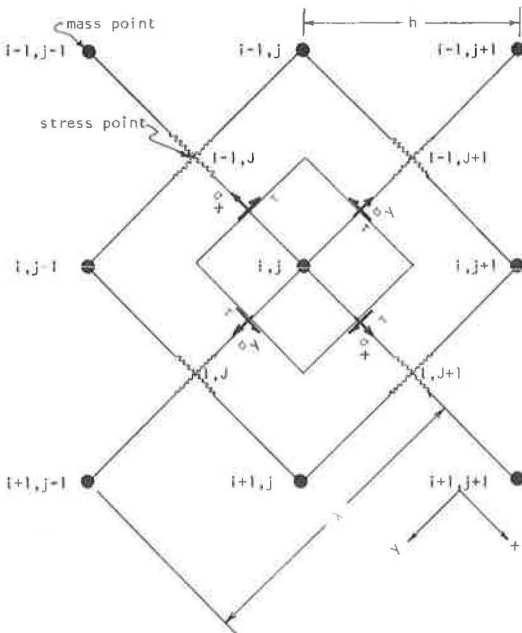

Figure 1.   A typical section of the interior of the discrete element model.

$$\epsilon_x = \frac{\partial u}{\partial x}, \quad \epsilon_y = \frac{\partial v}{\partial y}, \text{ and } \gamma_{xy} = \frac{\partial u}{\partial y} + \frac{\partial v}{\partial x}$$

where x and y are the two coordinate axes (Fig. 1), u and v are the deformations in the x and y directions respectively, E_x and E_y are the axial strains in the x and y directions respectively, and Y_{xy} is the shear strain (7). The corresponding central finite difference equations relating strain and deflection at stress point I, J (Fig. 1) are

$$\epsilon_{x_{I,J}} = \frac{u_{i+1,j} - u_{i,j-1}}{\lambda}$$

$$\epsilon_{Y_{I,J}} = \frac{v_{i+1,j+1} - v_{i,j}}{\lambda}$$

and

$$\gamma_{xy_{I,J}} = \gamma_{I,J} = \frac{u_{i+1,j-1} - u_{i,j}}{\lambda} + \frac{v_{i+1,j} - v_{i,j-1}}{\lambda}$$

where λ is the diagonal spacing of the mass points.

Again from elastic theory the equations relating stress and strain are

$$\sigma_x = C\epsilon_x + B\epsilon_y$$

$$\sigma_y = C\epsilon_y + B\epsilon_x$$

and

$$\tau_{xy} = G\gamma_{xy}$$

where

$$C = \frac{E(1-\mu)}{(1+\mu)(1-2\mu)}$$
$$B = \frac{E\mu}{(1+\mu)(1-2\mu)}$$
$$G = \frac{E}{2(1+\mu)}$$

σ_x and σ_y are the normal stresses in the x and y directions respectively, τ is the shear stress, E is Young's modulus of elasticity, and μ is Poisson's ratio (7). Since no differentials are involved in these equations, the central finite difference forms for these equations are identical with those for the elastic theory.

This problem is being solved in terms of deflections, and therefore the only other equations needed are the equilibrium equations. Assuming that body forces and accelerations are zero (4), the differential equation for equilibrium in the x direction is (7)

$$\frac{\partial \sigma_x}{\partial x} + \frac{\partial \tau_{xy}}{\partial y} = 0$$

The corresponding central finite difference approximation for this equation at mass point i, j (Fig. 1) is

$$\left(\sigma_{x_{I,J+1}}\right)\frac{\lambda}{2} + \left(\tau_{I,J}\right)\frac{\lambda}{2} - \left(\sigma_{x_{I-1,J}}\right) - \left(\tau_{I-1,J+1}\right)\frac{\lambda}{2} = 0$$

Dividing by the volume represented by each mass point $(\lambda^2/2)$ and rearranging gives

$$\frac{\sigma_{x_{I,J+1}} - \sigma_{x_{I-1,J}}}{\lambda} + \frac{\tau_{I,J} - \tau_{I-1,J+1}}{\lambda} = 0$$

The corresponding differential and finite difference equations for equilibrium in the y direction are

$$\frac{\partial \tau_{xy}}{\partial x} + \frac{\partial \sigma_y}{\partial y} = 0$$

and

$$\frac{\tau_{I,J+1} - \tau_{I-1,J}}{\lambda} + \frac{\sigma_{y_{I,J}} - \sigma_{y_{I-1,J+1}}}{\lambda} = 0$$

By substitution, the equilibrium equations for point i, j can be expressed in terms of the deflections of point i, j and the eight surrounding points. These equations are presented in the form of computational molecules as shown in Figure 2. A portion of the equilibrium equation in the x direction would be

$$\Sigma F_x = (C_{I-1,J}) u_{i-1,j-1} + (B_{I-1,J} + G_{I-1,J+1}) v_{i-1,j} + \cdots$$

$$+ (C_{I,J+1}) u_{i+1,j+1} = 0$$

Boundary Conditions

To apply the model to typical pavement structures it is necessary to define consistent boundary conditions for the model (5). Three types of boundary conditions must be evaluated: (a) the boundary conditions at the pavement surface, including a means for applying external forces; (b) boundary conditions for the remainder of the perimeter; and (c) the boundary conditions for the interfaces between layers.

The equations defining the surface boundary condition can be determined by defining the equilibrium of the surface mass points. The equilibrium equations can be developed in terms of the deflection of the mass points at the surface. A typical surface mass point with the stresses acting on the point is shown in Figure 3.

The computational molecules for the equilibrium equations of the surface mass points are shown in Figure 4. Note that the computational molecule is the same as the lower half of its corresponding molecule describing the equilibrium of an internal mass point but that the top half has been replaced by the function of applied stresses and λ shown on the right side of the equation.

The boundaries around the remainder of the perimeter are assumed to be immoveable, and values for u and v for mass points along the perimeter are set at zero.

The boundary condition between layers is assumed to be perfectly rough; that is, there can be no relative movement between any point on the bottom of the upper layer and the corresponding point on the top of the lower layer. This condition is satisfied for the numerical model by defining the boundary through a row of mass points and defining the material properties for
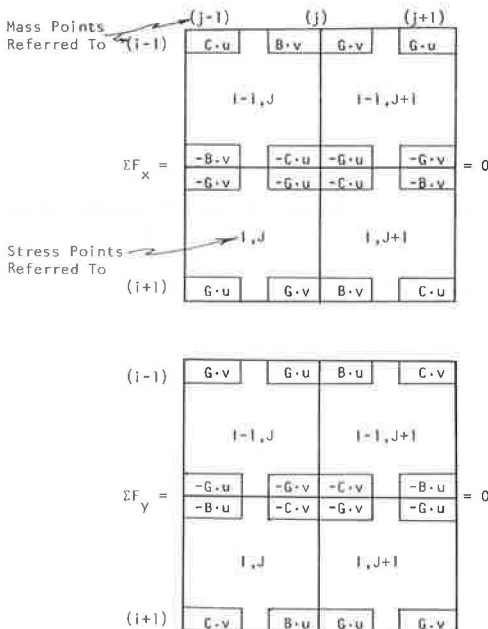
Figure 2. Computational molecules representing the equilibrium equations for an interior mass point in terms of deflections.
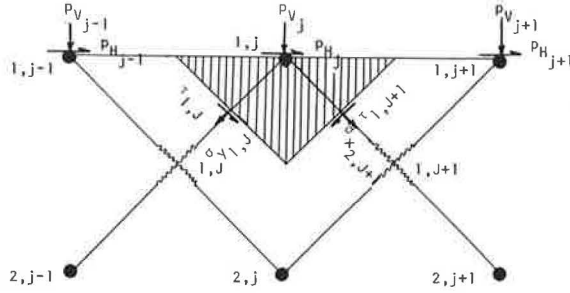
Figure 3. A typical section of the surface of the model.
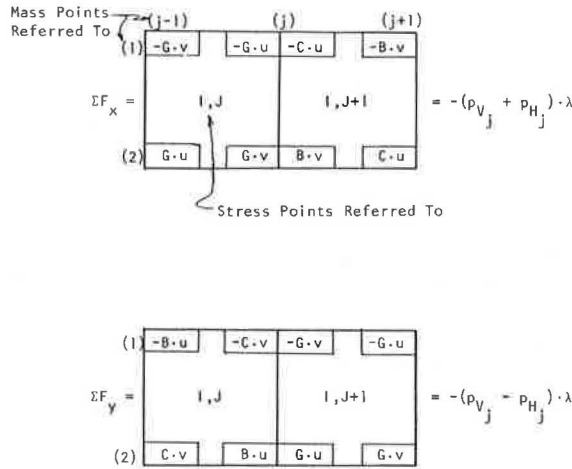
Figure 4. Computational molecules representing the
equilibrium equations for a surface mass point in terms
of deflections.

the stress points above the boundary to correspond with the material in the upper layer
and the properties below the boundary to correspond to the material below the boundary.

Solving the Equilibrium Equations for Unknown Deflections, Strains, and Stresses

The equilibrium equations must be solved for the deflections at each mass point in
the model. A modification of the Gauss elimination procedure was used to solve the
equations for this study. The form of the unmodified coefficient matrix is shown in
Figure 5.

The modification of the Gauss elimination procedure consists of operating on only
the non-zero coefficients in the matrix. Two large groups of zero coefficients are lo-
cated above and below the band of non-zero coefficients shown in Figure 6. Other
groups are located in the cross-hatched areas also shown in Figure 6. The modified
form of the coefficient matrix is shown in Figure 7.

The solutions to the equilibrium equations are obtained by operating on the modified
matrix using a bookkeeping system that relates the location of the coefficients in the

modified matrix to the corresponding coefficients in the unmodified matrix. The storage requirement for the modified matrix and constant vector is $4M^2N + 6MN$ for a model with $M \times N$ mass points and where $N \geq M$.

Generation and Assignment of Random Variables

A random number generator was used to assign the material properties to stress points in the model. The method used is based on the central limit theorem of statistics. To obtain a standard normal, pseudo-random variable this procedure, a series of 12 uniformly distributed pseudo-random numbers were generated, normalized, and summed. Since the mean of the sum was 6, with a standard deviation of 1.0, subtracting 6 from the sum resulted in a standard normal random variable; that is, a variable with a mean of 0 and standard deviation of 1.0. A frequency distribution of 100,000 pseudo-normal, random numbers was generated in this manner to test the validity of the procedure. This frequency distribution is shown in Figure 8.

Figure 5. Form of the coefficient matrix for the equilibrium equations for a problem 10 points deep and 5 points wide.

After the random material properties have been generated, they must be assigned to the stress points. The most straightforward method of assigning the values of a
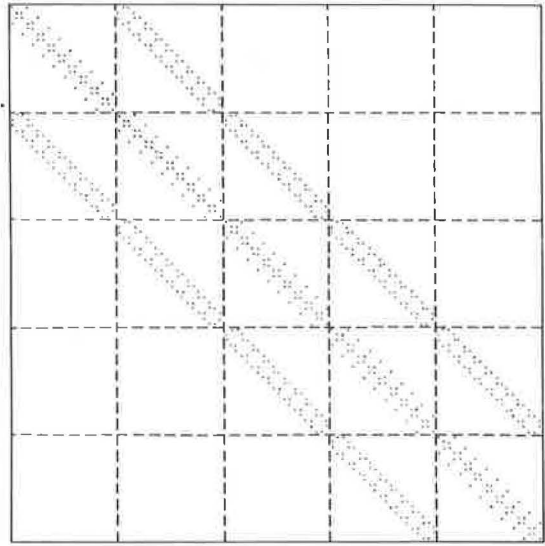

$$D = B + G$$
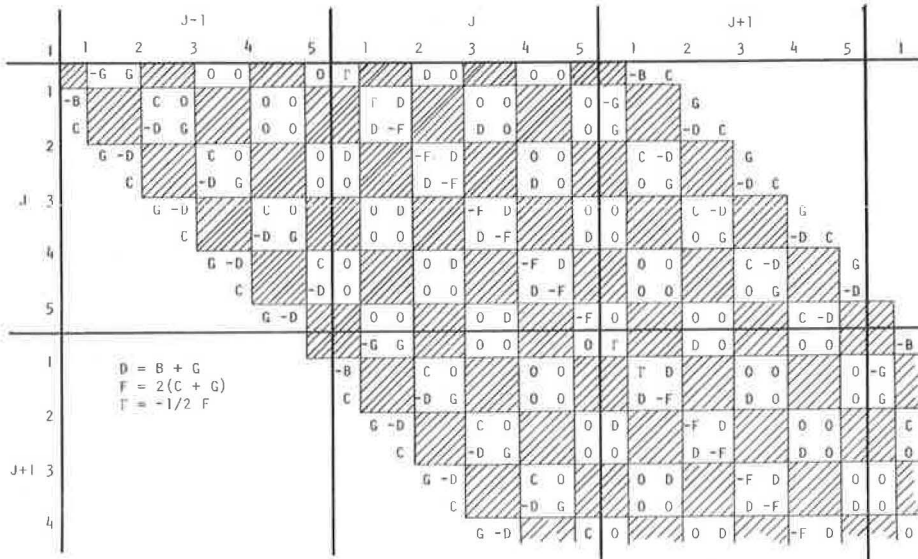$$F = 2(C + G)$$
$$\Gamma = -1/2 \ F$$

Figure 6. A section of the coefficient matrix of the equilibrium equations of a problem 5 points deep before the elimination of unneeded zeros.

random material property to the model is to generate a series of normal random values with the appropriate mean value and standard deviation and to assign each in turn to the stress points of the layer being considered. Typical assignments thus developed are shown in Figure 9.

When the material for a given pavement layer is produced by a batch type of process, a random step function must be used to represent the batch-to-batch variability. The level of each step in the step function is determined by generating normal random numbers using the mean value for the layer and the batch-to-batch standard deviation as parameters. The width of each step, except the first, is related to the area covered for a given batch size. In order to prevent a possible bias, the size of the first step is determined so that it will be a uniformly distributed random value that will be less than the size of the other steps in the layer. The within-batch variability of the material is superimposed on the random step function representing the batch means. By applying this procedure, material properties characterized by a batch-wise variability can be assigned to the stress points of any layer in the pavement. Figure 10 shows an example of two typical assignments.

J	K	1	2	3	4	5	6	7	8	9	10	11	12	13	B
1	1	X	X	X	X	X	X	Γ	D	0	0	0	-B	C	-Px
		X	X	X	X	X	X	Γ	D	0	0	0	-G	G	-Py
	2	X	X	X	X	X	D	-F	D	0	0	G	-D	C	0
		X	X	X	X	X	D	-F	D	0	0	C	-D	G	0
	3	X	X	X	X	0	D	-F	D	0	0	G	-D	C	0
		X	X	X	X	0	D	-F	D	0	0	C	-D	G	0
	4	X	X	X	0	0	D	-F	D	0	0	G	-D	C	0
		X	X	X	0	0	D	-F	D	0	0	C	-D	G	0
	5	X	X	0	0	0	D	-F	0	0	0	G	-D	0	0
		X	X	0	0	0	D	-F	0	0	0	C	-D	0	0
2	1	X	-G	G	0	0	0	Γ	D	0	0	0	-B	C	-Px
		X	-B	C	0	0	0	Γ	D	0	0	0	-G	G	-Py
	2	C	-D	G	0	0	D	-F	D	0	0	G	-D	C	0
		G	-D	C	0	0	D	-F	D	0	0	C	-D	G	0
	3	C	-D	G	0	0	D	-F	D	0	0	G	-D	C	0
		G	-D	C	0	0	D	-F	D	0	0	C	-D	G	0
	4	C	-D	G	0	0	D	-F	D	0	0	G	-D	C	0
		G	-D	C	0	0	D	-F	D	0	0	C	-D	G	0
	5	C	-D	0	0	0	D	-F	0	0	0	G	-D	0	0
		G	-D	0	0	0	D	-F	0	0	0	C	-D	0	0
3	1	0	-G	G	0	0	0	Γ	D	0	0	0	-B	C	-Px
		0	-B	C	0	0	0	Γ	D	0	0	0	-G	G	-Py
	2	C	-D	G	0	0	D	-F	D	0	0	G	-D	C	0
		G	-D	C	0	0	D	-F	D	0	0	C	-D	G	0
	3	C	-D	G	0	0	D	-F	D	0	0	G	-D	C	0
		G	-D	C	0	0	D	-F	D	0	0	C	-D	G	0
	4	C	-D	G	0	0	D	-F	D	0	0	G	-D	C	0
		G	-D	C	0	0	D	-F	D	0	0	C	-D	G	0

X = Locations not existing in the actual coefficient matrix

Figure 7. A section of the coefficient matrix and constant vector for a problem 5 points deep after the elimination of unneeded zeros.
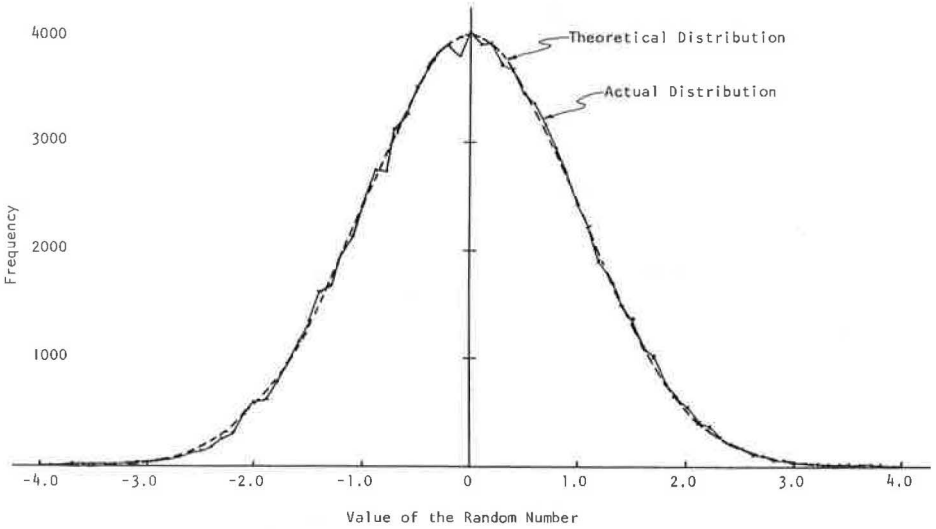
Figure 8. Frequency distribution of 100,000 normally distributed pseudo-random numbers.
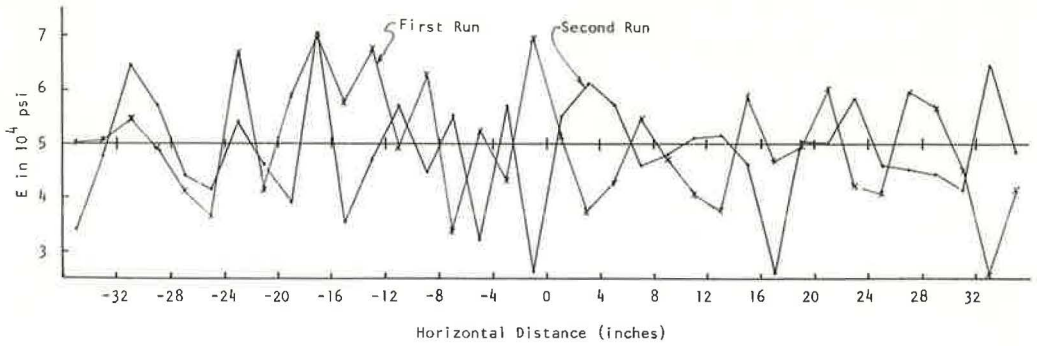
Figure 9.   Assignments of normal random numbers (mean = 5 x 10^4 psi, coefficient of variation = 20) assuming that each value is independent of all other values.
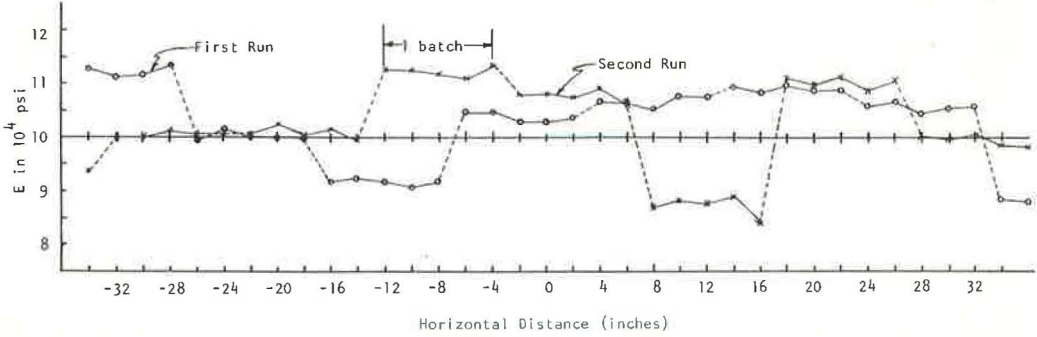
Figure 10.   Assignments of normal random numbers (mean = 1 x 10^5 psi, external coefficient of variation = 10 percent, internal coefficient of variation = 1 percent) to represent a batch process.

Figure 11.   Assignments of normal random numbers (mean = 5 x 10^4 psi, external coefficient of variation = 10 percent, internal coefficient of variation = 0 percent) to represent a continuous process.

When the material for a given layer is produced by a continuous type of process, a continuous random function can be used to represent the external variability. This function is generate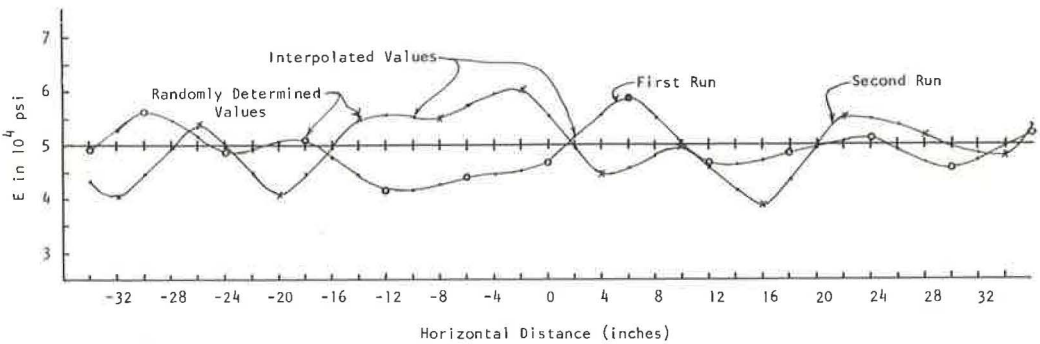d by passing an interpolation polynomial through equally spaced normal random variables, using the layer mean value and the external standard deviation as parameters. The spacing of the points is the minimum distance needed so that the values representing the material property are independent random variables from point to point. Again, the function can be translated a random distance horizontally so that bias due to maximum and minimum values occurring in the same place for successive solutions can be eliminated. The within-batch variability can then be superimposed upon this random function to provide values for all of the stress points in the layer. Examples are shown in Figure 11.

LIMITATIONS

Three possible sources of error that might decrease the value of the model for evaluating pavement systems are (a) the constraints due to the fixed boundaries of the model, (b) the spacing of the mass points, and (c) roundoff error. Sources a and b can be minimized if the computer system is large enough to handle very large problems with many mass points. Unfortunately, most computer systems available for general use do not have the storage capacity for handling large problems. Thus, the size of the model must be carefully chosen to give the maximum accuracy within the limits of the computer capability. The effect of each of the sources of error is examined in the following.

Boundary Constraints

The magnitude of the error involved by imposing finite boundaries on the layered half plane was determined by varying the size of the model while keeping the loading and mass point spacing constant. Values calculated from the model were compared with the corresponding values calculated from an analytical solution of the layered semi-infinite half plane developed by Iyengar and Alwar (8).

A study of the results reveals the following trends. The vertical stresses calculated in the model are in good agreement with those obtained by the theoretical solution for widths exceeding 60 in. The horizontal stresses and vertical deflections obtained using the model, however, are not in good agreement with those from the theoretical solution for practical model sizes. The disagreements are most likely caused by the zero deflection boundary conditions on the sides and bottom of the model. An increase of the modular ratio increases the error in the vertical stress. The rigid side boundaries are probably responsible for this increase.

One side boundary condition that was not evaluated but that would seem to eliminate most of the boundary condition errors is one using the boundary deflections obtained from the theoretical solution for homogeneous, two-dimensional layers rather than the zero deformations discussed above. This approach would eliminate much of the bridging of the fully restrained boundary and would provide for the deformation of the lower boundary. Also, since all theoretical deflection values used at the boundaries would appear in the constant term of each equation, use of this method would not increase the computer storage requirement.

Grid Spacing Errors

The grid spacing error results from the approximation of the differential equations in the theory of elasticity with finite difference equations. To estimate the magnitude of this error, a model of constant size representing a single layer of homogeneous material supported on a rigid base was used. To reduce the effect of the boundary condition error, the theoretical solution used for comparison consisted of two layers, the upper layer having an E and thickness the same as in the model, and the lower layer having a very high E value to represent the lower rigid boundary used in the model. The number of points in the model was varied to relate the grid spacing to the gird spacing error.

The magnitude of the grid spacing error in the vertical stress under the loaded area was on the order of 1 percent of the applied pressure for a grid spacing of 2 in. This error increased to about 10 percent of the applied pressure for a grid spacing of 8 in. Thus the grid spacing errors can be significant and should be considered when using this type of a model.

Roundoff Errors

The magnitude of error caused by roundoff during the solution of the equations is estimated by utilizing the fact that, for a layered half plane composed of homogeneous layers and loaded symmetrically, the deflection in the horizontal direction must be zero.

The results indicate that as the number of equations is doubled, the grid spacing error is increased by a factor of 6.5. The magnitude of the roundoff error in the horizontal deflection is fairly small, on the order of 0.6×10^{-6} for the largest problems that have been solved, but these errors propagate to the strain and then to the stresses. Roundoff errors in the stress and strain terms can be estimated by their deviation from symmetry. An estimate of this type revealed that the roundoff error in the stresses for the problem involving 1,400 equations was on the order of 0.01 psi, which is of little consequence.

A more complete discussion of all errors is presented by Levey (9).

TYPICAL SOLUTIONS AND RESULTS

The solution procedure described above was applied to the layered system shown in Figure 12 in order to demonstrate the ability of the procedure to determine the statistical nature of the response of such a system. For this analysis, the material is assumed to be elastic, and only the moduli of elasticity of the materials was assumed to vary. Coefficients of variation and the types of variability considered for the analysis are shown on the appropriate figures with the results.

The mean values and standard deviations for the vertical deflection, vertical stresses, horizontal stresses, and shear stresses respectively are shown in Figures 13 through 16. In these figures, the
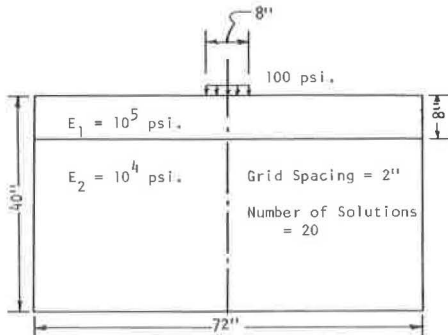
Figure 12. A diagram of the model used for obtaining the example solutions.
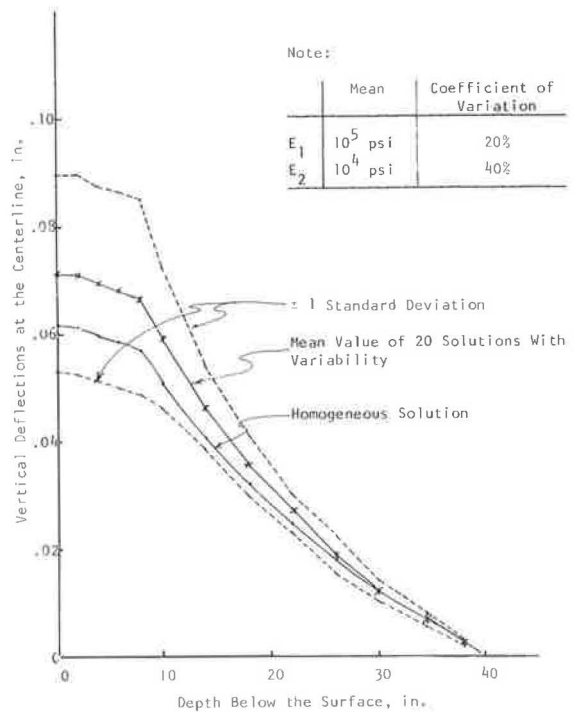
Figure 13. Effect of variability on vertical deflections.
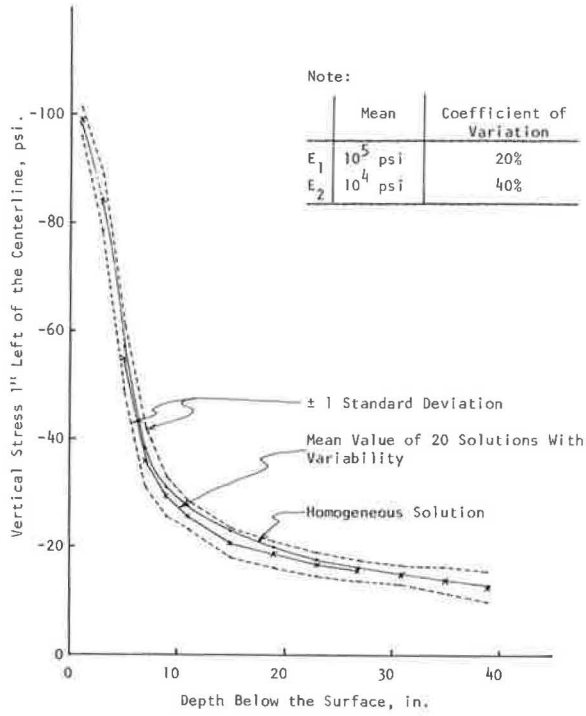
Figure 14. Effect of variability on vertical stresses.
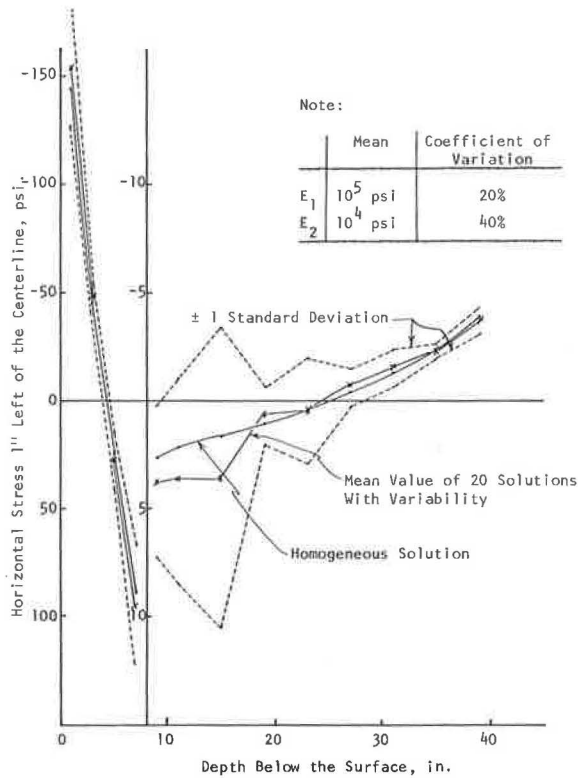
Figure 15. Effect of variability on horizontal stresses.
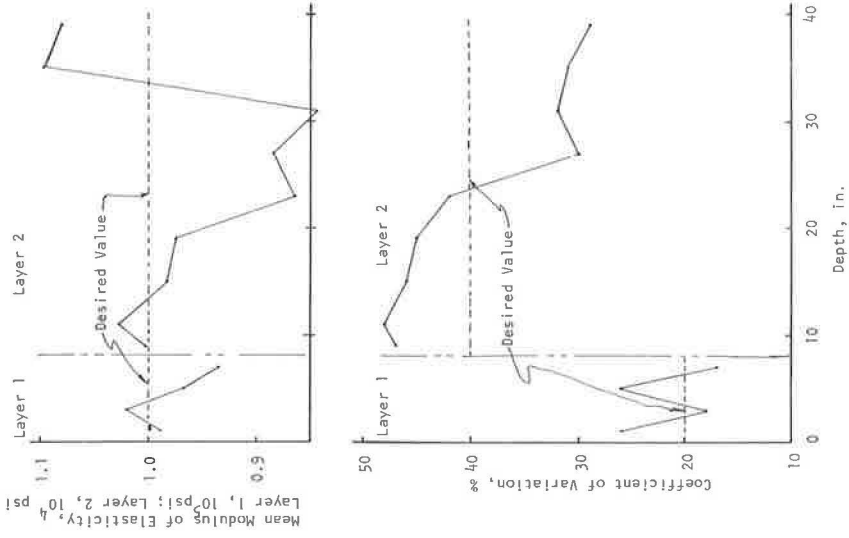
Figure 17. Mean values and coefficients of variation of the modulus of elasticity at the given depth and 1 in. from the centerline.
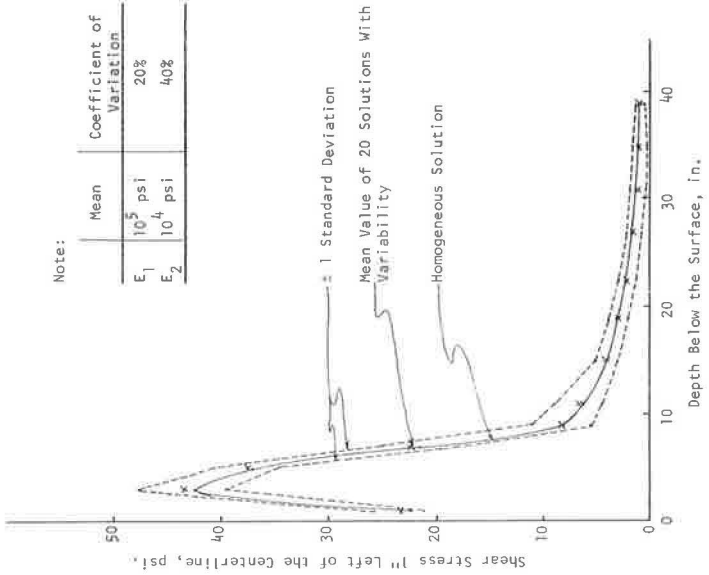
Figure 16. Effect of variability on shear stresses.

Figure 18. Frequency distributions of the stresses and vertical deflection for the upper layer.

Figure 19. Frequency distributions of the stresses and vertical deflection for the top 8 in. of the lower layer.

smooth curves represent the values of stresses and vertical deflections in the model when homogeneous materials are used, i.e., the coefficient of variation is zero. The broken curves connecting the x's represent the mean values of the stresses and vertical deflections in the model when variable materials are used. The dashed curves connect points that are one standard deviation above and below the corresponding means. Figure 17 shows the mean values and overall coefficients of variation of the moduli of elasticity that were generated and used in the 20 solutions. These values correspond to the same stress points as the vertical and horizontal stresses shown in Figures 14 and 15.

In all cases, the values of stress and deflections that were determined with homogeneous materials are within one standard deviation of the corresponding mean values determined with variable materials. However, the hypothesis that the mean values for heterogeneous materials approach the c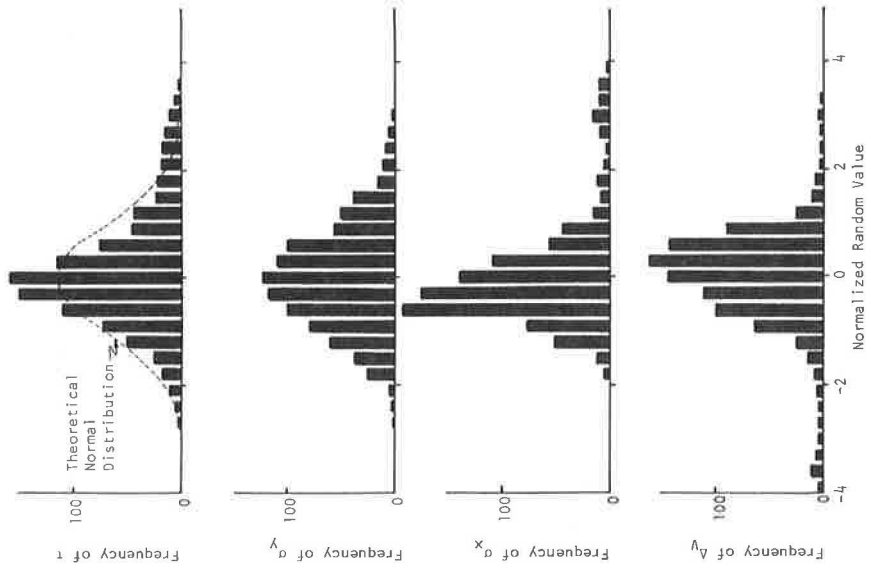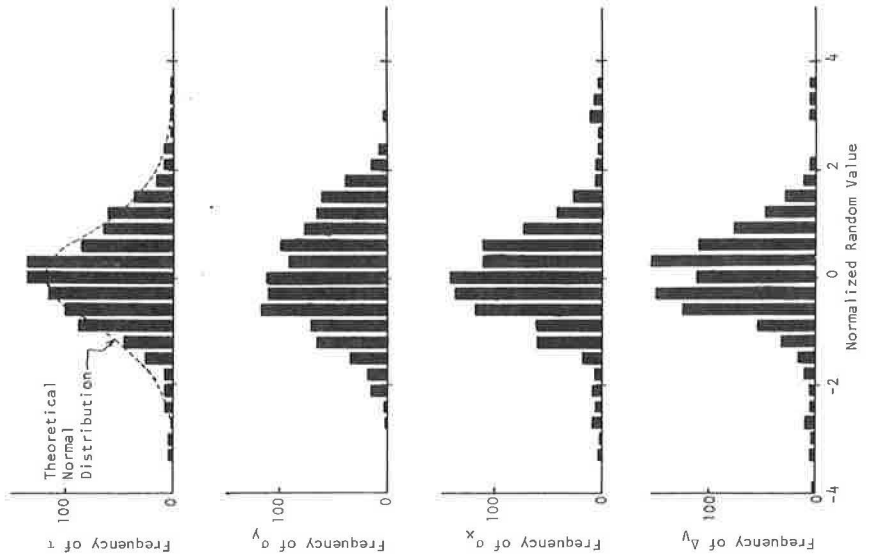orresponding values for homogeneous materials, which implies that the value obtained with the homogeneous material is within the limit of accuracy of the mean, cannot always be accepted at the 5 percent level ($\alpha = 0.05$). The deviation between the means for the heterogeneous materials and their corresponding values for homogeneous materials may be due to a difference between the mean modulus of elasticity that was actually generated at each point and the true mean.

The presentation of the data generated by the model in the format of the frequency distribution is not as straightforward as it might appear. If a frequency distribution were obtained for each stress, strain, and deflection at every mass point in the demonstration problem, 5,600 frequency distributions would be produced, and each one would consist of only 20 values. To get a better indication of the frequency distributions of the variables, the frequency distributions of the variables for points in the same region of the model can be lumped together. To do this, each value used in the composite frequency distribution must be normalized by subtracting its mean value and dividing by its standard deviation. A composite frequency distribution can then be compiled from all of the normalized values of the property within the desired region of the model.

Composite frequency distributions for the vertical deflection and the stresses are shown in Figures 18 and 19. The distributions in Figure 18 are for the area that extends 12 in. on either side of the centerline and the full depth of the upper layer. The distributions in Figure 19 are for the area of the model that extends 12 in. on either side of the centerline and includes the top 8 in. of the lower layer; 960 values are represented in each frequency distribution.

Most of the frequency diagrams shown in Figures 18 and 19 appear to resemble the normal distribution, although in some cases—the vertical deflection in particular—the tails of the distributions tend to extend farther than would be expected for a normal distribution. The only distribution that departs radically from a normal distribution is the distribution of the horizontal stress in the lower layer. Here a skewed distribution is produced by a random value that is physically restricted. In this case the horizontal stresses in the top of the lower layer must always be positive. Since the mean values of the horizontal stresses are near zero, the variability above the mean (zero on the composite frequency diagram) can be much greater than it can be below the mean; hence the skewed distribution.

CONCLUDING REMARKS

A procedure was developed that can analyze layered systems with nonuniform materials. High amounts of variability in the stresses and strains calculated in the typical problem shown indicate a need for establishing design criteria that consider this variability and also construction control criteria for controlling the material variability within economically acceptable limits.

Very limited work on defect size and degree indicated that the procedure can be used to determine the characteristics of critical defects. This information can be used in establishing statistical sampling plans or in establishing realistic rejection criteria for non-statistical sampling techniques.

It must be emphasized that this research did not produce an analysis of the statistical response of pavements to random material properties or of the defect problem mentioned above. Research using this or similar techniques will be needed to obtain these analyses. The technique mentioned can be used to study the effects of the elastic modulus and Poisson's ratio for most pavement structures if the changes in boundary conditions recommended are made. The model can be modified to analyze materials stressed above their yield points also, and the effects of yield point variability can be studied. When larger computing systems are variable and more efficient models and methods of formulating and solving the equations are developed, three-dimensional problems can be studied. This procedure can be extremely flexible and should be a valuable tool in the repertory of all serious pavement analysis.

REFERENCES

1. Proceedings, Highway Conference on Research and Development of Quality Control and Acceptance Specifications, Vol. 1. U.S. Bureau of Public Roads, 1965.
2. Huculak, N. A. Evaluation of Pavements to Determine Maintenance Requirements. Highway Research Record 129, pp. 12-27, 1966.
3. C.G.R.A. Field Performance Studies of Flexible Pavements in Canada. Proc. Second Internat. Conf. on the Structural Design of Asphalt Pavements, Ann . Arbor, Michigan, Aug. 1967.
4. The AASHO Road Test: Report 5—Pavement Research. HRB Spec. Rept. 61E, 1962.
5. Ang, Alfredo H.-S. Mathematically Consistent Discrete Models for Simulating Solid Continua. Computation of Underground Structural Response, DASA 1386, Final Report DA-49-146-XZ-104, Univ. of Illinois, 1963.
6. Ang, Alfredo H.-S., and Harper, Goin N. Analysis of Contained Plastic Flow in Plane Solids. Jour. Engineering Mechanics Div., ASCE, Vol. 90, No. EM5, pp. 397-418, Oct. 1964.
7. Timoshenko, S., and Goodier, J. N. Theory of Elasticity, 2nd Ed. McGraw-Hill, New York, 1951.
8. Iyengar, K. T., Raja, S., and Alwar, R. S. Stresses in a Layered Half Plane. Jour. Engineering Mechanics Div., ASCE, Vol. 90, No. EM4, pp. 79-96, Aug. 1964.
9. Levey, James R. A Method for Determining the Effects of Random Variations in Material Properties on the Behavior of Layered Systems. PhD thesis, Univ. of Illinois, Oct. 1968.

Stress Distribution in Rectangular
Concrete Slabs Under Wheel Loads

Y. H. HUANG, Department of Civil Engineering, University of Kentucky

•ENGINEERS have long used the theory of elasticity for determining the stresses in concrete pavements due to wheel loads. One of the best-known and most frequently used methods is Westergaard's analysis (1) for determining the maximum stress in an infinite large slab loaded at a corner, near an edge, or at the interior of a slab far from any edge. In order to check the validity of the theory, experimental pavements were constructed (2) and the maximum stress under a given wheel load was determined and compared with the theoretical solution. These comparisons based on the maximum stress generally could not give a definite indication on the applicability of the theory because the theoretical stress depends strongly on the modulus of elasticity and the Poisson's ratio of the concrete as well as the modulus of subgrade reaction, the exact values of which are quite difficult to ascertain. It is believed that a comparison between theoretical solutions and experimental measurements should be made on the distribution of stresses rather than just on the maximum stress. Although the distribution of stresses in concrete pavements was measured in the AASHO Road Test and contours of major and minor principal stresses were presented (3), because of the mathematical difficulty involved no effort has been made to compare these contours with those obtained by the elastic theory.

The purposes herein are twofold: (a) to introduce an approximate method for determining the stress distribution in rectangular concrete slabs, based on the theory of thin plates on elastic foundations; and (b) to determine theoretically the contours of principal stresses and compare them with those obtained experimentally from the AASHO Road Test.

The theoretical method employed in this study was first developed by Vint and Elgood (4) as early as 1935 for determining the deflections in a rectangular plate. In 1937 Murphy (5) applied the method to obtain stresses and deflections in a rectangular plate with four free edges. He showed that the method could easily be extended to the case where part of the plate is not in contact with the subgrade. Because the method is quite cumbersome and requires the solution of a large number of simultaneous equations, it has not received the attention it merits. However, this difficulty has been completely overcome with the advent of high-speed computers. The inclusion of partial contact between pavement and subgrade is an outstanding feature not considered in Westergaard's analysis.

In this method, the deflection function is represented by a double series in the form of two orthogonal functions. Under a given wheel load, the coefficients of the series can be determined by minimizing the total energy. Because of the particular deflection function selected, it is necessary to neglect the effect of Poisson's ratio when determining the moment and shear from the deflection so that the boundary condition that no moment exists at the free edge can be satisfied. This surely will lead to error, and the method may be considered as only approximate. However, the error is believed to be small, especially when the point at which the stresses are to be sought is not too far from the edge. Details of the method can be found elsewhere (4, 5).

Another difficulty in comparing theoretical solutions with the experimental data from the AASHO Road Test is that the former are based on free edges while dowel and tie

bars were used in the latter. Although the effect of dowel and tie bars on stress distribution is very significant when the load is close to the joints, their effect becomes smaller as the load moves farther away from the joints. For this reason, only the case when the load is at a distance of 6 ft from the transverse joint (Fig. 1) was used for comparison.

Figure 1 shows the contours of major and minor principal stresses in a 5-in. pavement over a 36-sq ft region bounded by the pavement edge and a transverse joint. A total load of 6 kips was applied to the pavement through 2 wooden pads, each having 11 × 14-in. area and spaced on 6-ft centers. The stress is considered positive when the top of slab is in tension and negative when in compression. Figure 1a shows the experimental stresses determined in the AASHO Road Test (3). The stresses were measured at the 15 points indicated by the black dots. Figure 1b shows the theoretical stresses based on the assumption that the slab and subgrade are in full contact. Figure 1c shows the theoretical stresses when a 0.6-ft strip adjacent to the outside edge is not in contact. In the theoretical calculations, the following data employed or determined in the Road Test were used: length of slab = 180 in., width of slab = 144 in., thickness of slab = 5 in., modulus of elasticity of concrete = 6.25 × 10⁶ psi, Poisson's ratio of concrete = 0.28, and modulus of subgrade reaction = 80 pci. The deflection function was approximated by 144 terms. The stresses were determined at 7 × 7 or 49 points, each 6 in. apart, and the contours of equal stresses were then interpolated. The method was programmed for the IBM 360 high-speed computer available at the University of Kentucky.

A comparison between the experimental stresses and the theoretical stresses based on full contact indicates that the general pattern of stress distribution is quite similar, although the magnitudes of the computed stresses are somewhat smaller than those of the measured stresses. This result is reasonable because the stresses were measured when the corners and edges of the slab were curled upward, whereas the theoretical
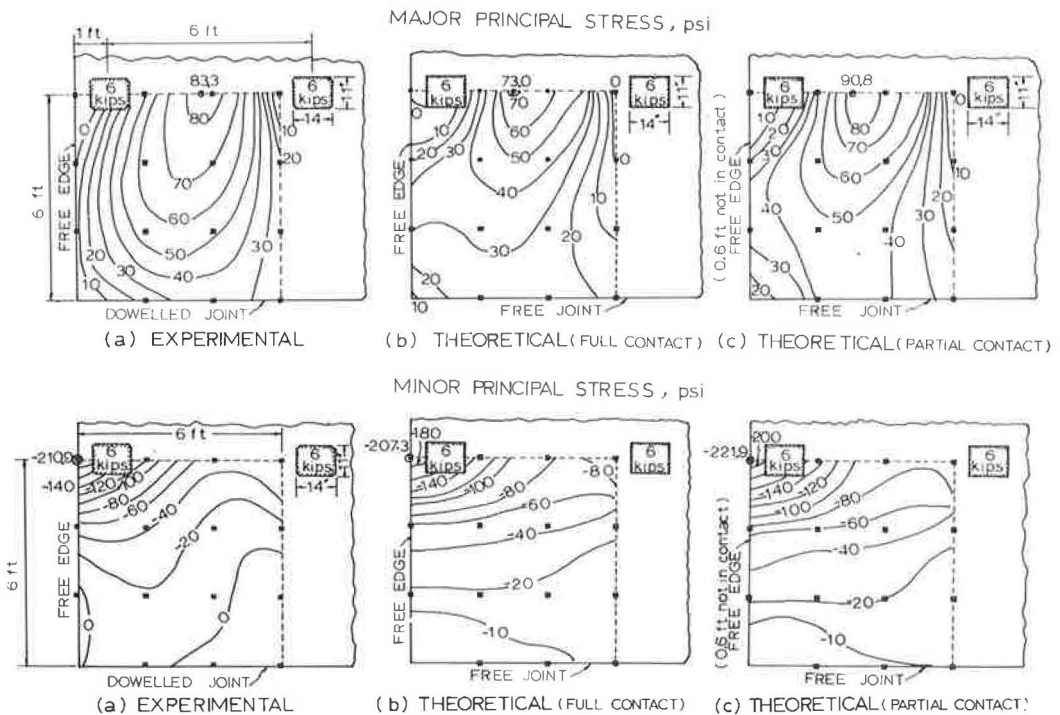

Figure 1. Contours of major and minor principal stresses, experimental vs. theoretical.

analysis is based on full subgrade contact. As can be seen from the figure, the assumption of partial contact gives stresses that check more closely with actual measurements than the assumption of full contact.

A note should be made on the case of partial contact. To compute the stresses based on partial contact, it is necessary to know the area over which the slab and subgrade are in contact. This area can be estimated by a method of successive approximations if the curling of the slab at various points is known. Because reliable information on the curling of the slab is not available, it is arbitrarily assumed that a 0.6-ft strip, or 5 percent of the slab width, adjacent to the outside edge is not in contact. The inside edge is at the longitudinal joint and is assumed in full contact. Although the area adjacent to the transverse joints may also be curled, its effect on stress distribution for the given loading position is comparatively small and can therefore be neglected.

The agreement between the theoretical and the experimental stress distribution for the 9.5-in. and 12.5-in. slabs is quite similar to that for the 5-in. slab. Because of space limitations, they are not presented here.

The close agreement between the theoretical solutions and the experimental measurements indicates that this approximate method, based on the theory of thin plates on elastic foundations, can be used to determine the stress distribution in concrete pavements when the load is far from the joints. Fortunately, this is also the most critical position as revealed by the AASHO Road Test.

REFERENCES

1. Westergaard, H. M. Stresses in Concrete Pavements Computed by Theoretical Analysis. Public Roads, April 1926, pp. 25-35.
2. Hudson, W. R. Comparison of Concrete Pavement Load-Stresses at AASHO Road Test With Previous Work. Highway Research Record 42, 1963, pp. 57-98.
3. The AASHO Road Test: Report 5—Pavement Research. HRB Spec. Rept. 61E, 1962, pp. 228-237.
4. Vint, J., and Elgood, W. N. The Deformation of a Bloom Plate Resting on an Elastic Base When a Load Is Transmitted to the Plate by Means of a Stanchion. The London, Edinburgh, and Dublin Philosophical Magazine and Journal of Science, Vol. 19, No. 124, Jan. 1935, pp. 1-21.
5. Murphy, G. Stresses and Deflections in Loaded Rectangular Plates on Elastic Foundations. Iowa Engineering Experiment Station Bulletin 135, 1937.

Elastic Properties of Pavement Components by Surface Wave Method

K. P. GEORGE, Department of Civil Engineering, University of Mississippi

The present study explores the feasibility of using vibration methods in determining the Rayleigh wave velocity and thereby the elastic properties of a three-layer pavement. When the intermediate layer in a three-layer composite pavement is stiffer than the surface layer, the existing procedure to determine the Rayleigh wave velocity of the former cannot be applied. A correction procedure is proposed in this study; the Rayleigh wave velocity and the thickness, determined accordingly, are both within 9 percent of the actual values.

•A KNOWLEDGE of the elastic properties and thickness of the pavement layers that make up the pavement is required for design, maintenance, and repair of highway pavements. In recent years, nondestructive methods have become of increasing interest in highway engineering practice (1, 2). A technique based on the measurements of surface waves was proposed by Jones (2, 3) where the elastic properties of two- or three-layered pavements were determined by using the theory of layered systems. Jones (2) dealt with the case of an intermediate layer that has a modulus of elasticity slightly less than that of the surface layer but considerably greater than that of the underlying medium. The present study, however, treats a three-layer system in which the surface layer has a modulus of elasticity less than that of the intermediate layer; a typical example is an asphalt-cement layer overlying the soil-cement base.

ELASTIC WAVES IN LAYERED SYSTEM

Road construction is regarded as being composed of layers of homogeneous, elastic materials and of infinite horizontal extent. In Figure 1, layer H_1 represents the asphalt surfacing, layer H_2 is the soil-cement base, and the uniform semi-infinite medium is the soil under the pavement.

Miller and Pursey (4) have shown that a vibrator on a circular base operating normal to the surface of a semi-infinite elastic solid radiates 67.4 percent of the power as a surface wave. The surface wave here is the Rayleigh wave, which has its maximum particle displacement normal to the surface. When vibrations of the Rayleigh wave type are propagated in a layered medium their velocity depends on the frequency of the vibrations and the thickness, density, and elastic properties of strata. Accordingly, the approach taken in this investigation has been to carry out the proper dynamical measurements on the layered system and to exploit the properties of surface waves to determine certain unknowns either pertaining to material constants or of geometrical origin.

Single-Layer Overlying the Semi-Infinite Medium

The derivation of the wave equation for the case of one surface layer over a semi-infinite medium involves the computation of a sixth-order determinant, which can yield more than one velocity at each frequency (5). The solution giving the lowest velocity

---

refers to the principal mode of propagation of the Rayleigh wave, and this particular mode can be shown to correspond to the fundamental flexural branch of a free plate. The evaluation of phase velocity from the sixth-order determinant can be simplified; for instance, when the wavelength is small compared with the thickness of the layer (i.e., $L/H \to 0$), the phase velocity of surface waves tends to correspond to the Rayleigh wave velocity appropriate to the top medium.

Figure 1. Section of a three-layer pavement: asphalt surface (layer 1), soil-cement slab (layer 2), and subgrade (semi-infinite medium).

"Free Plate" Approximation

A single-layer pavement over a conventional subgrade can be approximately treated as an elastic plate, the surface of which is free of stresses (3). The solutions obtained by Lamb (6) for the propagation of the longitudinal and flexural waves in a free plate are represented by $P = 0$ and $Q = 0$ respectively, where

$$P = b_1^2 \cosh \tfrac{1}{2} r_1 H_1 \sinh \tfrac{1}{2} s_1 H_1 - \frac{4 r_1 s_1}{k^2} \sinh \tfrac{1}{2} r_1 H_1 \cosh \tfrac{1}{2} s_1 H_1 \qquad (1)$$

$$Q = b_1^2 \sinh \tfrac{1}{2} r_1 H_1 \cosh \tfrac{1}{2} s_1 H_1 - \frac{4 r_1 s_1}{k^2} \cosh \tfrac{1}{2} r_1 H_1 \sinh \tfrac{1}{2} s_1 H_1 \qquad (2)$$

in which

$$r_1^2 = k^2 \left(1 - \frac{c^2}{\alpha_1^2}\right); \; s_1^2 = k^2 \left(1 - \frac{c^2}{\beta_1^2}\right); \; b_1^2 = 1 + \frac{s_1^2}{k^2};$$

$$c = \text{phase velocity}, \; k = \frac{2\pi}{L}, \; L = \text{wavelength};$$

H_1 = thickness of the layer; and

$\alpha_1, \beta_1, \gamma_1$ = compressional, shear, and Rayleigh wave velocity in the layer.

Therefore, if experimental measurements have been made at wavelengths short enough to define γ of the layer, its thickness can be determined by a nonlinear curve-fitting procedure (to satisfy $Q = 0$).

Two Surface Layers of Comparable Moduli of Elasticity

The propagation of Rayleigh waves in a system composed of two surface layers over a semi-infinite medium requires the solution of a tenth-order determinant (2, 6), and the computational work becomes almost prohibitive. However, the evaluation of phase velocity from the dispersion equation can again be simplified for the case of very small wavelength ($L/H \to 0$).

In a plate-subgrade system, when the plate is much stiffer than the underlying subgrade the propagation of the vibration becomes sensibly independent of the properties of the subgrade. Accordingly, in the present problem, when the phase velocity exceeds α_3 the propagation will depend almost entirely on the properties and thickness of the materials in the two layers, and the two surface layers may be regarded as a composite layer.

In practice the vibrations are excited and measured at the surface of the upper layer so that Eq. 2—the Lamb solution of flexural vibrations—with the appropriate parameters of the top layer is the solution that will apply. As the wavelength of the surface vibration exceeds $2H_1$, however, the experimental dispersion relation is seen to deviate
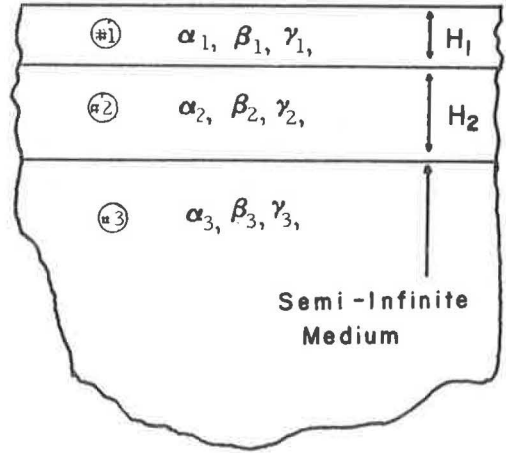
from the Lamb solution. A simple explanation of the observed deviation is that the surface waves are influenced by the second layer as well. Maxwell and Fry (8) strongly support this viewpoint when they assume that the surface waves are normally conditioned by the material from the surface to a depth equal to one-half of the length of the surface waves. Founded upon this hypothesis, the following empirical relationship is proposed to resolve the phase velocity of the composite plate into two component velocities appropriate to the individual layers:

$$c \, L/2 = c_1 H_1 + (L/2 - H_1) \, c_2 \tag{3}$$

where

$$2H_1 \leq L \leq 2(H_1 + H_2)$$

and

  c = phase velocity (surface wave) of the composite plate at wavelength L;
  c_1 = flexural wave velocity appropriate to the first layer at wavelength L; and
  c_2 = flexural wave velocity appropriate to the second layer at wavelength L.

When a number of points relating the wavelength and the phase velocity in the second layer have been obtained, extrapolation to zero wavelength can be accomplished by use of the Lamb flexural wave curve that offers the best fit to the data.

EXPERIMENTAL PROCEDURE

A two-layer composite pavement was constructed on a semi-infinite subgrade where the test slab consisted of a 0.32-ft thick soil-cement slab (8 ft by 6 ft, cement 10 percent by weight) overlaid by 0.27-ft thick dense-graded hot plant mix. To justify the assumption of an infinite slab in the horizontal direction, the edges of the slab were tapered.

Beam specimens, 3 by 3 by $11\frac{1}{4}$ in., were molded from both soil-cement and asphalt mixtures. Elastic constants of both materials were determined from the fundamental transverse vibration and torsional resonant frequency test (ASTM Designation C 215-58T).

Compressional Wave Velocity

Seismic tests (1) were made to determine compressional wave velocities in the soil-cement and the asphalt pavement.

Surface Wave Velocity

Vibration tests were conducted to determine the wavelength and thereby the phase velocity of the surface wave. The details of the equipment (the electromagnetic vibrator, cartridge pick-up, and preamplifier) and the technique used to detect the wavelength using a dual channel oscilloscope can be seen elsewhere (7).

RESULTS AND DISCUSSION

Single Surface Layer of Higher Elastic Moduli
Than the Underlying Subgrade

Attention herein is confined to a stiff slab (soil-cement base) over a relatively soft subgrade for which flexural wave dispersion curves conform adequately to the free plate approximation. When the measurements are made to a sufficiently high frequency, to define γ_2 for the slab material, the dispersion relation can be inverted to give the thickness of the slab (curve 1 in Fig. 2). The Rayleigh wave velocity for the soil-cement has been determined as 4,650 ft/sec, which compares favorably with the value computed from the resonant frequency tests (4,600 ft/sec). The thickness of the soil-cement slab is found to be 0.31 ft, which compares favorably with the actual thickness, 0.32 ft.

The Rayleigh wave velocity determined in conjunction with the compressional wave velocity by seismic method and the charts of Knopoff (5, p. 34) make possible the
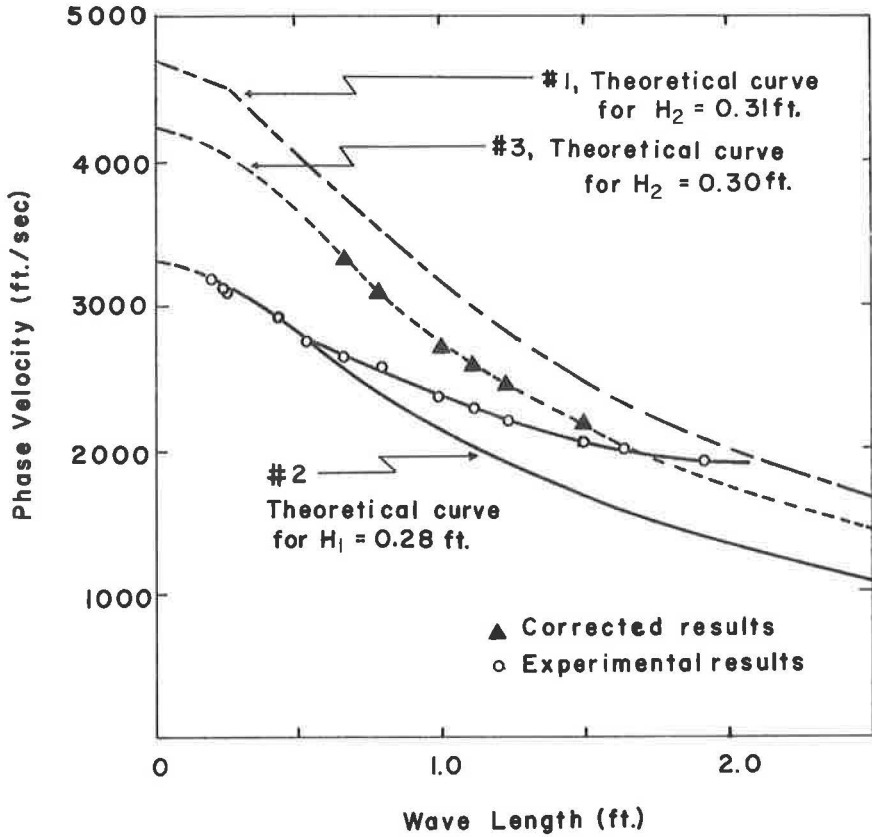
Figure 2. Phase velocity of flexural vibrations in a composite layer: theoretical solution from solving $Q = 0$.

determination of Poisson's ratio (0.23). The fact that the Poisson's ratio computed by an independent method—namely from transverse vibration and torsional resonant frequency—is in excellent agreement (0.22 vs. 0.23) validates the applicability of the surface wave technique.

Two Surface Layers of Comparable Moduli of Elasticity

Experimental results of phase velocity and wavelength at the surface of the three-layer construction are given by the open points in Figure 2. The results obtained at short wavelengths ($L \leq 2H_1$) permit the relation to be extrapolated to zero wavelength to provide a value of γ_1 in the asphaltic layer of 3,300 ft/sec. With this γ_1, the thickness, according to the Lamb solution, that best fits the experimental points is 0.28 ft, which is in excellent agreement with the actual thickness of 0.27 ft (curve 2 in Fig. 2).

As expected, when the wavelength exceeds $2H_1$, the experimental points lie to the right of the theoretical curve pertaining to the surface layer alone. The phase velocity for the soil-cement layer is calculated by the correction equation (Eq. 3) and given by solid points in Figure 2. The relation obtained by these data points may be extrapolated to get an approximate value of γ_2. Now that the Rayleigh wave velocity and thickness (thickness is normally known in new or old pavements) are approximately known, a theoretical curve that matches the computed data can be found by a judicious trial procedure (curve 3 in Fig. 2). The agreement between this curve and the Lamb curve, which fits the experimental data resulting from direct measurements, is remarkable.

Rayleigh wave velocity and the thickness of the soil-cement layer obtained by the procedure using the empirical correction equation are 4,200 ft/sec and 0.30 ft respectively, which compare well with the actual values (4,600 ft/sec and 0.32 ft).

It may be noted here that, by performing the vibration experiment alone, it is difficult to determine the relative stiffness of the first layer. The microseismic procedure described by Phelps and Cantor (1) is proposed for positive identification. Accordingly, if the slope of the travel-time graph is not changed, the top layer is stiffer than the bottom layer and the equation proposed by Jones (2) should be used for final correction. If the slope of the travel-time graph tends to change, however, the second layer is taken to be stiffer than its top counterpart and Eq. 7 is proposed in the final analysis.

CONCLUSIONS

The theory of wave propagation in layered media presented and the experimental technique developed provide an effective means of determining the Rayleigh wave velocity appropriate to the top slab in a two-layer pavement or to the top slab of a three-layer pavement. In the three-layer pavement, when the intermediate layer is stiffer than the top layer, the correction method proposed in the present study is satisfactory to determine the Rayleigh wave velocity and the thickness of the intermediate layer.

REFERENCES

1. Phelps, J. M., and Cantor, T. R. Detection of Concrete Deterioration Under Asphalt Overlays by Microseismic Refraction. Highway Research Record 146, 1966, pp. 34-49.
2. Jones, R. Surface Wave Technique for Measuring the Elastic Properties and Thickness of Roads: Theoretical Development. British Journal of Applied Physics, Vol. 13, 1962.
3. Jones, R., Thrower, E. N., and Gatfield, E. N. Surface Wave Method. Proc. Second Internat. Conf. on the Structural Design of Asphalt Pavements, Ann Arbor, 1967.
4. Miller, G. F., and Pursey, M. The Field and Radiation Impedance of Mechanical Radiators on the Free Surface of a Semi-Infinite Isotropic Solid. Proc. Royal Society, Vol. 223, 1954.
5. Ewing, W. M., Jardetzky, W. S., and Press, F. Elastic Waves in Layered Media. McGraw-Hill, New York, 1957.
6. Lamb, H. On Waves in an Elastic Plate. Proc. Royal Society, Series A, Vol. 93, 1916.
7. Lee, C. L. Elastic Properties of Pavement Components by Surface Wave Method. Unpublished MS thesis, Univ. of Mississippi, 1969.
8. Maxwell, A. A., and Fry, Z. B. A Procedure for Determining Elastic Moduli of In Situ Soils by Dynamic Techniques. Proc. Internat. Symposium on Wave Propagation and Dynamic Properties of Earth Materials, Albuquerque, N.M., 1967.

The Analysis of Highway Pavement Systems

A. C. LEMER and FRED MOAVENZADEH, Department of Civil Engineering,
Massachusetts Institute of Technology

This paper presents a model for describing the performance of an engi-
neered facility from the user's point of view. It is suggested that per-
formance may be described in terms of serviceability, reliability, and
maintainability. Serviceability is the quality of providing satisfactory
service to the user and is evaluated through applications of utility theory.
Reliability is the probability that adequate serviceability will be maintained
throughout the facility's design life; it may be predicted by use of a semi-
Markov process approach. Maintainability is a measure of the effort
required during a facility's service life to maintain adequate service-
ability. Methods for analysis are suggested and applied to existing data
to show how the model may be used in practice to yield engineered facilities
having good performance characteristics. The model and its use are
viewed in a perspective of the goals of the larger system of which the
engineered facility is a part.

•IN PROVIDING a pavement—a riding surface—the engineer is attempting to give a
service to the user of a transportation facility. In effect, the real problem the engi-
neer must face is not the design and construction of a physical, structural unit, but
rather the satisfaction of the user.

The pavement—in fact, the whole highway system—may be evaluated in terms of
three principal parameters: serviceability, reliability, and maintainability. Service-
ability is the quality of providing satisfactory service to the user (1). Serviceability
is not just a matter of transportation but of transportation in such a fashion as to fulfill
the user's needs. Reliability is the probability that serviceability will be maintained
at adequate levels, from a user's point of view, throughout the design life of the facility
(2). This concept is suggested in recognition of the uncertainty inherent in the sys-
tems with which the engineer deals. Maintainability is a measure of the effort required
to maintain adequate serviceability throughout the design life. Two types of mainte-
nance effort must be considered: normal maintenance is that regular, day-to-day ac-
tion planned to keep operation smooth; repair maintenance is an action required to cor-
rect a potential or actual loss of serviceability.

This paper attempts to show how these parameters may be evaluated and used by
the engineer to provide a facility that will exhibit qualities of satisfactory performance
throughout its design life. The framework suggested here is intended to assist the
engineer to provide such facilities in a most economical fashion.

SERVICEABILITY

The application of the serviceability concept may be based on utility theory as it is
being developed and used in economics and psychophysics. Utility is a general term
for the intrinsic value that a person attaches to some stimulus. In the present con-
text, a user would experience the ride over one pavement section as more or less com-
fortable than that over another section. The relative comfort felt may then be scaled
as utility against some objective measure of pavement roughness—for example, a
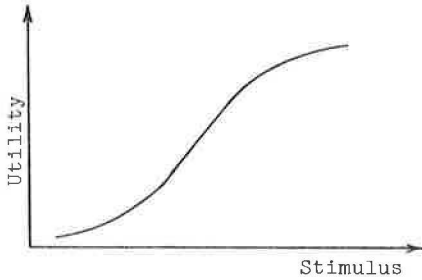roughometer reading.
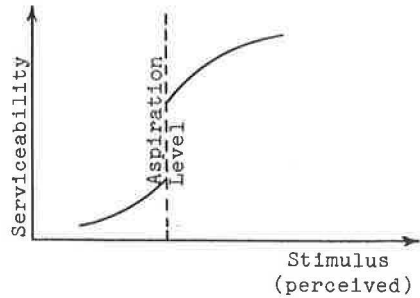
Figure 1. A uni-dimensional utility function.

Figure 2. A component of serviceability.

By direct or indirect questioning, one attempts to build up a picture of what the user's utility function is with respect to a stimulus (3). For example, the question might be posed, "How much money would you have to receive in order to make you twice as happy as receiving $10? How much would make you half as happy?" And so on. The utility scale is thus built up on a relative basis.

Figure 1 shows a typical utility function (4). Over a sufficiently broad range of stimulus, this typical s-shaped curve exhibits areas of relative indifference at either end of the stimulus scale and a central portion of maximum sensitivity. For example, consider the changes in user's utility derived from highway lane width. Narrow lanes have a value to the user approaching zero as the lane becomes too narrow for vehicle passage. In the range of typical lane widths, there is a rapid rise in utility up to, say, the size of current Interstate standards. Additional utility derived is small as lanes become oversized—there is more room than the user can appreciate. It is of interest to note that a decrease in overall serviceability may occur as lanes become so wide that safety is affected because weaving by drivers is encouraged.

For the typical engineering facility there will be several scales of utility that will be pertinent to the satisfaction of the user. For example, in the AASHO Road Test it was acknowledged that features such as grade, alignment, slipperiness, and glare enter into the consideration of how satisfactory a pavement is. But it is found that it is difficult, if not impossible, for the user to judge several dissimilar qualities at once (5), so it is necessary to deal with these qualities separately. In the case of the AASHO Road Test, all aspects of the pavement not directly related to the riding quality of the surface were excluded from consideration. In the case of a systematic analysis of the highway, serviceability is evaluated as a multi-dimensional quantity, a composite of several scales of utility.

A serviceability function of this sort—that is, a vectoral quantity—is difficult to use for comparisons of alternative actions. There are no satisfactory multi-dimensional optimization techniques, and it is somewhat out of the engineer's field of responsibility to make trade-off decisions among the various qualities the user might prefer. The establishment of the aspiration level (6) as a minimum acceptable level of performance, however, may provide the engineer with a measure with which to work. The aspiration level is described as that level of achievement (or performance, in this case) which the user expects, and which he considers reasonable. This level will be based on the user's perception of what is technologically possible and appropriate.

It has been suggested that the idea of an aspiration level may be used to set engineering requirements (4). As shown in Figure 2, part of the region of rapidly rising utility is eliminated from the curve. Specifically, the straight-line portion of the curve having maximum slope is cut, based on psychological considerations involved (6). This action associates a larger loss of serviceability with a small drop in performance at the aspiration level. Thus an effective failure criterion is established at the aspiration level, while optimization above this failure level is still practical.

RELIABILITY

In order to say whether a facility is satisfactory or not it is necessary to predict the behavior of the facility, in terms of levels of serviceability, for the duration of its design life. But this prediction can be made only in uncertain terms; reliability is a measure of the degree of this uncertainty. It is suggested that the lifetime behavior of a facility may be approximated by a Markov process. Such an approximation allows the engineer to predict serviceability with a particular degree of reliability throughout the design life.

Figure 3. Coin tossing as a Markov process.

The behavior of a facility may be represented as a set of states and interstate transition probabilities. The states—in the present context, levels of serviceability—are descriptions of possible conditions of the system being modeled. For example, in flipping a coin, the two states would be "heads" and "tails." The transition probabilities tell the chances that the system, given that it is in a known state now, will occupy a certain state at the next observation. This basic assumption of the Markov process is that the probability that the system will be in any state after a trial is dependent only on the state that is occupied immediately preceding that trial. Figure 3 shows a pictorial representation of such a process for the tossing of a coin.
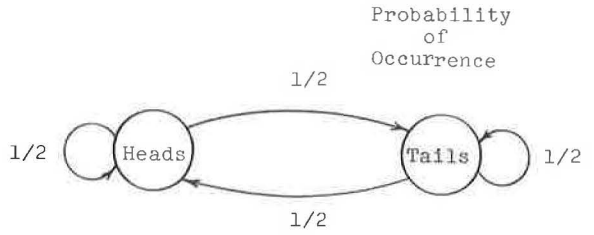
A variation of the Markov process allows one to describe time spent in a given state at any trial—that is, the time before an interstate transition is made—as a probabilistic variable. With this semi-Markov process, one can approximate the aging behavior of a facility. If the states are thought of as the levels of serviceability that the facility may occupy, this process will allow prediction of the service life history in a probabilistic manner. One then has the reliability of the facility, with respect to some serviceability level, as a function of time. This is the time-dependent probability that the facility will be in a certain state.

MAINTAINABILITY

In describing a facility's behavior as a semi-Markov process, some of the interstate transitions may represent maintenance and repair operations. Normal maintenance will have an influence on the distribution of time before a decrease in serviceability occurs. Repair maintenance is the way in which transitions from one state to another of higher serviceability may occur. The expected time during which the facility will occupy a state that represents failure, relative to the total design life, is a measure of maintainability.

Figure 4 shows two possible expected life histories for two similar facilities. It is expected that one will experience a greater number of failures than the other, but a failure in the second case will take much longer to repair than the multiple failures of the first. The second facility would have a lower maintainability. That this time lost—and hence the maintainability—is directly related to user cost and comfort may be realized by considering the case of a bridge that must carry heavy traffic. The execution of a difficult maintenance action may require the closure of a lane, resulting at least in the slowing of traffic flow and losses of time

Figure 4. Possible life histories.

to the commuter or, quite likely, the disruption of traffic patterns within a sizable radius of the bridge.

It should be noted that in both cases it is possible for the facility to give adequate service throughout its design life, with no failures. Life history is probabilistically predicted. This point admits the possibility that one may learn by experience, changing planned normal maintenance and operating policies to suit the exhibited performance of the facility. The most efficient selection and adjustment of such policies is essentially a problem in statistical decision theory and is beyond the scope of this paper.

AN EXAMPLE OF APPLICATION

The foregoing discussion has been directed toward describing what is basically a systems analytic approach to engineered facilities. A brief example should help to illuminate the way in which these ideas fit together. What follows is rough, intended only to present in outline of how the engineer might proceed to use this approach.

It has been suggested that a satisfactory highway pavement will be one which is rideable, safe, and possesses structural integrity (2). This goal statement gives three components of serviceability for the highway pavement; the first step is to develop the functions for evaluating these components.

Rideability is the most apparent quality for the immediate user of the road, and the most complex. A variety of evaluation schemes have been suggested, ranging from purely subjective (8) to very objective (9). For this example the AASHO Road Test is a useful source of information. The AASHO definition of serviceability is essentially what is meant here by rideability (10). Figure 5a shows a plot of the percentage of people finding a pavement to be acceptable vs. a subjective scale of rideability. This function may be interpreted as a mean value utility function for rideability. It would be more correct to show the variations among individuals and to say that there is a certain probability that a given percentage of people will find a pavement of given rideability satisfactory. Figure 5b shows how this function may be transformed (4) for use in an engineering context. The aspiration level is defined and the curve adjusted. The serviceability scale is derived by a geometric (and in this case quite direct) transformation of the utility scale.

In trying to predict pavement safety, one faces a wide assortment of studies and conclusions as to what is important and how pavement affects accidents and vehicle driver characteristics. It is beyond the scope of this example to try to formulate a coherent definition of when and why a pavement is safe. For purposes of illustration it will be assumed that skid resistance, as affected by pavement roughness, is of primary importance because of its influence on accidents.

It has been suggested that characteristics of the microscopic roughness of the pavement surface may be related to the coefficient of friction (11), which in turn may be related to the occurrence of accidents (12). With this rationale, approximations may
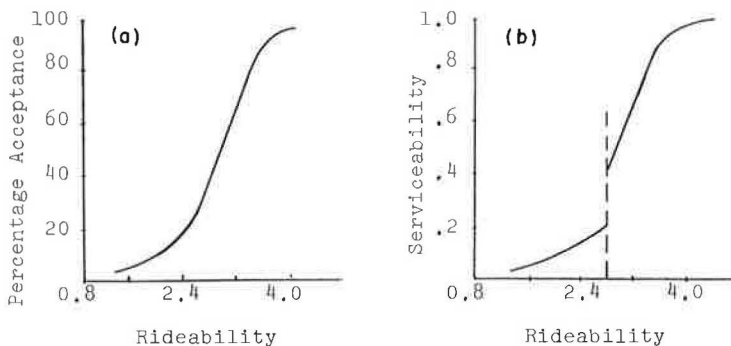

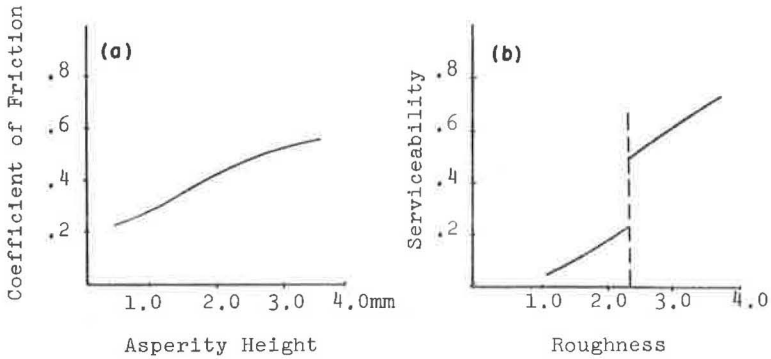Figure 5. Rideability component of serviceability.

Figure 6. Safety component of serviceability.

be made to give Figure 6. Relative safety is meant to relate to skidding resistance at a given speed and to accident frequency; the roughness scale is related to asperity height. Figure 6b gives the converted serviceability function.

Structural integrity is the classical problem of the engineer. Does the structure resist the loads to which it is subjected? The safety factor with respect to loads is an adequate prediction of this component of serviceability. Figure 7 shows this func-tion. When the ratio of applied load to structural capacity rises above unity—a factor of safety with respect to load of less than unity—a structural failure may be expected. Such a failure will represent a complete loss of structural integrity and a decline of serviceability effectively to zero. As long as the system can resist the loads applied, full serviceability with respect to structural integrity would be retained. In cases where a partial loss of serviceability is possible—for example, some plastic yielding without complete structural collapse—this serviceability function would not be such a severe single step.

The specification of the multi-dimensional serviceability function in such a way as to allow comparisons of alternative actions is another difficult problem that cannot be adequately treated here. For the purposes of this example, the product of the three scales can represent gross serviceability. Failure occurs when this gross service-ability falls to an unacceptably low level.

Having set up serviceability measures, one next uses these measures as a basis for describing the service behavior of a facility. In a detailed study, the various physical conditions and processes leading to losses of serviceability might be represented in the Markov process. For this example, however, the representation has been simpli-fied to include only discrete steps in ride-ability, without regard to cause. Figure 8 shows a state transition diagram for pave-ment aging. Dashed lines indicate mainte-nance actions. Numbers for the states are taken from Figures 5, 6, and 7.

Some additional simplification concern-ing transition probabilities will be used here to ease computation. It was stated earlier that interstate transitions are in general stated as time-dependent-probability functions. Work is currently under way to develop such functions from theoretical and statistical analysis of data such as labora-tory tests and those gathered in the AASHO
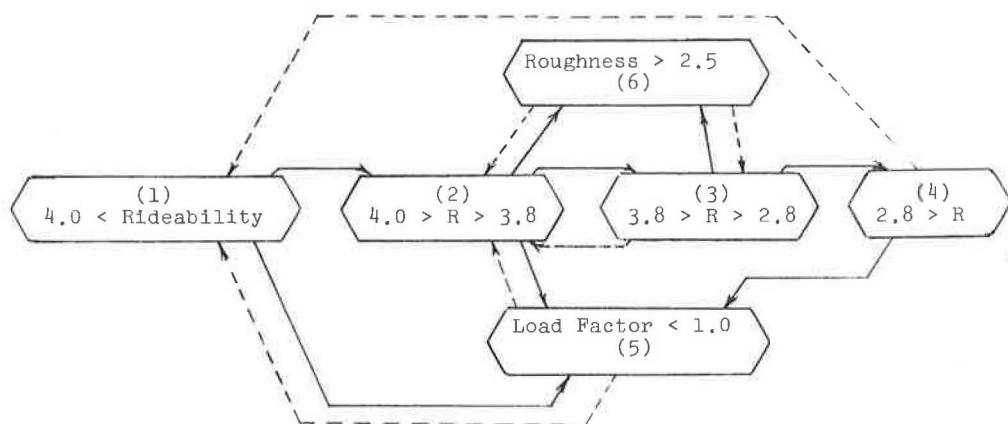
Figure 7. Structural integrity component of serviceability.

Figure 8. A Markov process for highway pavement.

Road Test. It is expected that these techniques will be described in future papers. For current purposes, it will be assumed that these functions are given. Further, this example deals only with the overall probabilities that a particular transition will occur, given that a transition does occur. That is, it may be assumed that pertinent convolution integrals have been computed for the transition functions, yielding the numerical probabilities shown in Figure 8. Parentheses indicate that a decision regarding maintenance activity has been made for the case shown. The aspiration level is defined and the curve adjusted. Also shown in Figure 8 is the transition matrix for this process. Each entry P_{ij} in this matrix is the probability that the system will be in state j after the next transition, given that it is in state i now. The picture (a flow graph representation) and matrix are equivalent. Implicit in all of the numbers are decisions regarding operating policies, expected traffic, economic design life, etc. What remains after these assumptions is a simple Markov process.

Computations may be made using flow-graph or matrix methods in the transform domain (13). It may be shown that the probability matrix P_{ij} (n), where P_{ij} is the probability that the system will be in state j after n transitions, given that it starts in state i, is given by the inverse transform of

$$P^g (z) = [I - Pz]^{-1}$$

where P is the transition matrix. This expression applies to the current example and uses geometric transforms. Analogous results are obtained using Laplace transforms for the continuous time case.

In this example, probabilities refer to continuous time processes reduced to the facility's design life, as described above. The overall lifetime behavior to be expected of the system is given as the steady-state limit of this process. Expected serviceability, reliability, and a coefficient of maintainability (equal to one over the relative time used in maintenance) may thus be computed. Table 1 summarizes the results of

TABLE 1

SUMMARY OF CASES

Case	Transition Matrix						Evaluation Parameters
Normal	0	0.95	0	0	0.05	0	Expected Serviceability = 0.49
	0	0	0.90	0	0.05	0.05	
	0	0.40	0	0.45	0.10	0.05	Reliability = 0.72
	0.10	0	0.65	0	0.25	0	
	0.25	0.75	0	0	0	0	Coefficient of Maintainability = 3.58
	0	0.50	0.50	0	0	0	
Normal Maintenance-Intensive	0	0.95	0	0	0.05	0	Expected Serviceability = 0.50
	0	0	0.9	0	0.05	0.05	
	0	0.6	0	0.25	0.1	0.05	Reliability = 0.81
	0.1	0	0.8	0	0.1	0	
	0.25	0.75	0	0	0	0	Coefficient of Maintainability = 5.25
	0	0.5	0.5	0	0	0	
Innovation	0	0.95	0	0	0.05	0	Expected Serviceability = 0.34
	0	0	0.9	0	0.05	0.05	
	0	0.5	0	0.3	0.05	0.15	Reliability = 0.45
	0.1	0	0.65	0	0.25	0	
	0.25	0.75	0	0	0	0	Coefficient of Maintainability = 1.82
	0	0.5	0.5	0	0	0	

several design options for the process described. In the maintenance-intensive case, normal maintenance-type transition probabilities are set higher. The "normal" case is as shown in Figure 8. The "innovation" case involves a supposition that some new material of higher initial cost is used that gives this pavement a very low probability of going from a rideability of 3.2-2.8 to the failure state—i.e., improved durability, at the expense of maintenance funds, after initial deterioration, something like work hardening.

It is now up to the engineer to consider the costs involved in the various alternative actions and the benefits derived from varying levels of serviceability—all in terms of the specific goals for the pavement under consideraction—and to arrive at a decision. The decision problem is made very complex by the multitude of non-engineering factors that must be considered. A benefit-cost type of analysis must be undertaken with care (14).

CONCLUSIONS

This paper has attempted to present a framework for the systematic analysis of constructed facilities such as highway pavements. It is expected that this approach will benefit not only the engineer, by helping him to order problems and solutions, but also the user of the engineer's services. With the increasingly wide recognition of a need for a systems approach to engineering problems, it is hoped that the approach described here will be of some modest use in filling an apparent lack of operationally useful suggestions.

ACKNOWLEDGMENT

REFERENCES

1. Carey, W. N., Jr., and Irick, P. E. The Pavement Serviceability-Performance Concept. HRB Bull. 250, 1960, pp. 40-58.
2. Moavenzadeh, F., and Lemer, A. C. An Integrated Approach to the Design and Analysis of Highway Pavement. Report R68-58, M. I. T. Dept. of Civil Engineering, 1968.
3. Galanter, E. Direct Measurement of Utility and Subjective Probability. Amer. Jour. of Psychology, Vol. 75, 1962, pp. 208-220.
4. Lifson, A. Evaluation Technology. Unpublished notes, U. C. L. A., 1968.

5. Stevens, S. S.   Measurement, Psychophysics, and Utility.   In Measurement: Definitions and Theories (Churchman and Ratoosh, ed.), Wiley, New York, 1959.
6. Siegel.   Level of Aspiration and Decision Making.   Psychological Review, Vol. 64, 1957, pp. 253-262.
7. Shepard, R. N.   On Subjectively Optimum Selections Among Multi-Attribute Alternatives.   In Decision-Making (Edwards and Tversky, ed.), Penguin, Baltimore, 1967.
8. Canadian Good Roads Assn.   Pavement Evaluation Studies in Canada.   Proc. Internat. Conf. on the Structural Design of Asphalt Pavements, Ann Arbor, 1962.
9. Quinn, B. E., and Wilson, C. C.   Can Dynamic Tire Forces Be Used as a Criterion of Pavement Condition?   Report 32, JHRP, Purdue Univ., 1963.
10. The AASHO Road Test: Report 5—Pavement Research.   HRB Spec. Rept. 61E, 1962.
11. Colley, B. E., Christensen, A. P., and Nowlen, W. J.   Factors Affecting Skid Resistance and Safety of Concrete Pavements.   HRB Spec. Rept. 101, 1969, pp. 80-99.
12. Beaton, J. L., Zube, E., and Skog, J.   Reduction of Accidents by Pavement Grooving.   HRB Spec. Rept. 101, 1969, pp. 110-125.
13. Howard, R.   Dynamic Programming and Markov Processes.   M. I. T. Press, Cambridge, 1960.
14. Marglin.   Criteria for Evaluation of Public Investment.   M. I. T. Press, Cambridge, 1968.

Optimal Design of Flexible Pavement Sections

S. S. HEJAL, Purdue University;
S. R. YODER, Indiana State Highway Commission; and
J. C. OPPENLANDER, University of Vermont

Although several methods are available for the design of flexible pave-
ments, no existing technique explicitly considers the optimal combination
of flexible pavement components to minimize the total in-place cost of the
pavement system. The purpose of this systems analysis was to develop a
rational method for the optimal selection of the arrangement of the various
pavement components. This cost minimization must be realized within the
boundary conditions imposed by the practical limitations of the design pa-
rameters. The design model consists of an objective function and various
constraint equations. The total cost of the pavement system is quantita-
tively described by this objective function, and a minimum-cost solution
is obtained for each combination of material costs and design conditions.
The various constraining equations quantify the boundary conditions to
which the design of a flexible pavement is subject. These physical limi-
tations complete the realism of the mathematical model in describing the
real-world situation of flexible pavement design. The design model was
solved by a modified linear programming technique. In developing prac-
tical solutions to the design model, optimal flexible pavements are de-
signed for cross sections without subbase, cross sections with subbase
through shoulders, and cross sections with subbase and subdrains. The
design requirements for the various components are predicted on the de-
sign parameters of traffic conditions, soil support values, pavement ma-
terial characteristics, environmental effects, and pavement performance
requirements, and on unit costs of pavement components. Substantial
cost savings result in the selection of flexible pavement sections by this
design procedure.

•THE PRIMARY OBJECTIVE of highway pavement design is to provide an acceptable
roadway surface that can withstand the deteriorating effects of traffic and environment
for the service life of the facility. In addition, the pavement structure must adequately
serve the demands of the road users at an acceptable level of performance. A properly
designed, constructed, and maintained pavement is a major factor in providing eco-
nomical, efficient, safe, convenient, and comfortable highway travel. This goal is an
integral part of the total highway transportation program.

Although several design techniques are available for determining reasonable thick-
nesses of flexible pavements to satisfy the specified design parameters, no present
method explicitly considers an optimization of flexible pavement components to mini-
mize the total cost of the pavement system. Of course, this cost minimization must
be realized within the boundary constraints imposed by the selected values of the de-
sign parameters. The purpose of this systems analysis was to develop a rational
method for the optimal design of flexible pavement sections.

The objective of flexible pavement design in this investigation is to select the vari-
ous pavement components so that the total pavement cost is minimized within the limi-
tations of the various design parameters. Minimum-cost designs are determined for

---

flexible pavements to satisfy the demands of traffic and environment on the system of pavement structure and soil support. Therefore, this technique affords a practical and economical solution to the problem of designing flexible pavements. This approach to design embodies the essence of sound engineering.

CONCEPTUAL MODEL

A flexible pavement distributes the traffic loads through a system of pavement components to the subgrade. These pavement layers are generally identified as surface, base, and subbase. Several different thickness combinations of the materials comprising the various components may adequately satisfy the structural design of the highway pavement. However, all satisfactory thickness arrangements may not provide an economical solution to the engineering problem of pavement design. In general, only one pavement structure is an optimal selection of the flexible pavement components for the designated design conditions.

The concept for this flexible pavement design procedure is illustrated by the logic diagram in Figure 1. The total pavement system is described by the various design parameters representing traffic conditions, soil support values, pavement material characteristics, environmental effects, and pavement performance requirements. In addition, unit costs of pavement components and alternate cross section designs are considered in the selection of the optimum flexible pavement section.

The structural requirements of flexible pavements are predicated on an estimated number of equivalent 18-kip single-axle load repetitions and on an appropriate measure of the soil support afforded by the subgrade. The elements of pavement performance and environment are also incorporated as initial and terminal serviceabilities and regional factor respectively. The combined effect of traffic loading, soil support, pavement performance, and environment is denoted as a structural number (SN) according to the interim design guide for flexible pavements of the American Association of State Highway Officials (1). Pavement component thicknesses are then selected to reproduce the specified structural number by a linear combination of layer thickness times its coefficient of relative strength. A minimum pavement thickness is equal to the summation of the component thicknesses.

Consideration of significant environmental factors, such as depth of frost penetration, provides another control on the selection of a minimum pavement thickness. This design procedure specifies a minimum pavement thickness (T_{min}) to account for various influencing environmental conditions. This minimum thickness is based on a design procedure that requires a selected design wheel load and a specified soil support value. The greater minimum thickness value becomes the design requirement.

To account for varying design practices, several types of pavement cross sections are available as possible alternatives in this procedure for designing flexible pavements. These arrangements include cross sections without subbase, cross sections with subbase through shoulders, and cross sections with subbase and subdrains. Finally, the unit costs of the pavement components are specified to permit the design of an acceptable pavement structure for the least cost. This cost-effectiveness approach provides both an optimal and a practical solution to the problem of flexible pavement design.

In a real sense, the minimum thicknesses represent design constraints and not design objectives. The design objective is to produce a flexible pavement system at the least total cost within the specified boundary conditions. The in-place unit costs of the component materials depend on the locale in which the flexible pavement is to be constructed. In addition to the traffic loading, soil support, pavement performance, and environmental constraints, practical limitations on layer thicknesses are specified in concurrence with present highway construction practices.

DESIGN MODEL

The logic diagram for this optimal design of flexible pavements is shown in Figure 1. A detailed description of this design technique is presented in the following sections,
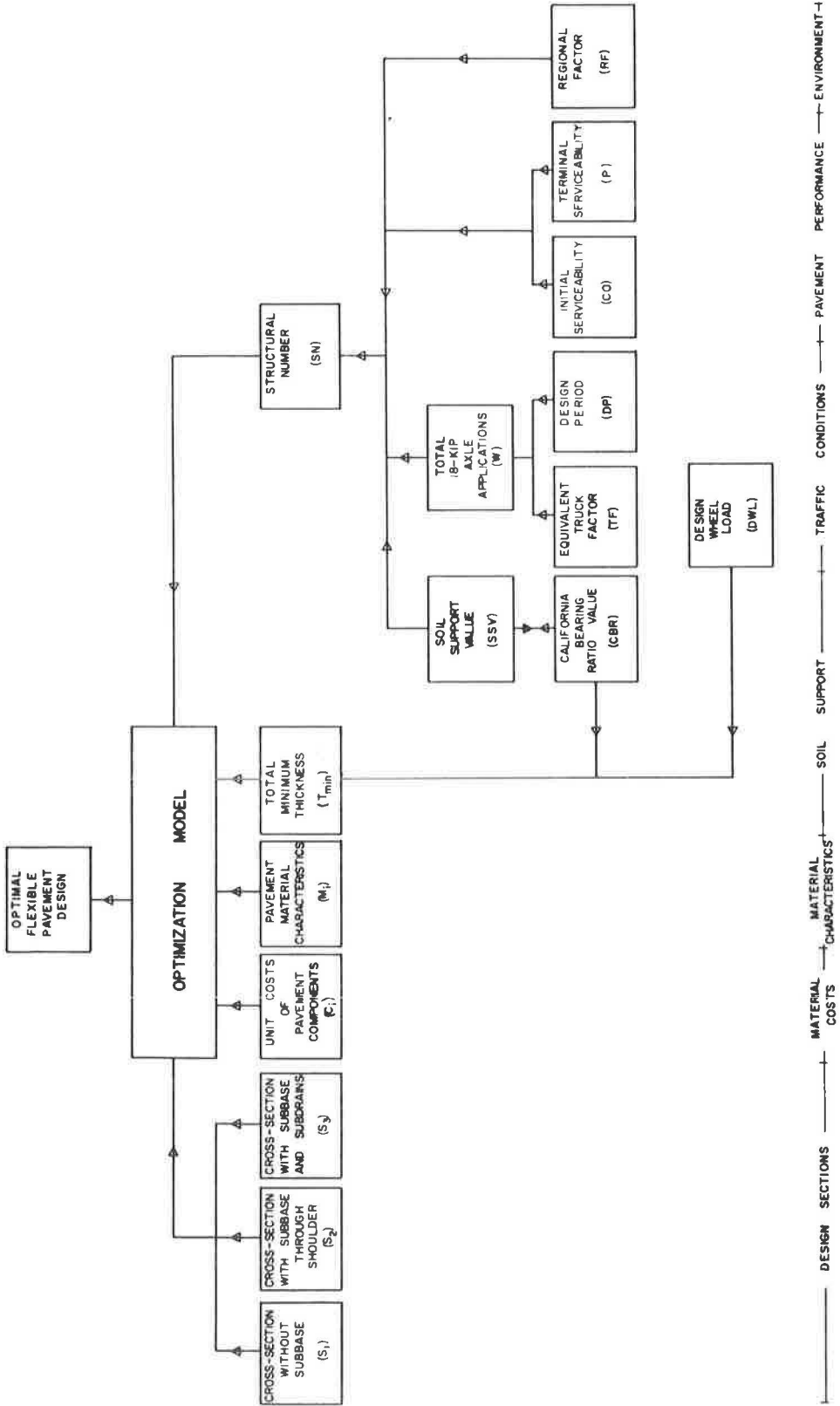
Figure 1. Design concept.

which provide the various computational procedures and design features for determining the optimal selection of flexible pavement sections.

Design Parameters

Design parameters represent the various measures of traffic conditions, soil support, pavement material properties, environmental effects, and pavement performance requirements. The results of these evaluations provide the summary quantities that are necessary for the optimal design of flexible pavements.

The initial measure of the stability of the subgrade soil is determined by the standard California bearing ratio (CBR) test. This soil strength is then translated into the soil support value (SSV) as defined by AASHO (1). In this study the following equation was developed to relate soil support values to CBR measures:

$$SSV = 4.90 \log_{10} (CBR)$$

where SSV is the soil support value and CBR is the California bearing ratio.

The traffic conditions are expressed as the number of 18-kip single-axle load repetitions for the service life of the pavement. These load applications are estimated from an evaluation of the formula

$$W = 365 (TF) (DP)$$

where

 W = total number of equivalent 18-kip single-axle load repetitions during the pavement design period,
 TF = truck factor (18-kip single-axle load applications per day), and
 DP = design period (years).

To develop a measure of the truck factor, a correlation was derived between the number of 18-kip single-axle load applications and the percentages of various truck types in the traffic stream. The following expression was obtained from loadometer data collected on highways in Indiana:

$$TF = \left[\frac{(ADT_1) + (ADT_2)}{4} \right] \left[\frac{11.7(TR)(LU) + 0.83(TR)(LU)(CT)}{10,000} \right]$$

where

 TF = truck factor (18-kip single-axle load applications per day),
 ADT_1 = average daily traffic volume at the start of the design period (vehicles per day in both directions),
 ADT_2 = average daily traffic volume at the end of the design period (vehicles per day in both directions),
 TR = percentage of all trucks,
 CT = percentage of combination trucks, and
 LU = truck lane use factor (1.0, 0.9, and 0.8 for two-, four-, and six-lane highways respectively).

The various measures of traffic conditions, soil support, environmental effects, and pavement performance requirements are now combined into a single design parameter defined as the structural number (SN). Two nomographs have been prepared by AASHO to quantify this structural requirement (1). However, the following equation was developed from these nomographs to use in the computer program for this design procedure:

$$\log_{10}(W) = 9.36 \log_{10} [(SN) + 1] - 0.20$$

$$+ \log_{10} \left[\frac{(CO) - (P)}{(CO) - 1.5} \right] \Bigg/ \left\{ 0.40 + \frac{1,094}{[(SN) + 1]^{5.19}} \right\}$$

$$+ 0.37756 [(SSV) - 3.0] - 0.97 \log_{10} (RF)$$

where

W = total number of equivalent 18-kip single-axle load repetitions during the pavement design period,

SN = structural number,

CO = initial pavement serviceability index (4.2 for all highways),

P = terminal pavement serviceability index,

SSV = soil support value, and

RF = regional factor.

The effects of the environment are numerically summarized in the regional factor (2), and the desired pavement performance is specified by selected values for the initial and terminal pavement serviceability indexes. An iterative procedure is used to solve this equation for the structural number of a particular design situation.

Another consideration of environmental influences is determining a minimum thickness as a design against the detrimental effects of frost action and the loss of subgrade strength in the spring break-up period. Design charts developed by Hicks (3) provide correlations between bearing capacity and CBR and between pavement thickness and bearing capacity. Adverse subgrade conditions are represented by using a 4-day soaked value for the selected CBR. The following relationships were prepared from these design charts for 9-kip and 10-kip wheel loads respectively:

$$T_{min(9)} = 4.723 + \frac{61.037}{(CBR)^{1.05}} - 45.18 \, e^{-(CBR)}$$

$$T_{min(10)} = 4.423 + \frac{52.706}{(CBR)^{0.90}} - 19.884 \, e^{-(CBR)}$$

where

$T_{min(9)}$ = minimum pavement thickness for 9-kip design wheel load (inches),

$T_{min(10)}$ = minimum pavement thickness for 10-kip design wheel load (inches), and

CBR = California bearing ratio for reduced strength conditions.

The 10-kip wheel load is considered satisfactory for the design of primary highways, whereas the 9-kip wheel load is applicable for flexible pavements on secondary routes. In the computer input for this design model, the highway engineer specifies the design wheel load for either a primary or a secondary highway. This minimum-thickness determination accounts for environmental effects by highway classification and provides another realistic constraint in selecting optimal flexible pavement sections.

The characteristics of each pavement material are described by the in-place density and the coefficient of relative strength. These values depend on the local materials used in the construction of flexible pavements. The evaluation of the pavement material characteristics permits the application of the design model for the prevailing construction practices.

The foregoing descriptions numerically define the various design components of the flexible pavement system. Although the selected equations provide reasonable evaluations of these parameters, other expressions can be used to satisfy local design conditions.
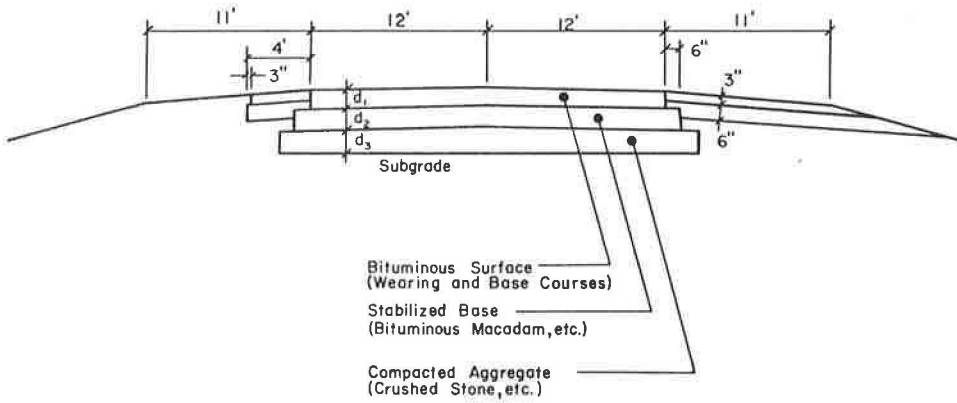
Figure 2. Typical cross section of a flexible pavement without subbase for a four-lane highway, one direction.
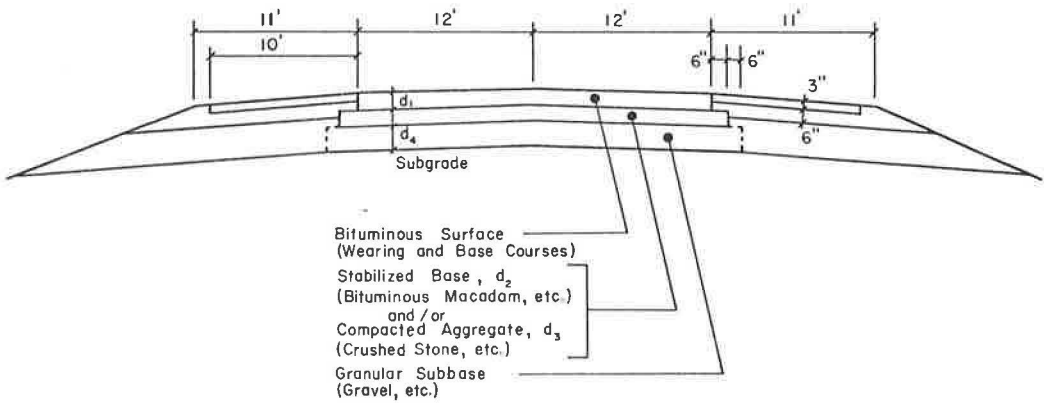
Figure 3. Typical cross section of a flexible pavement with subbase through the shoulder for a two-lane highway.
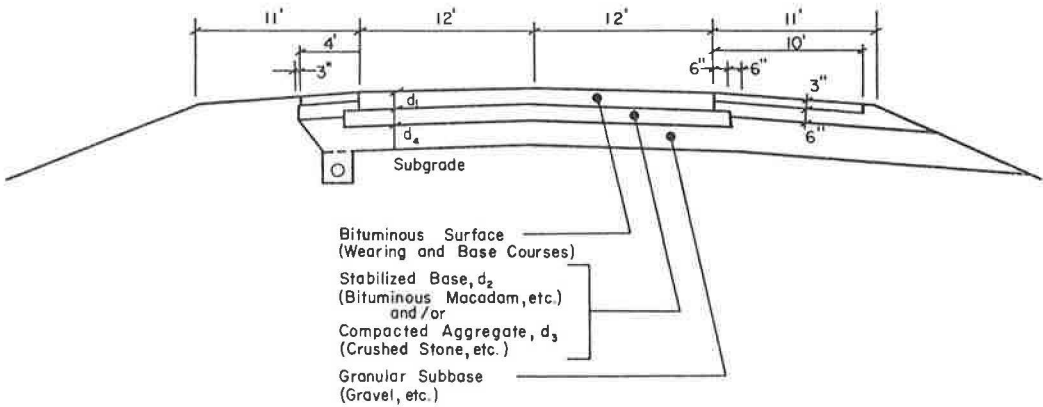
Figure 4. Typical cross section of a flexible pavement with subbase through the shoulder for a four-lane highway, one direction.
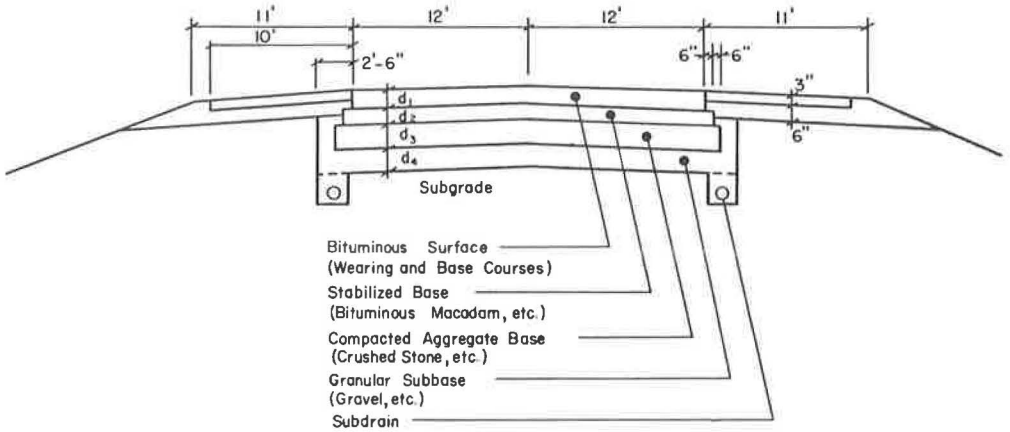
Figure 5. Typical cross section of a flexible pavement with subbase and drain for a two-lane highway.
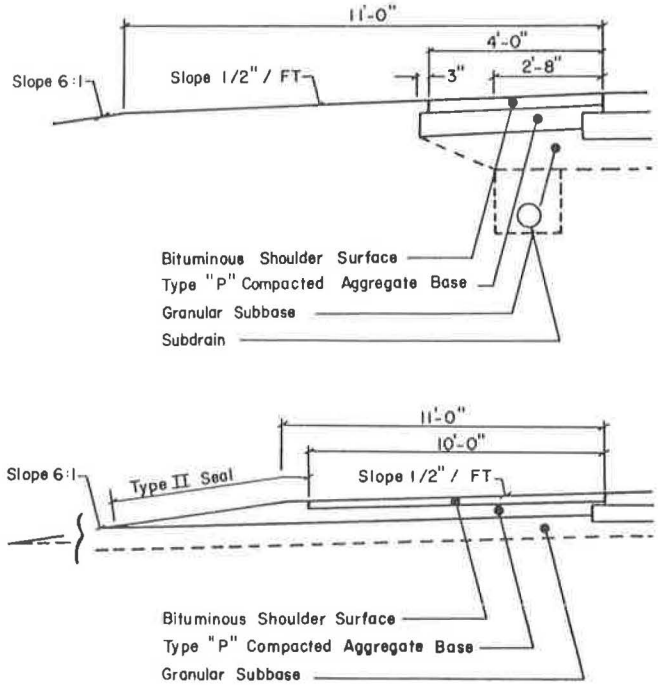
Figure 6. Shoulder details.

Design Sections

Because reasonable variations exist in the design of highway elements, three acceptable cross sections were selected for two-lane and divided multilane highways to provide several alternative designs in the model. These arrangements include the following distinct designs:

1. Cross sections without subbase, S_1;

2. Cross sections with subbase, S_2, extended through the shoulders for two-lane highways and extended through the right shoulder with subdrain under the left shoulder for divided multilane highways; and

3. Cross sections with subbase and subdrains under both shoulders, S_3.

Typical details of these cross-sectional designs are shown in Figures 2, 3, 4, and 5 respectively. The shoulder designs are further detailed in Figure 6 for cross sections with subbases and with subdrains.

Of course, additional cross-sectional arrangements may be incorporated into this design model. Because each section represents a different design, an objective function is required for each cross section to permit the optimal selection of flexible pavement sections. The best design then is the cross section that minimizes the total pavement cost for the specified design parameters.

Optimization Model

The optimal design of flexible pavement sections is depicted by the following objective functions for the three different design sections.

1. Cross sections without subbase:

$$\text{Min. } S_1 = \left(\frac{C_1 D_1 L k_1}{12 \times 2{,}000} \right) d_1 + \left(\frac{C_2 D_2 L k_j}{12 \times 2{,}000} \right) d_2$$

$$+ \left(\frac{C_3 D_3 L k_j}{12 \times 2{,}000} \right) d_3 + E_\ell + H_\ell$$

2. Cross sections with subbase through shoulders:

$$\text{Min. } S_2 = \left(\frac{C_1 D_1 L k_1}{12 \times 2{,}000} + \frac{C_4 A}{12 \times 27} \right) d_1$$

$$+ \left(\frac{C_2 D_2 L k_j}{12 \times 2{,}000} + \frac{C_4 A}{12 \times 27} \right) d_2$$

$$+ \left(\frac{C_3 D_3 L k_j}{12 \times 2{,}000} + \frac{C_4 A}{12 \times 27} \right) d_3$$

$$+ \left[\frac{C_4 (L + A)}{12 \times 27} \right] d_4 + E_\ell + H_\ell + M_\ell - Y_\ell$$

3. Cross sections with subbase and subdrains:

$$\text{Min. } S_3 = \left(\frac{C_1 D_1 L k_1}{12 \times 2{,}000} + \frac{C_4 B}{12 \times 27} \right) d_1$$

$$+ \left(\frac{C_2 D_2 L k_j}{12 \times 2{,}000} + \frac{C_4 B}{12 \times 27} \right) d_2$$

$$+ \left(\frac{C_3 D_3 L k_j}{12 \times 2{,}000} + \frac{C_4 B}{12 \times 27} \right) d_3$$

$$+ \left[\frac{C_4 (L + B)}{12 \times 27} \right] d_4 + E_\ell + H_\ell + N - Z_\ell$$

where

- S = total cost of pavement system (dollars per longitudinal foot);
- C_i = unit cost of material i (dollars per ton for materials 1, 2, 3, 5, and 8; dollars per cubic yard for materials 4 and 6; and dollars per foot for material 7);
- D_i = density of material i (pounds per cubic foot);
- L = pavement width (24 ft for two-lane and one-way section of divided four-lane highways and 36 ft for one-way section of divided six-lane highways);
- d_i = thickness of material i (inches); with $i = 1$ for bituminous surface, 2 for stabilized base, 3 for compacted aggregate base, 4 for granular subbase, 5 for bituminous shoulder surface, 6 for subdrain granular fill, 7 for subdrain pipe, and 8 for wearing surface;
- k_j = adjustment factor for increase in width of pavement layers; with $k_1 = 1.00$ for first layer, $k_2 = 1.04$ for second layer, $k_3 = 1.08$ for third layer, and $k_4 = 1.12$ for fourth layer;
- E_ℓ = cost of shoulder (dollars per longitudinal foot), where, for two-lane highways,

$$E_1 = 20 \times 3.0 \left(\frac{C_5 D_5}{12 \times 2,000} \right) + 31 \times 6.0 \left(\frac{C_3 D_3}{12 \times 2,000} \right)$$

and for divided multilane highways,

$$E_2 = 14 \times 3.0 \left(\frac{C_5 D_5}{12 \times 2,000} \right) + 19.75 \times 6.0 \left(\frac{C_3 D_3}{12 \times 2,000} \right)$$

- H_ℓ = adjustment for the additional cost of the wearing surface, where, for two- and four-lane highways,

$$H_1 = \frac{(C_8 - C_1)}{12 \times 2,000} \ D_1 \times \left(\frac{90}{110} \right) \times 24$$

and for six-lane highways,

$$H_2 = \frac{(C_8 - C_1)}{12 \times 2,000} \ D_1 \times \left(\frac{90}{110} \right) \times 36$$

- A_ℓ = width of shoulder subbase for an embankment slope of 6:1 (feet), where, for two-lane highways,

$$A_1 = \left[\ 22 + \frac{2(d_1 + d_2 + d_3)}{3} \right]$$

and for divided multilane highways,

$$A_2 = \left[\ 14.375 + \frac{(d_1 + d_2 + d_3)}{3} \right]$$

- B_ℓ = adjusted width of shoulder subbase when subdrains are provided (feet), where, for two-lane highways, $B_1 = 5.0$, and for divided multilane highways, $B_2 = 5.875$;
- M_ℓ = cost of subdrain when used under median shoulder only (dollars per longitudinal foot), where, for two-lane highways, $M_1 = 0.0$, and for divided multilane highways, $M_2 + 1.1 (0.075 C_6 + C_7)$;
- N = cost of subdrains under both shoulders (dollars per longitudinal foot), where, for all highways, $N = 2 \times 1.1 (0.075 C_6 + C_7)$;
- Y_ℓ = adjustment for the amount of subbase material replaced by the shoulder surface and base (dollars per longitudinal foot), where, for two-lane highways,

$$Y_1 = \frac{258 \times C_4}{12 \times 27}$$

and for divided multilane highways,

$$Y_2 = \frac{162 \times C_4}{12 \times 27}$$

Z_ℓ = adjustment for the amount of subbase material added above the level of the pavement subbase under the shoulders, where, for two-lane highways,

$$Z_1 = \frac{50 \times C_4}{12 \times 27}$$

and for divided multilane highways,

$$Z_2 = \frac{60 \times C_4}{12 \times 27}$$

Thus, the objective of this optimal selection of flexible pavement components is to minimize the total cost of the pavement system. The various material and layer notations of the design model are graphically described in the figures illustrating the design sections.

To quantify the boundary conditions to which the optimal design of the flexible pavement components is subject, the following constraint equations are necessary to complete the realism of this design model.

1. The selection of layer thicknesses must satisfy the structural number requirement:

$$a_1d_1 + a_2d_2 + a_3d_3 + a_4d_4 \geq SN$$

where a_i = coefficient of relative strength of material i, and SN = structural number for design. The coefficients of relative strength are given in Table 1 for the four pavement materials used in this design model.

2. The total thickness of the flexible pavement must be at least equal to the minimum thickness required by an influencing environmental consideration:

$$d_1 + d_2 + d_3 + d_4 \geq T_{min}$$

where T_{min} = total minimum thickness of flexible pavement to satisfy environmental conditions.

The remaining constraining equations are required to account for the physical limitations inherent in the construction of the various layers of a flexible pavement. The following seven relationships complete the mathematical representation of the concept for the optimal selection of flexible pavement components.

3. The bituminous surface course of a primary highway is at least 3.0 in. in thickness; that is, $d_1 \geq 3.0$.

4. If a stabilized base is selected for the pavement system, the minimum thickness is 4.0 in.; that is, $d_2 = 0$ or $d_2 \geq 4.0$.

5. If a compacted aggregate base is included in the flexible pavement, a minimum thickness of 4.0 is necessary for construction purposes; that is, $d_3 = 0$ or $d_3 \geq 4.0$.

TABLE 1

PAVEMENT MATERIAL SPECIFICATIONS

Material Notation	Material Description	Coefficient of Relative Strength (a_i)
d_1	Bituminous surface	0.44
d_2	Stabilized base	0.24
d_3	Compacted aggregate base	0.14
d_4	Granular subbase	0.08

6. If a granular subbase is specified from the optimal selection, at least a 4.0-in. layer is required; that is, $d_4 = 0$ or $d_4 \geq 4.0$.

7. Because rutting and shoving of the pavement may result under high load repetitions for excessive thicknesses of bituminous mixtures, the maximum thickness of the bituminous surface is 10.0 in.; that is, $d_1 \leq 10.0$.

8. The maximum thickness of the stabilized base is established at 10.0 in. because of large vertical deformations that may result in this base course if excessive thicknesses of bituminous mixtures are used; that is, $d_2 \leq 10.0$.

9. An upper limit of 20.0 in. is set for the thickness of the granular subbase to conform with present construction practice in Indiana; that is, $d_4 \leq 20.0$.

In summary, the optimal design of flexible pavement components is predicated on determining that minimum-cost combination of layer thicknesses that satisfies the real and practical constraining conditions. The selection of actual in-place construction costs enhances the mathematical representation of the flexible pavement design process and provides further economies in the highway construction industry.

SOLUTION

The final step in determining the optimal design of flexible pavement sections is to obtain a solution to the design model. This solution optimizes the objective function and is subject to the set of constraining situations. The design model was programmed for solution on digital computers using FORTRAN IV language.

The optimization process is performed in two stages. In the first phase, the following nine separate arrangements of flexible pavement components are optimized by a linear programming algorithm:

1. Bituminous surface and stabilized base;
2. Bituminous surface, stabilized base, and compacted aggregate base;
3. Bituminous surface, stabilized base, and granular subbase with subbase through shoulders;
4. Bituminous surface, stabilized base, and granular subbase with subdrains;
5. Bituminous surface, stabilized base, compacted aggregate base, and granular subbase with subbase through shoulders;
6. Bituminous surface, stabilized base, compacted aggregate base, and granular subbase with subdrains;
7. Bituminous surface and compacted aggregate base;
8. Bituminous surface, compacted aggregate base, and granular subbase with subbase through shoulders; and
9. Bituminous surface, compacted aggregate base, and granular subbase with subdrains.

Six of these nine layered combinations of pavement components represent all possible flexible pavement systems for the cross sections with subbase, S_2, and for the cross sections with subbase and subdrains under both shoulders, S_3. Only three arrangements of these components are possible for the cross sections without subbase, S_1; they include combinations 1, 2, and 7.

The other phase of the solution involves the selection of that pavement-component arrangement that minimizes the total cost of the pavement system for the selected unit costs of the pavement materials. This final solution exists for the specified pavement design and material cost parameters. Each flexible pavement section fulfills the design objectives for the least total cost.

DESIGN EXAMPLES

To illustrate the application of this design model, two typical examples for the design of flexible pavements are shown in Figure 7. In each case, the computer output provides a listing of the stipulated design data and the material specifications. After these design parameters are summarized, the optimal solution is tabulated in terms of the best design section and the required thicknesses of the pavement components.

DESIGN DATA

NUMBER OF LANES	2
CBR	4.00
AVERAGE DAILY TRAFFIC 1966	2900. VEH./DAY
	BOTH DIRECTIONS
AVERAGE DAILY TRAFFIC 1986	5220. VEH./DAY
	BOTH DIRECTIONS
DESIGN PERIOD	20.00 YEARS
PERCENT TRUCKS	20.00
PERCENT MULTIPLE UNITS	25.00
DESIGN WHEEL LOAD	10000. LB.
REGIONAL FACTOR	1.00
PAVEMENT TERMINAL SERVICABILITY	2.50

DESIGN DATA

NUMBER OF LANES	4
CBR	2.30
AVERAGE DAILY TRAFFIC 1968	9438. VEH./DAY
	BOTH DIRECTIONS
AVERAGE DAILY TRAFFIC 1988	17830. VEH./DAY
	BOTH DIRECTIONS
DESIGN PERIOD	20.00 YEARS
PERCENT TRUCKS	17.00
PERCENT MULTIPLE UNITS	50.00
DESIGN WHEEL LOAD	10000. LB.
REGIONAL FACTOR	1.00
PAVEMENT TERMINAL SERVICABILITY	2.50

MATERIALS SPECIFICATIONS

	COST	DENSITY
BITUMIN. WEARING SURFACE	10.00 $/TON	145. LB/FT3
BITUMINOUS SURFACE BASE	5.00 $/TON	145. LB/FT3
STABILIZED BASE	8.00 $/TON	135. LB/FT3
COMPACTED AGGREGATE BASE	3.25 $/TON	140. LB/FT3
GRANULAR SUBBASE	3.15 $/YD3	
SHOULDER SURFACE	8.50 $/TON	145. LB/FT3
AGGREGATE FOR SUBDRAIN .	5.00 $/YD3	
PIPES FOR SUBDRAIN	0.70 $/FT	

MATERIALS SPECIFICATIONS

	COST	DENSITY
BITUMIN. WEARING SURFACE	6.85 $/TON	145. LB/FT3
BITUMINOUS SURFACE BASE	5.92 $/TON	145. LB/FT3
STABILIZED BASE	5.53 $/TON	135. LB/FT3
COMPACTED AGGREGATE BASE	2.87 $/TON	140. LB/FT3
GRANULAR SUBBASE	3.33 $/YD3	
SHOULDER SURFACE	7.95 $/TON	145. LB/FT3
AGGREGATE FOR SUBDRAIN .	4.35 $/YD3	
PIPES FOR SUBDRAIN	0.72 $/FT	

SOLUTION

NUMBER OF LANES	2
PERCENT MULTIPLE UNITS	25.00
STRUCTURAL NUMBER	3.95
TOTAL THICKNESS	19.2 INCHES
TRUCK FACTOR	132. 18K/DAY

SOLUTION

NUMBER OF LANES	4
PERCENT MULTIPLE UNITS	50.00
STRUCTURAL NUMBER	5.67
TOTAL THICKNESS	27.3 INCHES
TRUCK FACTOR	555. 18K/DAY

OPTIMAL SOLUTION

CROSS-SECTION WITHOUT SUBBASE

	THICKNESS
BITUMINOUS SURFACE	4.2 INCHES
STABILIZED BASE	0. INCHES
COMPACTED AGGREGATE BASE	15.0 INCHES
GRANULAR SUBBASE	0. INCHES

COST .. 19.32 $ PER LONG. FT.

OPTIMAL SOLUTION

CROSS-SECTION WITHOUT SUBBASE

	THICKNESS
BITUMINOUS SURFACE	6.1 INCHES
STABILIZED BASE	0. INCHES
COMPACTED AGGREGATE BASE	21.2 INCHES
GRANULAR SUBBASE	0. INCHES

COST .. 18.25 $ PER LONG. FT.

ALTERNATIVE SOLUTION (SUBOPTIMAL)

CROSS-SECTION WITH SUBDRAIN

	THICKNESS
BITUMINOUS SURFACE	6.0 INCHES
STABILIZED BASE	0. INCHES
COMPACTED AGGREGATE BASE	4.0 INCHES
GRANULAR SUBBASE	9.2 INCHES

COST .. 21.45 $ PER LONG. FT.

ALTERNATIVE SOLUTION (SUBOPTIMAL)

CROSS-SECTION WITH SUBDRAIN

	THICKNESS
BITUMINOUS SURFACE	9.0 INCHES
STABILIZED BASE	0. INCHES
COMPACTED AGGREGATE BASE	4.0 INCHES
GRANULAR SUBBASE	14.3 INCHES

COST .. 20.39 $ PER LONG. FT.

ALTERNATIVE SOLUTION (SUBOPTIMAL)

CROSS-SECTION WITH SUBBASE THROUGH SHOULDER

	THICKNESS
BITUMINOUS SURFACE	6.0 INCHES
STABILIZED BASE	0. INCHES
COMPACTED AGGREGATE BASE	4.0 INCHES
GRANULAR SUBBASE	9.2 INCHES

COST .. 22.63 $ PER LONG. FT.

ALTERNATIVE SOLUTION (SUBOPTIMAL)

CROSS-SECTION WITH SUBBASE THROUGH SHOULDER

	THICKNESS
BITUMINOUS SURFACE	9.0 INCHES
STABILIZED BASE	0. INCHES
COMPACTED AGGREGATE BASE	4.0 INCHES
GRANULAR SUBBASE	14.3 INCHES

COST .. 23.14 $ PER LONG. FT.

Figure 7. Example 1, design of flexible pavement for primary highways.

To permit a cost-effectiveness evaluation, the next two best solutions are generated for the remaining design sections. These alternate suboptimal solutions provide an economic measure of the additional cost for designs other than the optimal cross section.

The first situation involves a two-lane highway with a primary classification. The other example is a four-lane highway with pavement material costs that differ from those corresponding values in the first illustration. The rather significant increases in flexible pavement costs are evident when the alternate suboptimal solutions are compared to the optimal solutions in the two design examples.

Real economies are achieved when engineering designs are formulated to permit the selection of the optimal answer. This design model affords the highway engineer a practical and realistic method for the optimal design of flexible pavement sections.

REFERENCES

1. AASHO Interim Guide for the Design of Flexible Pavement Structures. American Association of State Highway Officials, 1961.
2. Buick, T. R. Analysis and Synthesis of Highway Pavement Design. Purdue Univ., Master's thesis, June 1968.
3. Hicks, L. D. Structural Design of Flexible Pavements in North Carolina. Proc., Internat. Conf. on Structural Design of Asphalt Pavements, Univ. of Michigan, Aug. 1962.